

Improving flight performance of DelFly II in hover by improving wing design and driving mechanism

Bart Bruggeman B.Sc.

October 19, 2010

Faculty of Aerospace Engineering · Delft University of Technology

Improving flight performance of DelFly II in hover by improving wing design and driving mechanism

MASTER THESIS

For obtaining the degree of Master of Science in Aerospace
Engineering at Delft University of Technology

Bart Bruggeman B.Sc.

October 19, 2010



Delft University of Technology

Copyright Bart Bruggeman B.Sc.
All rights reserved.

DELFT UNIVERSITY OF TECHNOLOGY
DEPARTMENT OF
SYSTEM ENGINEERING AND AIRCRAFT DESIGN

The undersigned hereby certify that they have read and recommend to the Faculty of Aerospace Engineering for acceptance a thesis entitled **“Improving flight performance of DelFly II in hover by improving wing design and driving mechanism”** by **Bart Bruggeman B.Sc.** in partial fulfillment of the requirements for the degree of **Master of Science.**

Dated: October 19, 2010

Head of department:

Prof. dr. ir. M.J.L. van Tooren

Committee chairman:

Prof. dr. ir. H. Bijl

Supervisor:

Ir. H.M. Ruijsink

Reader:

MSc. ing. B.D.W. Remes

Reader:

Dr. ir. J.F.L. Goosen

Abstract

Recent years have seen an increasing interest in micro aerial vehicles (MAV). The same can be said about flapping flight. The Delft University of Technology started to develop a flapping wing MAV in 2005, "DelFly", which relies on a flapping biplane wing configuration for thrust and lift generation. DelFly has evolved significantly during the last years. At the time of writing there are already three version of DelFly; DelFly I, DelFly II and DelFly Micro. The test subject of this study is DelFly II because of its stable and broad flight envelope.

The aim of this study is to improve flight performance of the DelFly II. Hereto, in this thesis report, a wing geometry study is performed in order to improve the aerodynamic performance of the wing and the driving mechanism is improved in order to increase the efficiency of energy transfer from the battery to the movement of the leading edges. The current study resulted in a increase of thrust-to-power ratio of 5% due to the wing design and 20% due to the new crank-shaft mechanism.

Acknowledgements

The present work is the final step towards my graduation at the Systems Engineering and Aircraft Design (SEAD) chair at the faculty of Aerospace Engineering at Delft University of Technology. During the past years in Delft I have learned a lot about aerospace and the things in life.

First of all I want to thank my supervisor Rick Ruijsink and Bart Remes for providing assistance during the whole period of my thesis. They both gave me tips and tricks about both the practical and theoretical insight of my subject. Hester Bijl and Bas van Oudheusden I also wish to thank for their knowledge about the aerodynamics aspect of the subject. They gave valuable feedback during the meetings.

I would like to express my thanks to the other members of the MAVLAB team as well: Christophe De Wagter for helping me with all the electronics of the experimental set-up and for the adaptations in the software. Although he had lots of work, he always managed to help me with my "small questions". Furthermore, I wish to thank Guido de Croon who has given me more insight in the field of data analysis and how to get the most out of my data.

Special mention goes out to Mark Groen, he was my colleague during this research. We have spent numerous hours together in the MAVLAB building and fixing the DelFly model over and over again. I want to thank Peter, Guido and Dennis for grabbing the opportunity to build DelFly wings for me. And Maarten for helping me with the cover.

I wish to thank all my friends here in Delft for giving me a very pleasant time for the last couple of years. Thanks goes out to the guys in my graduation room for the great moments we spent together. It was a real pleasure being in a room where there was always time for an intermezzo. Thank you guys!

Last but not least I am grateful to my family for supporting me during the last couple of years. Moe, thank you for giving me the opportunity to become an aerospace engineer. Bert, thanks for reviewing my thesis. And special thanks goes out to my girlfriend Karolien. She was always there for me and kept on believing in me. Thanks for your patience and for listening to all my annoying stories after a bad day.

Bart Bruggeman
Delft, The Netherlands
October 19, 2010

Contents

Abstract	v
Acknowledgements	vii
List of Figures	xvii
List of Tables	xix
Nomenclature	xxi
1 Introduction	1
1.1 Project description	1
1.2 Outline of the report	2
2 Test subject: DelFly II	5
2.1 Past, present and future	5
2.2 Wing configuration	8
2.3 Flight Kinematics	10
2.4 Driving mechanism	11
2.4.1 DelFly I	11
2.4.2 DelFly II	12
2.4.3 DelFly Micro	12
2.4.4 New DelFly II mechanism	12
2.5 Basic flapping aerodynamics	13
2.5.1 Insect-like flapping flight	14
2.5.2 DelFly flapping mechanism	16

3	Experimental set-up	19
3.1	The experiment	19
3.2	Working principle	20
3.2.1	Micro-controller board	23
3.2.2	DelFlyControl program	24
3.2.3	Speed controller	25
3.2.4	Hall sensor	25
3.2.5	Force sensors	26
3.2.6	Instrumentation amplifier	26
3.2.7	Voltage, current and frequency measurement	27
3.2.8	Accuracy of the system	27
3.3	DelFly in Forward Flight	28
3.4	DelFly in Hover	29
4	New crank-shaft mechanism	31
4.1	Shortcomings in the old DelFly II crank-shaft mechanism	31
4.2	New crank-shaft mechanism	32
4.2.1	Improvements	32
4.2.2	Gear ratio	33
4.2.3	Manufacturing of the different components	34
4.3	Weight breakdown	45
4.4	Comparison between old and new mechanism	46
5	Results and discussion of wing study	49
5.1	Raw data processing	49
5.1.1	Noise filtering	49
5.1.2	Mean value calculation	50
5.1.3	Accuracy of the measurements	53
5.2	Wing design	57
5.2.1	Effect of orientation and location stiffeners	57
5.2.2	Effect of stiffener thickness	64
5.2.3	Effect of different area distribution	65
5.2.4	Effect of different aspect ratio	67
5.2.5	General remark	69
5.3	Additional measurements	70
5.3.1	Clap & peel effect for DelFly II	70
5.3.2	Endurance test	72
5.3.3	Vacuum test	73
5.4	Overall increase in performance	75

6	Wing manufacturing process	79
6.1	Important building parameters	79
6.2	Overview of the options	80
6.2.1	Traditional cut & glue method	80
6.2.2	MEMS method	82
6.2.3	Advanced cut & glue method	84
6.3	Trade-Off	87
6.4	Advanced cut & glue method in practice	88
6.4.1	Draw the wing in a CAD program	88
6.4.2	Milling	89
6.4.3	Building the wing	90
6.4.4	Some remarks	94
6.5	Comparison of advanced cut & glue method with traditional cut & glue method	95
6.5.1	Manufacturing time comparison	95
6.5.2	Quality comparison	96
7	Conclusions & Recommendations	99
7.1	Conclusions	99
7.1.1	Experimental set-up	99
7.1.2	New crank-shaft mechanism	100
7.1.3	Results of wing study	100
7.1.4	Manufacturing method	102
7.2	Recommendations	102
7.2.1	Experimental set-up	102
7.2.2	New crank-shaft mechanism	102
7.2.3	Experiments	103
7.2.4	Wing manufacturing process	103
	References	105
A	DelFly II parameters	109
B	Specifications of Q70x5x9-H sensors	111
C	Technical drawings of the new crank-shaft mechanism	113
D	DelFly II wing design	121
D.1	Influence of stiffener location	121
D.2	Influence of area distribution	123
D.3	Influence of aspect ratio	123

List of Figures

2.1	DelFly I.	6
2.2	DelFly II (Jaap Oldenkamp).	7
2.3	DelFly Micro.	7
2.4	DelFly I (right), DelFly II (left) and DelFly Micro (middle).	8
2.5	Geometric flapping parameters of DelFly II.	9
2.6	Wing shape of DelFly II with position of the carbon rods (dotted line).	9
2.7	Schematic representation of the different velocity vectors (De Clercq [2009]). The morphological lower surface is indicated by a triangle at the leading edge.	10
2.8	Schematic representation of the wing path in forward flight (A) and hover (B) (De Clercq [2009]). The morphological lower surface is indicated by a triangle at the leading edge. Lift (perpendicular to the wing path) and drag (tangent to the wing path) are represented with red arrows.	10
2.9	Crank-shaft mechanism of DelFly I (<i>DelFly</i> [2010]).	11
2.10	Sideview (right) and frontview (left) of the old crank-shaft mechanism of DelFly II (<i>DelFly</i> [2010]).	12
2.11	Crank-shaft mechanism of DelFly Micro.	13
2.12	New crank-shaft mechanism of DelFlyII.	13
2.13	Schematic representation of half strokes during insect flapping (Ansari et al. [2008]).	15
2.14	Schematic illustration of the clap & fling mechanism; streamlines are illustrated in black, light blue vectors are net forces and dark blue vectors represent the induced velocities (Sane [2003]).	15
2.15	Schematic illustration of the clap & peel mechanism; streamlines are illustrated in blue, D-shape represents the cross section of the leading edge (De Clercq [2009]).	16
2.16	Pear-shaped heaving trajectory (Lehmann & Pick [2007]).	17

3.1	Strain gauge balance of Kristien De Clercq(De Clercq [2009]).	20
3.2	Picture of the new balance. One can see the L-shaped strain gauges. One vertical and one horizontal.	20
3.3	SolidWorks model of full scale DelFly II model with strain gauges and rotating point indicated in red.	21
3.4	Flow chart of the experiment.	22
3.5	Micro controller with different connections.	23
3.6	Interface of DelFly Control program.	24
3.7	Micro Variateurs Brushless VARBL2 Speed controller (<i>Micro Plane Solutions</i> [2010]).	25
3.8	Speed controller is mounted on the DelFly model.	25
3.9	Hall sensor.	26
3.10	Hall sensor mounted on DelFly II model.	26
3.11	Q70x5x9-H force sensor(<i>Zemic</i> [2010])	27
3.12	Datasheet force sensor (<i>Zemic</i> [2010]).	27
3.13	Picas amplifier.	27
3.14	Experimental apparatus in forward flight conditions	28
3.15	Experimental apparatus in hover conditions	29
4.1	Representation of the new crank-shaft mechanism.	32
4.2	Illustration of the old gear mechanism with a gear ratio of 20.	34
4.3	Illustration of the new gear mechanism with a gear ratio of 21.33.	34
4.4	Gear box drawings. The exact dimensions can be found in appendix C.	35
4.5	Cross section of the motorhousing together with the rotor, stator and bearings of the motor. The exact dimensions can be found in appendix C.	36
4.6	Motor pinion drawing. The exact dimensions can be found in appendix C.	37
4.7	Intermediate gear drawings. The exact dimensions can be found in appendix C	38
4.8	Main gear drawings. The exact dimensions can be found in appendix C.	39
4.9	Detail of the main gear.	40
4.10	Push rod drawings. The exact dimensions can be found in appendix C.	41
4.11	Inner and outer hinge of the old mechanism.	41
4.12	Symmetrical hinge of the new mechanism.	41
4.13	Push rod drawings. The exact dimensions can be found in appendix C.	42
4.14	Dimensions of the steel rivets (see also appendix C).	43
4.15	Wing holder drawings. The exact dimensions can be found in appendix C.	44
4.16	Performance plots of the comparison between old and new mechanism. The red lines represent two different wings on the old mechanism. The green line represent the same wings on the new mechanism	47
5.1	Thrust plot of both the raw (blue) and filtered (red) data of one clap cycle at 13 Hz.	50

5.2	Program flow diagram.	52
5.3	Measured thrust points (blue) are corrected for air pressure (red). The linear fit (green) through the corrected values has a slope of $-8.3e - 5 N/sample$. Flapping frequency is set to 12 Hz.	54
5.4	Measured power points (blue). Linear fit (green) has a slope of $-4.7e - 5 W/sample$. Flapping frequency is set to 12 Hz.	54
5.5	Thrust generation of 8 different wings.	55
5.6	Power consumption of 8 different wings.	56
5.7	Thrust-to-power ratio of 8 different wings.	56
5.8	Schematic representation of half wing with stiffener location of wing0 (cyan), wing31 (magenta), wing63 (blue), wing77 (green), wing90 (red) and the standard wing (wing5424) (dotted).	58
5.9	Performance plots of the parallel test series. Colors are according figure 5.8. The brown line represents a mean value of DelFly II weight at 0.16 N.	58
5.10	Schematic representation of half wing with stiffener location of wing6331 (red) and wing5163 (green).	59
5.11	Performance plots of the parallel test series. Colors are according figures 5.8 and 5.10. The brown line represents a mean value of DelFly II weight at 0.16N.	60
5.12	Schematic representation of half wing with stiffener location of (1)wing6331 (red), (2)wing6326 (solid magenta), (3)wing6328 (dashed magenta), (4)wing7731 (solid green), (5)wing6931 (dashed green), (6)wing6928 (solid blue), (7)wing9039 (dashed blue), (8)wing11663 (dotted blue).	61
5.13	Performance plots of the converging test series. Colors are according figures 5.12. The brown line represents a mean value of DelFly II weight at 0.16N.	61
5.14	Schematic representation of half wing with stiffener location of wing7731 (green), wing9039(blue) and wing8435 (red).	62
5.15	Performance plots of wing7731 (green), wing9039(blue) and wing8435 (red). The brown line represents a mean value of DelFly II weight at 0.16 N.	63
5.16	Schematic representation of half wing with stiffener location of standard wing (black) and wing8435(red).	64
5.17	Performance plots of standard wing (black) and wing8435(red). The brown line represents a mean value of DelFly II weight at 0.16N.	64
5.18	Performance plots of wings with different stiffener thickness. The brown line represents a mean value of DelFly II weight at 0.16 N.	65
5.19	Schematic representation of wing8436 (blue), bat-like wing (red) and reversed wing (green).	66
5.20	Performance plots of wing8436 (blue), bat-like wing (red) and reversed wing (green). The brown line represents a mean value of DelFly II weight at 0.16N.	67
5.21	Schematic representation of wing8436 with AR = 1.75 (blue), wing with AR = 2.20 (red) and wing with AR = 1.45(green).	68
5.22	Performance plots of wing8436 with AR = 1.75 (blue), wing with AR = 2.20 (red) and wing with AR = 1.45(green). The brown line represents a mean value of DelFly II weight at 0.16 N.	69

5.23	Comparison of thrust generation of a biplane DelFly II wing (red solid line) and a single DelFly II wing (dotted blue line). The doubled values of the single wing are presented by the solid blue line. The mean gain in thrust due to the clap & peel effect is 8% over the whole frequency range for DelFly II.	71
5.24	Comparison of power consumption of a single DelFly II wing (blue) and a half biplane wing (green).	71
5.25	Rupture at the tip of left wing.	72
5.26	Rupture at the rear of the root.	72
5.27	Results from the endurance test. The blue dots are the measuring points, the red dots are two measuring points after the wing was torn and the green line represents a linear fit through the blue dots.	73
5.28	Performance plots of vacuum tests. Solid lines represent tests in normal air conditions, dotted lines are tests in vacuum.	74
5.29	Comparison of current development at 13 Hz between a wing in air (blue) and a wing in vacuum (green) for one flap cycle. The thrust generation is shown in red.	75
5.30	Performance plots of four cases: Old wing - Old mechanism, New wing - Old mechanism, Old wing - New mechanism and New wing - New mechanism.	76
5.31	Simplified electric scheme of DelFly.	77
5.32	'Cyclone 130' 130mAh, 20C Lithium Polymer Cell discharge curve (<i>Atomic Workshop</i> [2010]).	77
5.33	Detail of discharge curve (<i>Atomic Workshop</i> [2010]).	77
6.1	Overview of the cut & glue method. 1) A4 is taped to the table; 2) Mylar is taped over the A4 paper; 3) Stiffeners are glued to the Mylar; 4) Detail of reinforcement tape at the end of a stiffener; 5) Detail of reinforcement around the semi-ellipse; 6) Leading edges are glued to the Mylar and the wing is cut out.	82
6.2	Building process of MEMS wings (Pornsir-Sirirak et al. [2000]).	84
6.3	SolidWorks representation of the MDF plate after milling the wing contours and holes (left). Detail of the holes on both sides of the contour (right).	85
6.4	After elastically stretching the foil, the brown line is displaced again over the groove. Therefore, no tension is present in the wing.	85
6.5	Cross-section of stiffener in jig with the Mylar.	86
6.6	Trade-off diagram between different methods.	88
6.7	AutoCAD drawing of a wing. Dimensions are in mm.	89
6.8	Tool for milling the contour, location of the leading edges and location of the stiffeners in the MDF plate. D1=0.6 mm, L1=4 mm, D2=3 mm, L2=38.1 mm (<i>STEP-FOUR</i> [2010]).	89
6.9	MDF plate after milling the wing contours	90
6.10	Tool for cutting the contour of the Mylar foil. D=3mm, L=40mm and $\delta = 15^\circ$ (<i>STEP-FOUR</i> [2010])	92
6.11	Overview of the advanced cut & glue method. 1) Placing the Mylar onto the vacuum table; 2) Glue the stiffeners; 3) Secure stiffeners with tape; 4) Cut out the half-ellipse; 5) Glue leading edges; 6) Cut out the contour; 7) Glue foil around leading edges; 8) Finished.	93

6.12	Microscopic view of an engraver cut with speed 12 mm/min.	94
6.13	Microscopic view of an engraver cut with speed 100 mm/min.	94
6.14	Microscopic view of an engraver cut with speed 500 mm/min.	95
6.15	Microscopic view of a razor blade cut.	95
6.16	Performance plots of wings made with the advanced method (red) and wings made with the traditional method	97
A.1	Geometry of the old DelFly II wing.	109
A.2	Geometry of the new DelFly II wing.	110
B.1	Dimensions of the force sensor (<i>Zemic</i> [2010]).	112
C.1	Dimensions (in mm) of the motor pinion.	113
C.2	Dimensions (in mm) of the gearbox.	114
C.3	Dimensions (in mm) of the intermediate gear.	115
C.4	Dimensions (in mm) of main gear.	116
C.5	Dimensions (in mm) of the pushrod.	117
C.6	Dimensions (in mm) of the hinge.	118
C.7	Dimensions (in mm) of the steel rivets.	119
C.8	Dimensions (in mm) of the wing holder.	120
D.1	Step 1.	121
D.2	Step 2.	122
D.3	Step 3.	122
D.4	Step 4.	122
D.5	Area distribution.	123
D.6	Aspect ratio.	123

List of Tables

3.1	Parameters of the <i>.log</i> file.	23
4.1	Diameter overview for loose and push fits.	44
4.2	Comparison of weight breakdown between old mechanism, the SolidWorks model and new mechanism.	45
4.3	Overview of different cases when comparing the old and new mechanism .	46
5.1	Parameters of the <i>.log</i> file.	50
5.2	List of standard deviations of thrust, power and thrust-to-power ratio for every measured frequency.	57
5.3	Stiffener properties.	65
5.4	List of different slopes.	69
5.5	List of power used for mechanics with respect to total power.	74
6.1	Milling parameters	90
6.2	Engraver cutting specifications	94
6.3	Differences between the Traditional and Advanced method	95
6.4	Overview of building time of one set of DelFly wings (two wings) for both traditional method and advanced method	96
A.1	Design parameters of DelFly.	109
B.1	Specifications of Q70x5x9-H sensors (<i>Zemic</i> [2010]).	111

Nomenclature

Latin Symbols

A	Wing area	$[m^2]$
C_L	Lift coefficient	$[-]$
C_T	Thrust coefficient	$[-]$
D	Drag force	$[N]$
d	Reference diameter	$[mm]$
$I_{measured}$	Measured motor current	$[mA]$
L	Lift force	$[N]$
m	Module	$[mm/number\ of\ teeth]$
n	number of teeth	$[-]$
n_1	number of teeth of the first gear	$[-]$
n_2	number of teeth of the second gear	$[-]$
p	Air pressure	$[hPa]$
p_0	Standard air pressure at sea level	$[hPa]$
R	Specific gas constant	$[J/(kgK)]$
T	Temperature	$[K]$
T	Thrust force	$[N]$
V	Velocity	$[m/s]$
$V_{measured}$	Measured motor voltage	$[V]$
V_{thrust}	Thrust in volts	$[V]$

Greek Symbols

α	Angle of attack	[deg]
ν	Kinematic viscosity	[kg/ms]
ψ	Dihedral angle	[°]
ρ	Air density	[kg/m ³]
φ	Stroke angle	[°]
φ_s	Clearance angle	[°]

Abbreviations

AR	Aspect Ratio
ASTI	Aerospace Software and Technologies Institute
CNC	Computer Numerical Control
DSE	Design Synthesis Exercise
DUT	Delft University of Technology
FMAV	Flapping Micro Air Vehicle
GR	Gear ratio
HF	Hydrofluoric
LEV	Leading Edge Vortex
MAVLab	Micro Aerial Vehicle Lab
MAV	Micro Air Vehicle
MEMS	Micro-Electro-Mechanical Systems
PC	Poly Carbonate
PIV	Particle Image Velocimetry
POM	Polyoxymethylene
RP	Rapid Prototyping
TAT	Turn-Around Time
Ti	Titanium
UAV	Unmanned Air Vehicle

Chapter 1

Introduction

1.1 Project description

Commercial and military airplanes have fixed or rotary wings. Birds, insects and bats on the other hand flap their wings. The way humans developed a way of flying differs quite a lot from the way nature does this. Due to its millions of years head start in flapping wings, it is safe to assume that this has to be an effective way of flying, of course within the constraints of these animals such as their relative small size. Over the last two decades, scientific interest in this way of flying has risen and research activity has started to cover the field systematically. However, many aspects have yet to be fully understood.

One of the fields where flapping wings are applied, is the field of Micro Air Vehicles (MAV's). MAV's are small Unmanned Air Vehicles (UAV). Both the civil and military values are of great importance and lead to multiple specifications such as low speeds, small size, great manoeuvrability at low speeds, hover capabilities and carrying small payload. All these specifications can be fulfilled with flapping wings.

DelFly is such an ornithopter, designed and developed at the Aerospace Faculty at Delft University of Technology. This ornithopter will be the test subject of this master thesis. Since the initial DelFly I design in 2005, many improvements have been implemented and resulted in the next generation MAV, called DelFly II. This second version of the DelFly family will be the test subject of this thesis.

Although the flight characteristics of DelFly II are good, both in hover and forward flight, room for improvement still exists. There are many possibilities to improve the aerodynamic efficiency of MAV's. Two of these possibilities are:

1. Improving the mechanics
2. Improving the wing design

By improving the mechanics, it is possible to use the electrical power of the battery in a more efficient way such that the battery of the MAV can perform longer which can

be translated in a longer flight time. In order to reach this objective, a new driving mechanism is designed during this project.

Changing the wing design can also result in a more efficient power consumption. Because the wings of a flapping MAV are not only responsible for the lift generation but also for the thrust generation it is of key importance that the aerodynamic properties such as high thrust and lift forces can be generated. This will result in a longer flight time as well. The old wing of DelFly II has a geometry which is mostly derived from literature. Although this type of wing seems to work pretty well on DelFly, little research has been done on the effectiveness of this type of wing and on possible other type of wings. Therefore it is necessary to carry out deeper research and tests in order to identify if a better wing is possible.

In order to manufacture and test these different type of wings a new manufacturing process and an experimental test set-up is built. This research is focusing on the hover condition because this is the most demanding flight condition.

When considering this, the project goal can be summarized as follows:

Project Goal

”Improve flight performance of DelFly II in hover by improving wing design and driving mechanism”

This research is closely related to the research of Mark Groen (Groen [2010]). He did his thesis work simultaneously, his work is focusing on the flow visualization around a DelFly wing with the aid of PIV measurements.

1.2 Outline of the report

The test subject of this thesis research, DelFly II, is discussed in chapter 2. This chapter will elaborate about the history of the DelFly project and the different versions of DelFly. The special wing configuration, biplane wings, will be explained in detail together with the flight kinematics. At the end of this first chapter the basics of flapping aerodynamics are discussed. Being able to test DelFly wings, involves having a good experimental set-up. The working principle and the different components of this experimental set-up are described in chapter 3. How the system works for forward flight and hover is explained in more detail in this chapter as well. In chapter 4 the driving mechanism of DelFly II is discussed. The chapter will explain why a new driving mechanism was needed and how it is created. The different components of this new crank-shaft mechanism are discussed in detail. The results of the wing study in order to improve the wing performance are presented in chapter 5 together with a discussion of additional tests in order to get a better understanding of the influence of certain wing parameters on the performance. Because of the high production number and reproducibility of wings during this thesis research, a different manufacturing method has to be created in order to make more consistent wings in a faster way. Different methods are described in chapter 6 and a trade-off has

been performed to select the best method for this research. Finally, conclusions and recommendations are stated in chapter 7.

Test subject: DelFly II

This chapter will give the reader more insight in the MAV "DelFly II", which is the test subject of this thesis work. Section 2.1 will give an overview of the history of the DelFly project and the different members of the DelFly family. More information about the wing configuration can be found in section 2.2. In sections 2.3 and 2.4 the flight kinematics and driving mechanism are described respectively. Finally, the basics for understanding flapping aerodynamics are explained in section 2.5.

2.1 Past, present and future

The DelFly project started as a student project in April 2005 at the Aerospace Faculty of Delft University of Technology (DUT). This project, the Design Synthesis Exercise (DSE), is the final phase of the Bachelor course at the faculty. During the DSE, ten students have to tackle a design problem in ten weeks time. The assignment of one group was: *"Impress the jury of the first US-European Micro UAV Competition by designing a flapping wing, vision based MAV, using commercially off the shelf products, within a budget of €5000, with eleven students in ten weeks time"* (DSE [2005]). In those ten weeks, the students developed a design of a Flapping Micro Aerial Vehicle (FMAV), DelFly I, which was inspired by nature, more specifically inspired by a dragonfly. The students built their design in the summer of 2005 and went to the international MAV competition in Germany where they impressed both the jury and the public with their design. Although they did not manage to complete the competition's mission, the DelFly was nominated as "Best Exotic Design". This first version of DelFly had a length of 410 mm, 330 mm span and a weight of 21 g (DSE [2005]). The frame is manufactured out of carbon and balsa wood, Mylar foil is used for the wing's membrane, the stiffeners are carbon rods and the leading edges are carbon-balsa-carbon constructions. A picture of DelFly I can be seen in figure 2.1.

Since the success of DelFly I at the IMAV '05 the interest in flapping MAV's at DUT increased. A valorisation institute at the aerospace faculty, Aerospace Software and Technologies Institute (ASTI), started to improve the DelFly I design. After one year of



Figure 2.1: DelFly I.

adapting DelFly I, in 2006, DelFly II was born (figure 2.2). DelFly II differs in many aspect from DelFly I:

- The size of DelFly II is smaller than the size of DelFly I. DelFly II has a span of 280 mm and a length of 240 mm. From flight tests, it could be seen that placing the tail closer to the wings had a beneficial effect on the flight efficiency.
- DelFly II is lighter than DelFly I, it weighs only about 16 g.
- The wing shape is slightly altered with respect to DelFly I.
- The frame of DelFly II is mainly built out of carbon.
- Lighter and smaller electronics are used.
- The brushed DelFly I motor is replaced by a brushless motor.

All these changes resulted in an exceptional flight envelope. DelFly II has the ability to hover, fly forward up to 15 m/s and backward up to 0.5 m/s (*DelFly* [2010]). All this can be done while carrying a payload in the form of one or two cameras for streaming live images to a ground station. DelFly II was again the first flying ornithopter of such a small size that could carry a camera. It also performed the first successful autonomous flight at the IMAV 2008. During this test, DelFly II had to follow a path of white A4 papers on the ground while maintaining a fixed altitude. The combination of these abilities makes DelFly a good platform for both military and civil use.

In 2008, the members of the MAVlab were able to downscale the DelFly II even further. DelFly Micro (see figure 2.3) has a span of 100 mm, a length of 107 mm and a weight of 3.07 g. Although DelFly Micro is not yet able to perform as well as DelFly II, it has flown successfully with a camera on board while sending the images to a ground station. DelFly Micro is not yet able to hover. Further work has to be done on DelFly Micro in order to become a stable platform such as DelFly II.

At the moment of writing the DelFly family has three different members, DelFly I, DelFly II and DelFly Micro. It has already been a successful story up till now, but the story is not finished yet. On the long term an even smaller DelFly than DelFly Micro is planned, the DelFly Nano. This flapper will be 50 mm in span and will also be able to carry a camera.

The DelFly I, DelFly II and DelFly Micro can be seen together in figure 2.4



Figure 2.2: DelFly II (Jaap Oldenkamp).

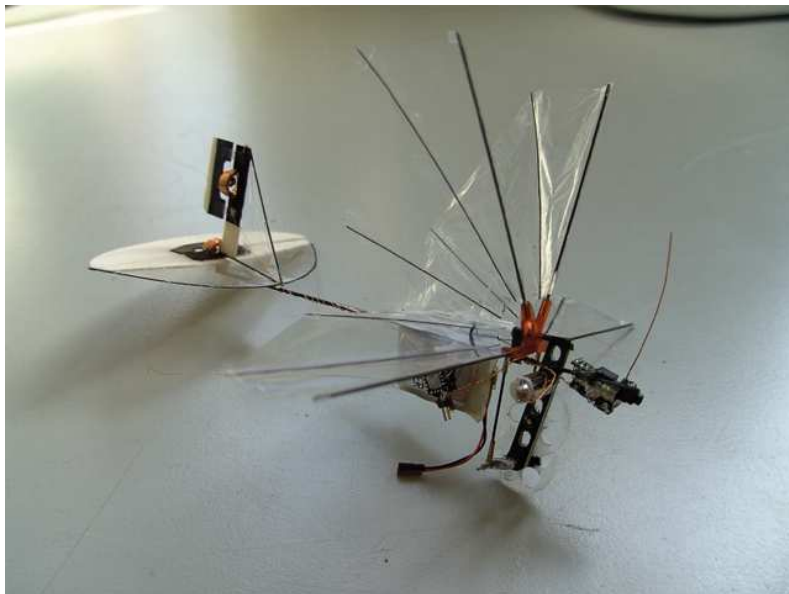


Figure 2.3: DelFly Micro.



Figure 2.4: DelFly I (right), DelFly II (left) and DelFly Micro (middle).

2.2 Wing configuration

With the aim of creating a stable platform for a camera, a biplane wing configuration was elected for the DelFly, see figure 2.5. The configuration consists of two pairs of wings that flap in anti-phase to reduce the plunging motion of the fuselage and thereby creating a stable platform for the camera images. "Biplane" means that the two pairs of wings are placed on top of each other in order to maximize the wings surface for a limited span and to gain extra lift from the clap & peel effect (see section 2.5). The wings are placed symmetrically with respect to the fuselage to obtain lateral stability during forward flight (De Clercq [2009]). The wings are placed under a dihedral angle, ψ of 12° . A small clearance angle, φ_s , is used to prevent damage due to collision between the upper and lower wing during flapping. The maximum stroke angle, φ , is 44° . Both the upper and lower wing flap with the same frequency. The wings are hinged in one point and move by means of a crank-shaft mechanism which will be enlightened in chapter 4. The leading edges move in a single plane due to this crank-shaft mechanism, this is the translational phase of a flap cycle. Due to aerodynamic and inertial forces the wings rotate around the leading edges between subsequent strokes, this is called the rotational phase. The wings are passively twisted due to elasticity and inertial forces.

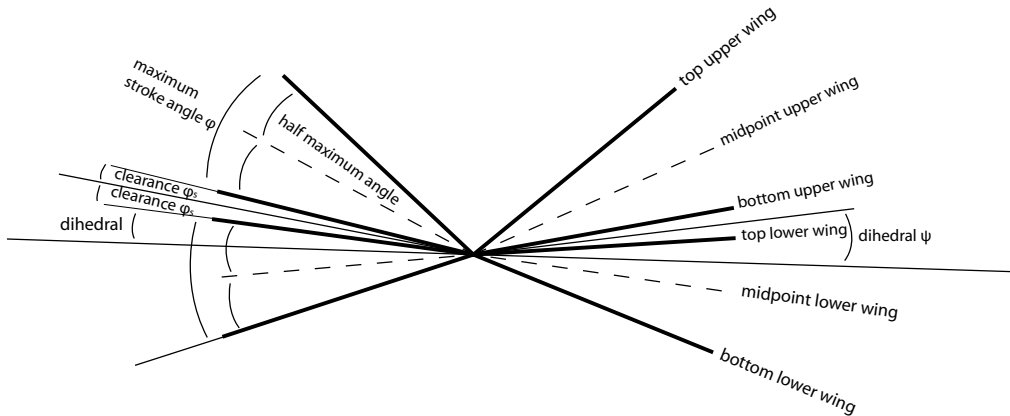


Figure 2.5: Geometric flapping parameters of DelFly II.

The membrane of the wing is made out of $5 \mu\text{m}$ thick Mylar, which is a strong, light and thin polyester film. This Mylar is reinforced with carbon rods of 0.28 mm diameter to give some rigidity and be able to passively control the dynamic twist of the wing due to the flapping motion. D-shaped carbon rods of $1.4 \text{ mm} \times 0.7 \text{ mm}$ are used for the leading edges. In figure 2.6 one can see the shape of the DelFly wing with the dimensions.

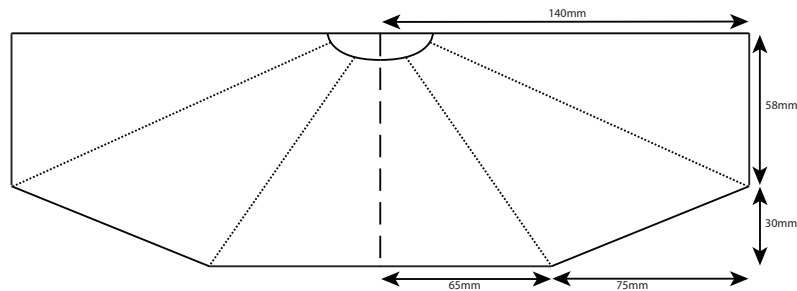


Figure 2.6: Wing shape of DelFly II with position of the carbon rods (dotted line).

The shape of the DelFly II wing is derived from the wing of DelFly I. DelFly I had a semi-elliptical wing shape (DSE [2005]) and was designed for the dimensions of DelFly I. The edges of the semi-elliptical wing were curling up between the stiffeners because there was not enough tension in that part of the wing to resist the forces which are generated during flapping. For this reason the wings of DelFly II have straight edges. For this research the wing design is altered in order to improve the flight characteristics of DelFly II. This will be explained further in the report.

The flapping frequency can vary between 0 Hz and 18 Hz . For level flight this frequency is around 11 Hz and around 14 Hz in hover, depending on the weight of DelFly II. The flapping frequency for level, forward flight is lower because of the aerodynamic benefit the wings have due to this forward flight. The wings of DelFly produce a lift force due to the dynamic twist and curvature of the wings, in analogy with conventional wings.

2.3 Flight Kinematics

In order to explain the broad flight envelope of DeFly II, a simplified analysis is made of both forward flight and hover. The relative velocity, $V_{relative}$, that the wing feels is a summation of three different velocity vectors: (1) the flight velocity, V_{flight} , (2) the flapping velocity, V_{flap} , and (3) the downwash velocity, $V_{downwash}$, as can be seen in figure 2.7. This $V_{relative}$ is tangent to the wing path. According to the definition of lift and drag force, these forces are respectively perpendicular and tangent to this wing path.

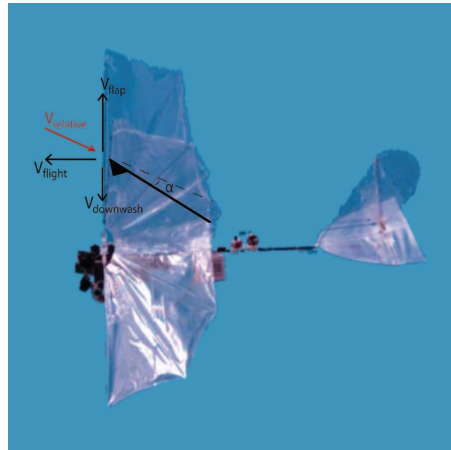


Figure 2.7: Schematic representation of the different velocity vectors (De Clercq [2009]).
The morphological lower surface is indicated by a triangle at the leading edge.

In figure 2.8(A) a schematic representation of the wing path is given for forward flight. Here, the stroke plane is positioned vertical and the fuselage horizontal, minimizing drag. The tail is used as a conventional tail.

The hover condition is represented in figure 2.8(B). Hovering can be done by pulling the elevator up, this induces a nose-up pitching moment and flight speed decreases until the stroke plane becomes horizontal. Eventually the flight speed becomes zero. $V_{relative}$ is now only the sum of V_{flap} and $V_{downwash}$.

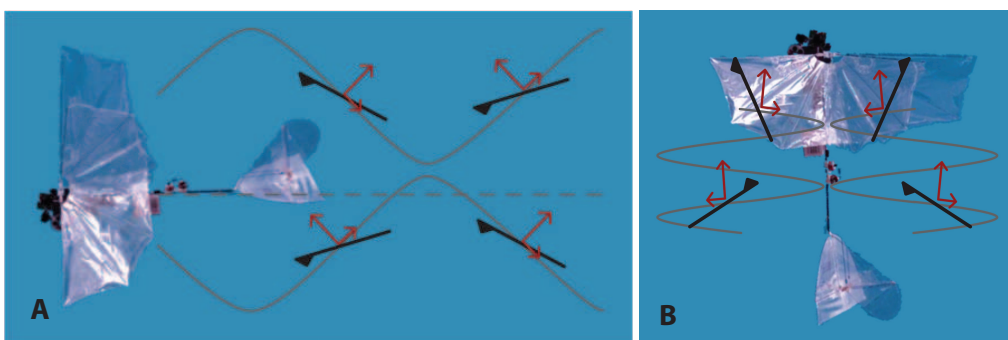


Figure 2.8: Schematic representation of the wing path in forward flight (A) and hover (B) (De Clercq [2009]). The morphological lower surface is indicated by a triangle at the leading edge. Lift (perpendicular to the wing path) and drag (tangent to the wing path) are represented with red arrows.

2.4 Driving mechanism

The driving mechanism of the DelFly is a crank-shaft mechanism. This type of driving mechanism is used for all versions of the DelFly family. However, changes are made between the different versions. The idea of a crank-shaft mechanism is that the spinning of the motor is responsible for the spinning of the gears, which are responsible for an optimal transmission due to different radii and different number of teeth. The main gear is connected to push rods which are connected to the leading edges. These push rods push and pull the leading edges up and down which causes the flapping motion of the wings.

2.4.1 DelFly I

DelFly I has a crank-shaft mechanism which is mainly manufactured of birch plywood and steel wire pins as illustrated in figure 2.9. The motor, gears, push rods and leading edges all move in the same plane. The main gear is directly driven by the motor pinion. Both push rods are connected to this main gear by means of a steel wire. This type of mechanism is responsible for asymmetric movement of the push rods and thus asymmetric flapping which caused the DelFly to make small roll movements.

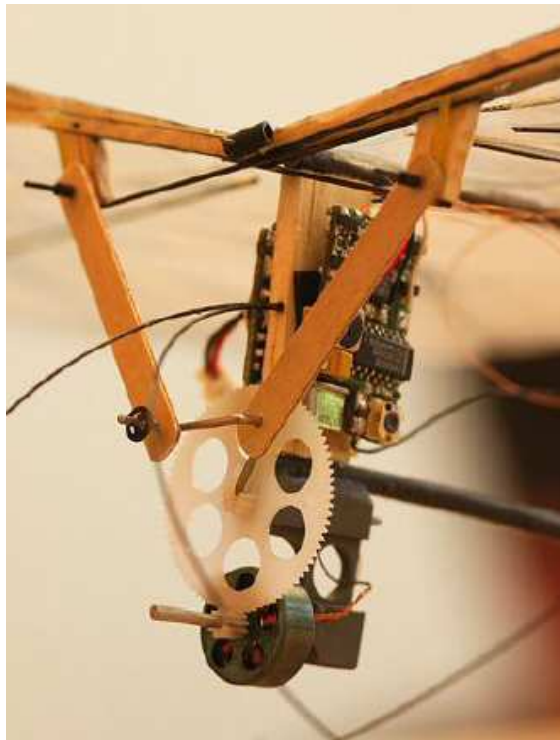


Figure 2.9: Crank-shaft mechanism of DelFly I (*DelFly* [2010]).

2.4.2 DelFly II

For DelFly II, a sandwich gearbox of carbon-balsa-carbon is used which is stronger, lighter and more accurate for placing the gears. The concept of having the gears, motor, push rods and leading edges in parallel planes was changed in placing the motor and gears in a plane perpendicular to the stroke plane as can be seen in figure 2.10. The main reason for this change is to get symmetric flapping in a compact system. Both push rods are each linked to a crank, a mechanism that is responsible for symmetric movement of both push rods. A two stage gearbox provides the right gear ratio to match the motor rpm to the flapping frequency.

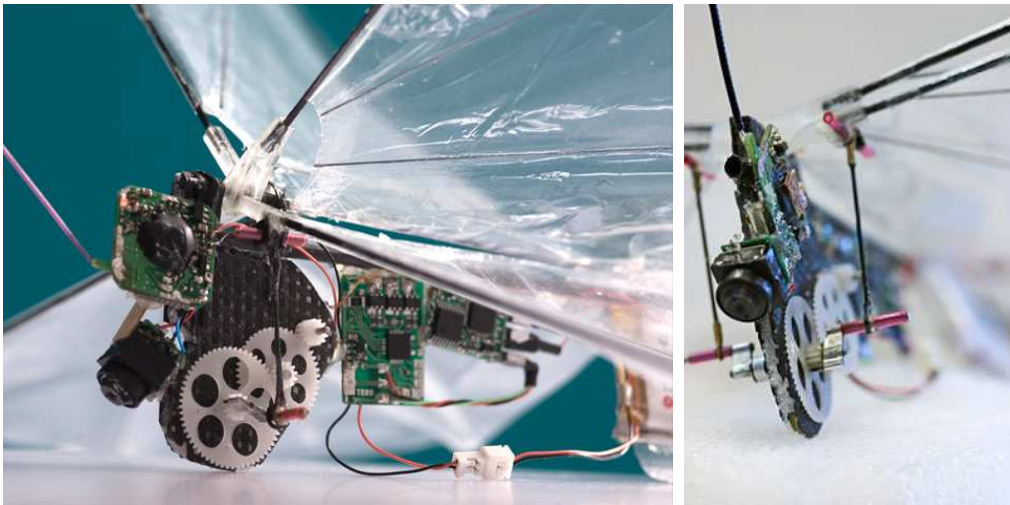


Figure 2.10: Sideview (right) and frontview (left) of the old crank-shaft mechanism of DelFly II (*DelFly* [2010]).

2.4.3 DelFly Micro

A scaled down version of the DelFly II mechanism is used for the driving mechanism of DelFly Micro (figure 2.11). Like for DelFly II, a two stage gearbox is used with another total gear ratio to match the specific DelFly Micro conditions.

2.4.4 New DelFly II mechanism

A new mechanism is developed during this thesis. The new mechanism is lighter, more efficient and more accurate than the previous one. A detailed description of this mechanism and its components can be found in chapter 4. Figure 2.12 shows the new mechanism. All the gears, the motor and the stroke plane are again in one plane like the DelFly I mechanism. However, the flapping motion is now symmetric due to the application of two counter rotating main gears.

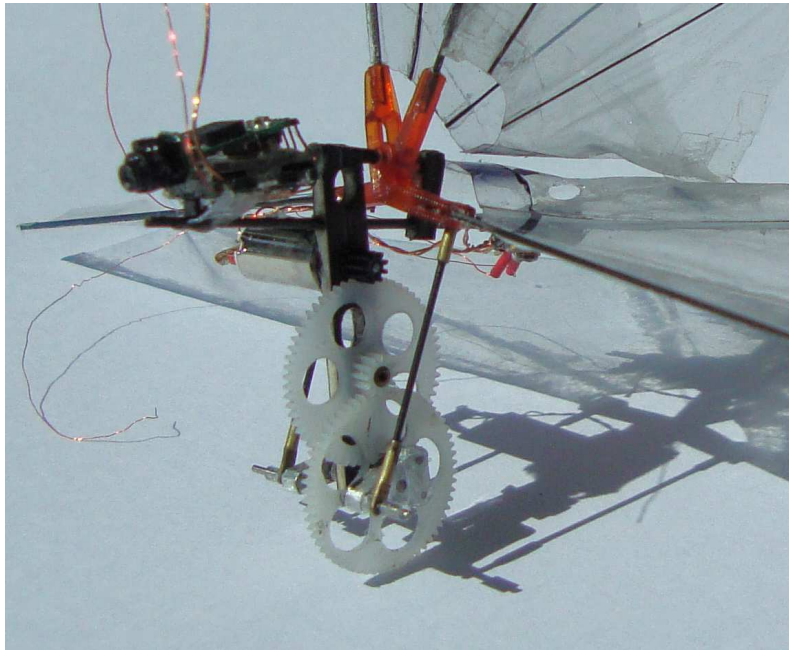


Figure 2.11: Crank-shaft mechanism of DelFly Micro.

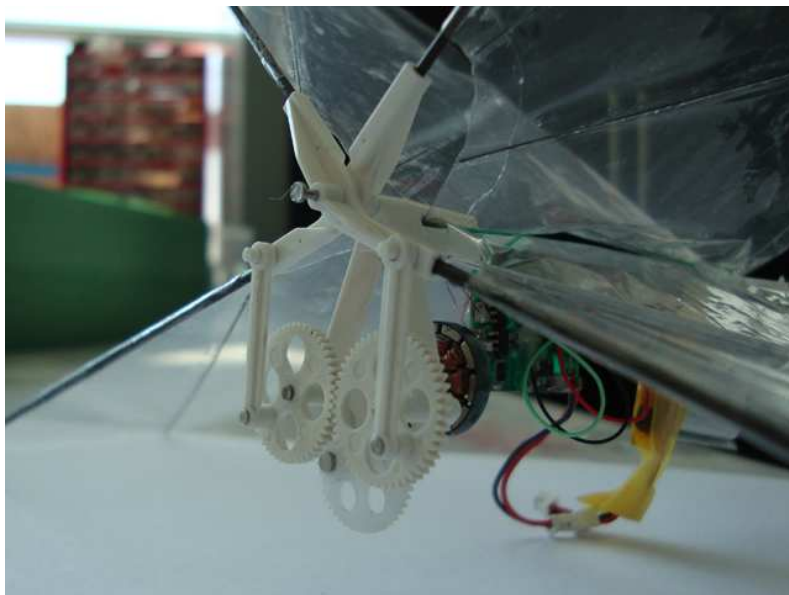


Figure 2.12: New crank-shaft mechanism of DelFlyII.

2.5 Basic flapping aerodynamics

To provide some understanding why DelFly is able to fly, some theoretical aerodynamic concepts are explained. DelFly, which is inspired by nature, is based on flapping flight. Nature uses this type of flight for several hundreds of million years. There are fundamental differences in flapping flight between animals of different sizes such as big birds, small birds, bats and different insects. The flapping motion of DelFly mostly resembles the

motion of an insect or bat because of the flight kinematics, in a more simplified manner. Despite its well adapted use in nature, understanding is not yet fully complete. Insects, however, uses a far more complicated manner of flapping flight than DelFly. In order to understand the global picture, it is necessary to take a brief look at insect flight before discussing DelFly flight. The flapping aerodynamics of DelFly are also discussed in the thesis of Mark Groen (Groen [2010]), who specialized more on the aerodynamic part of the project.

2.5.1 Insect-like flapping flight

The research is focusing on hover. Therefore, only the important flow features of this condition will be discussed. More detailed information of flapping aerodynamics can be found in C. P. Ellington [1995], Lehmann [2004] and Sane [2003]. The flow regime under consideration is that of an incompressible, unsteady flow at low Reynolds number. The relatively large forces that are generated during flapping flight cannot be explained with conventional fixed-wing aerodynamic theory. Therefore these forces need to be explained by the presence of the unsteady flow effects and the presence of strong vertical structures in the flow.

Insects use a reciprocating movement of the wings for flight. In figure 2.13 one can see a schematic approach of one flap cycle. In this movement three phases can be distinguished: the translational phase (moving the wing fore and aft), the rotational phase (when the pitch angle of the wing is changing substantially) and the heaving and plunging phase (upwards and downwards movement of the leading edges). The two half-strokes that make up the flap cycle are called the down-stroke and the up-stroke. These two strokes are predominantly translational movements. The change in pitch angle during these movements is rather small. At the end of a half-stroke the rotational phase takes place, during this phase stroke reversal occurs and the wing pitches rapidly.

Of the aerodynamic mechanisms that make insect flight possible, two mechanisms which are of greatest importance in this study are the occurrence of leading edge vortices (LEVs) and the clap & fling (or in the case of the DelFly, clap & peel) mechanism. The LEV is the result of flow separation at the wing leading edge, due to the thin airfoil and high angles of attack of the wing. Instead of stalling completely, the wing stall is delayed and the flow is able to reattach further downstream. A LEV is created in the separated part, which adds extra vorticity to the bound circulation of the wing, producing therefore an increase in lift (and also drag, depending on the wing orientation)(C. Ellington et al. [1996]). Another mechanism that contributes to the lift production is the clap & fling mechanism (or Weis-Fogh mechanism (Weis-Fogh [1972])). It has been discovered that certain insects and birds make use of the clap & fling mechanism, sometimes for a limited time in order to generate higher lift during for example the take-off phase (Lehmann [2004]). They do so by increasing the wing stroke to such an extent that the wings touch each other during the stroke reversal. During the clap the leading edges of the wings touch before the trailing edges do so. When the gap between the wings is closed progressively, the circulation of both wings cancels each other out. The air between the wings is expelled down in the form of a momentum jet enhancing lift (De Clercq [2009]), see figure 2.14 A-C. When the leading edges move away from each other, in the fling phase air is sucked

into the gap that is created. Due to this suction an increase in circulation is generated which means an increase in lift, see figure 2.14 D-F.

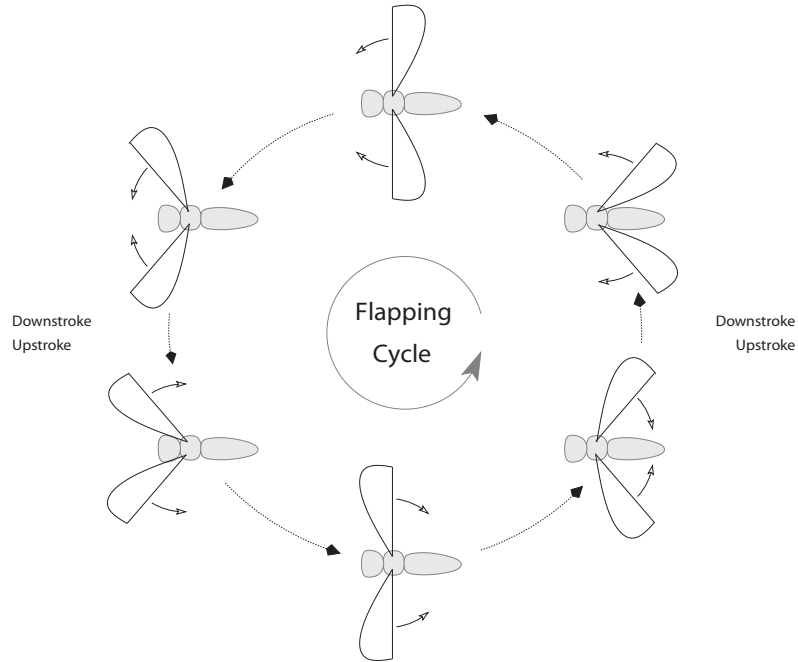


Figure 2.13: Schematic representation of half strokes during insect flapping (Ansari et al. [2008]).

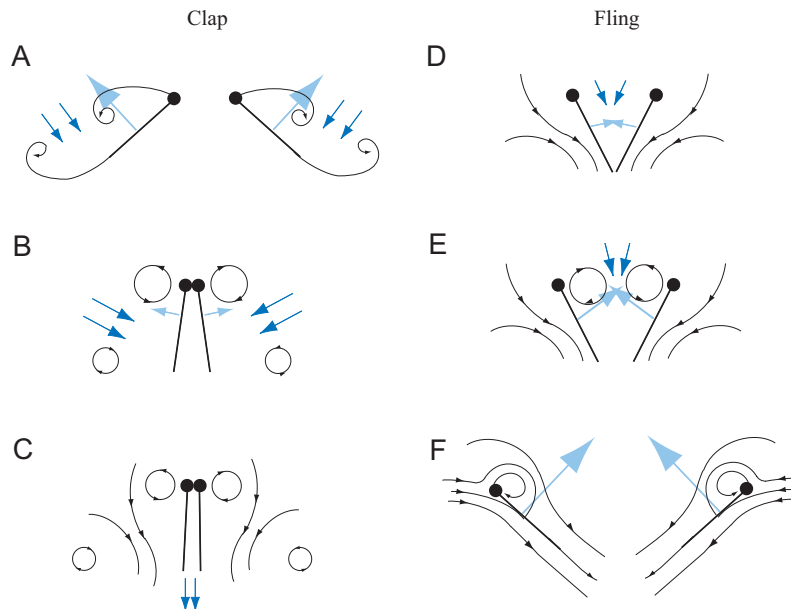


Figure 2.14: Schematic illustration of the clap & fling mechanism; streamlines are illustrated in black, light blue vectors are net forces and dark blue vectors represent the induced velocities (Sane [2003]).

2.5.2 DelFly flapping mechanism

DelFly does not use the aerodynamic mechanisms in the same manner as most insects do because the mechanism is kept more simple. The mechanics explained in the previous section are applied to a two-winged insect. DelFly, as said before is inspired by a dragonfly, which has four wings instead of two. The essential difference between the dragonfly's wing configuration and that of DelFly however, is that DelFly uses a biplane wing configuration with the wings on top of each other while the wings of a dragonfly are behind each other (tandem configuration). Because the wings are placed on top of each other, the wing area can be doubled without increasing the size of the MAV. In addition, early tests showed that a tandem configuration on DelFly uses more power for the same wing area (Croon et al. [2009]).

Because of the biplane wing configuration and the fixed flap amplitude, clap & fling will be present every flap cycle and not only during flight phase where high lift is demanded. Furthermore, clap & fling is actually clap & peel when talking about DelFly. Instead of flinging apart more rigidly, the wings peel apart due to fluid-structure interaction between the air and the flexible membrane wings. This gives a more gradual build-up of the circulation, which can prevent an unstable LEV from shedding into the wake (De Clercq [2009]). This can be seen in figure 2.15(D-F).

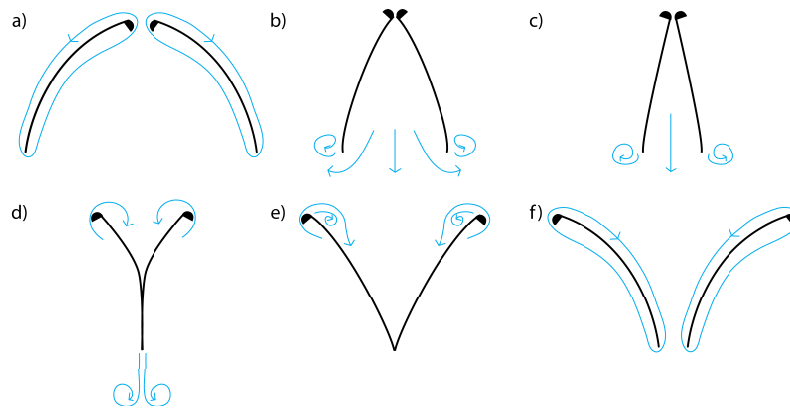


Figure 2.15: Schematic illustration of the clap & peel mechanism; streamlines are illustrated in blue, D-shape represents the cross section of the leading edge (De Clercq [2009]).

Another difference with common insect flight is the heaving or plunging movement that accompanies the flapping. It has been assumed that the wings make a heaving motion perpendicular to the stroke plane, which contributes to a better aerodynamic trajectory (Lehmann & Pick [2007]). The influence of this motion is not yet fully understood. Various patterns of heaving motion have been observed by insects, like for example the pear-shaped trajectory, see figure 2.16

Tests on DelFly shows that there is also a heaving motion in the DelFly flapping trajectory. Though, this motion is not actively triggered. It is a passive effect of the stiffness of the leading edges. Preliminary tests showed that DelFly was not able to fly as stable with circular carbon rods for leading edges as with D-shaped carbon rods. The difference between the two is the stiffness perpendicular to the stroke plane. Because the D-shaped

rods have a lower stiffness in that direction, the leading edges will bend easier in that direction than for circular rods. The result is a more beneficial tension in the wing during flapping. This change in stiffness gave DelFly the opportunity to hover.

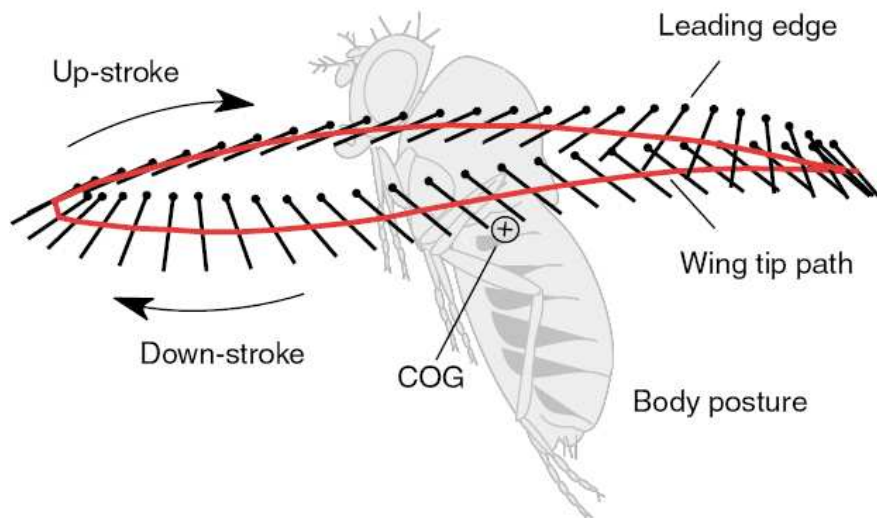


Figure 2.16: Pear-shaped heaving trajectory (Lehmann & Pick [2007]).

The parameters of DelFly II are presented in appendix A. As all DelFly's are built by hand, none of them is exactly the same so the weight differs slightly. With the weight, the wing flapping frequency required for sustained hovering flight also differs. When a DelFly is hovering, all the energy has to be put in lifting the whole weight of the DelFly, which means that the thrust to weight ratio is equal to 1. A lower wing flapping frequency is needed in forward flight because of aerodynamic benefits analogous to rotor aircrafts. In forward flight, the thrust has to overcome the drag and part of the weight, which results in a thrust to weight ratio smaller than 1. Under hovering conditions, the Reynolds number based on the mean wing tip velocity and the mean chord is typically of the order of 14,000.

Experimental set-up

For the actual testing of the DelFly II wings, an experimental set-up is built. This set-up has to measure power of the motor, flapping frequency, lift and thrust. Later on, this experimental apparatus is used in combination with a Particle Image Velocimetry (PIV) system for the thesis research of Mark Groen (Groen [2010]).

In section 3.1 the purpose of the experiment is explained. Next, the working mechanism of the experimental set-up together with the different parts of the system is discussed in detail in section 3.2. Finally, in sections 3.3 and 3.4 both the forward flight and hover conditions are explained.

3.1 The experiment

Performance tests have to be done on the wings of DelFly II. Therefore a full scale model of DelFly II is built in order to test the thrust generation and power consumption of a certain set of wings. The experimental set-up is based on the strain gauge balance of Kristien De Clercq' thesis research (De Clercq [2009]) (see figure 3.1) and on the work of Kawamura (Kawamura et al. [2008]) for changing the angle of attack.

The model has no tail, no servos for pitch and yaw control and no camera. There is evidence that the presence of a tail has influence on the airflow around the wing. For example, placing the tail closer to the wing has a positive influence on the stability of DelFly. This interaction between tail and wing is not captured in this study for simplification reasons. The model is mounted on a set-up with strain gauges for force measurements and connected with a micro-controller board which is responsible for a constant sample frequency. This micro-controller can measure the different parameters like current, voltage, frequency etc. The wings are evaluated for force generation, power consumption and ratio of these two parameters. The initial intension was to test both hover and forward flight conditions, therefore the set-up is able to change the angle of attack of DelFly II. Unfortunately, due to a lack of time this work focuses on hover flight only. The experimental set-up can be seen in figure 3.2

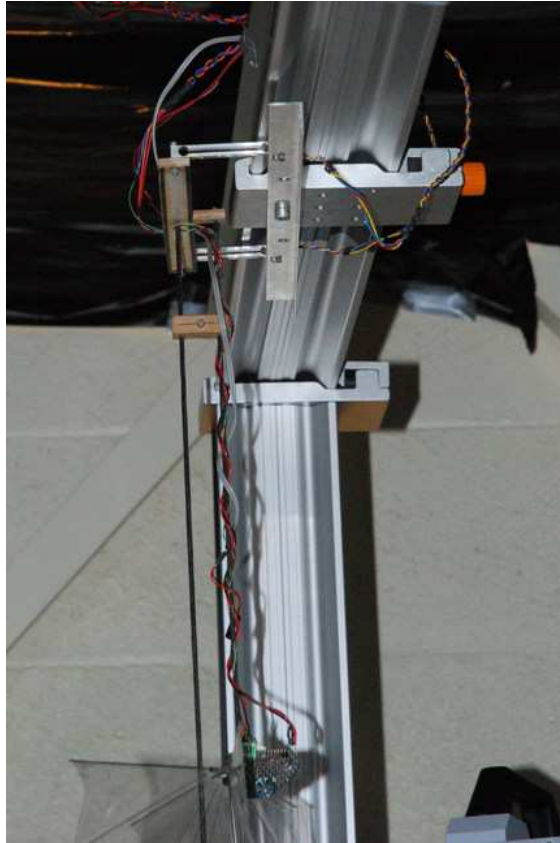


Figure 3.1: Strain gauge balance of Kristien De Clercq(De Clercq [2009]).

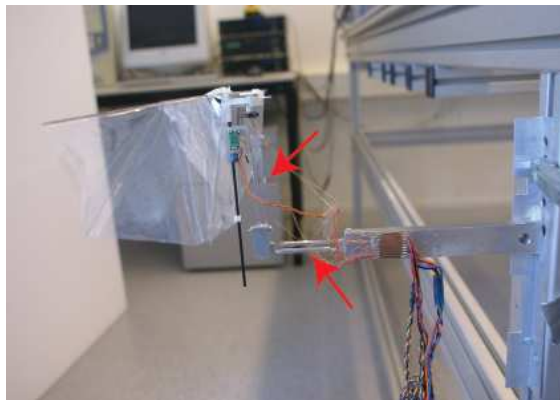


Figure 3.2: Picture of the new balance. One can see the L-shaped strain gauges. One vertical and one horizontal.

3.2 Working principle

As mentioned above, the strain gauge balance that Kristien De Clercq used, had a few limitations:

1. The balance can only measure the thrust force in hover conditions. This force is

also the lift force in hover.

2. The model is mounted on carbon tubes which are connected to the strain gauges and then to the earth. The carbon tubes are not stiff enough to counteract the vibrations due to the flapping. Although these vibrations damp almost completely out after initiation of the airflow, it still has effect on the strain gauge measurements.

In order to overcome these problems and limitations, a modified balance is made:

1. To enable measurements in both forward and hover conditions, the set-up has to be able to rotate, allowing a change in angle of attack.
2. Two strain gauges are placed in an L-shape under an angle of 90° . Both lift and thrust force in forward flight can now be calculated when the angle of attack is known.
3. Minimizing vibrations is done by means of a stiff construction. The connection between the DeIFly to the strain gauges is as light and stiff as possible. By doing this, the vibrations between model and strain gauges are minimized. To minimize the vibrations between model-strain gauge and the earth, solid aluminum beams are used to make the construction as stiff as possible. Here, more mass can be beneficial.
4. De Clercq used two Q70x5x9-H sensors with a capacity of 20 g (De Clercq [2009]) (*Zemic* [2010]) for the new balance one sensor for each direction is used. A sensor with double capacity (at least 40 g) for measuring of the thrust force is used. For the direction perpendicular to the thrust direction, a smaller capacity is used because of the smaller forces in that direction.

In figure 3.3 a 3D drawing is shown of the model with the strain gauges and the rotating mechanism.

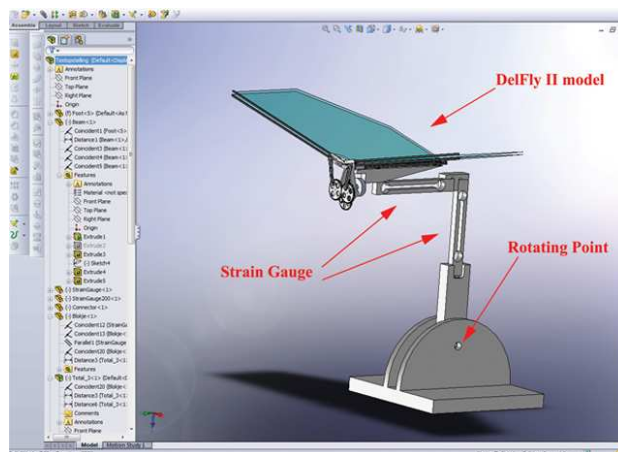


Figure 3.3: SolidWorks model of full scale DelFly II model with strain gauges and rotating point indicated in red.

The diagram in figure 3.4 gives a global overview of how the different components of the set-up are connected to the system and how they work together.

An external power supply keeps the system running and replaces the normal DelFly II battery. The input of the DelFlyControl program is sent to a micro-controller board which sends the information to the speed controller. The speed controller drives the motor which results in a flapping motion of the DelFly model through the gear connections. A feedback connection between the motor and the micro-controller board is used for the control of the flapping frequency by counting the motor phase. Voltage and current signals are sent to the micro-controller board. Due to the flapping motion, force sensor 1 and force sensor 2 measure voltage differences over their strain gauges which are amplified by an instrumentation amplifier and sent to the micro-controller board. A hall sensor counts the flap cycles and these signals are sent to the micro-controller board as well. Finally, all the information on the micro-controller board is processed and sent to the computer program and saved as usable data in a *.log* file. The different parameters which are logged can be found in table 3.1

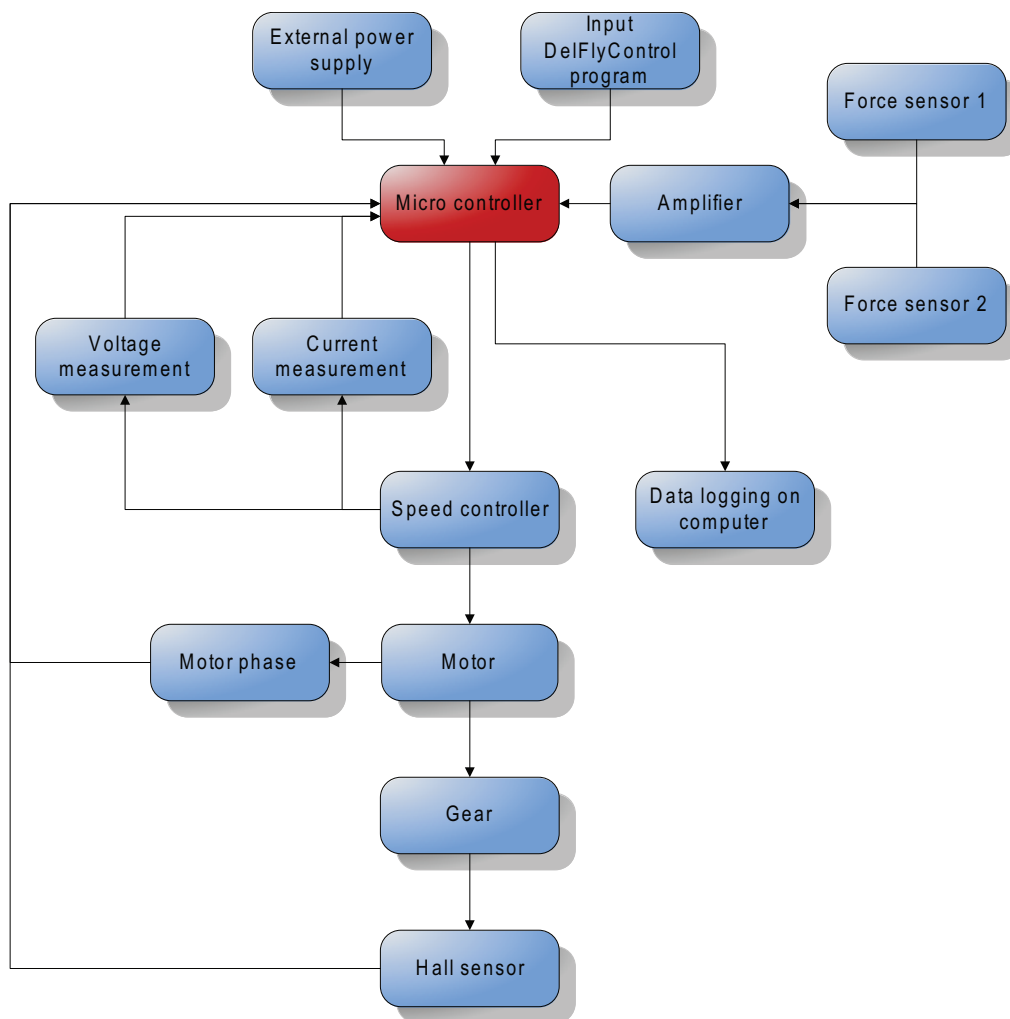


Figure 3.4: Flow chart of the experiment.

Parameter	Unit
Computer time	[sec]
Force sensor 1	[V]
Force sensor 2	[V]
Force sensor 3 (not used)	[V]
Voltage	[V]
Current	[mA]
Flapping frequency	[Hz]
Throttle	[-]
Motor counter	[-]
Hall sensor counter	[-]

Table 3.1: Parameters of the *.log* file.

In the following sections, the different components of the system are discussed in more detail.

3.2.1 Micro-controller board

The control of the DelFly II model (control of the flapping frequency) and the processing of all data is done by a custom made micro-controller board (figure 3.5), which is developed by Christophe De Wagter of the MAVlab. A high and accurate sampling frequency of 1860 Hz can be reached with the micro-controller board. The micro-controller board is the "heart" of the set-up as can be seen in figure 3.4. A serial connection is present between the micro-controller board and the PICAS instrumentation amplifier which is responsible for the force data. Data from the DelFly II model such as flapping frequency, voltage measurements, current measurements, throttle and motor counter is sent to the micro-controller board via one connector together with the external power supply. The Hall sensor has a separate connection. The PIV cameras are triggered through the two white BNC connectors. A detailed description of the PIV triggering can be found in the thesis report of Mark Groen (Groen [2010]). Finally, a USB connection is present as a linkage with the computer.

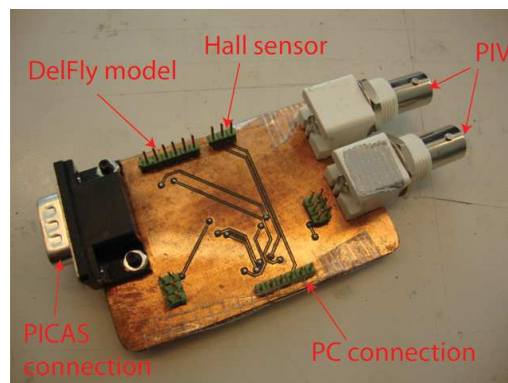


Figure 3.5: Micro controller with different connections.

3.2.2 DelFlyControl program

The micro-controller board is connected to a computer with a USB connection. This connection allows the user to control the DelFly model with a custom made computer program, developed by Christophe De Wagter, called "DelFlyControl.exe". This computer program allows the user to control the throttle and thereby control the flapping frequency. It also allows the user to set the flapping frequency to a certain value or to adjust the PID controller which controls the speed controller. The user can also trigger the moment of the laser for PIV measurements. The program translates the different signals from the micro-controller board into numerical data, see table 5.1.

The interface of the program can be seen in figure 3.6. With the slider on the left hand side of the interface, the user can control the throttle. When the user slides the bar upwards, the motor of the DelFly model will start to spin faster. This can only be done when the *Manual* button is selected. If the *Auto* button is selected, the user can give an input in the *Auto_Hz* field. For instance, if the user gives an input of 12, the motor will start to spin up until the flapping frequency is 12 Hz. In the *P*, *I*, *D* and *trim* fields, the user can tune the PID controller for controlling the motor. The standard values can be found in figure 3.6. *Comport* is the number of comport of the computer that the USB connection uses. *0 Phase* and *plaats flash* are parameters that can be set in combination with the PIV system (Groen [2010]). The fields *Force 1 [V]* and *Force 2 [V]* show the voltage of the strain gauges which are already amplified by the instrumentation amplifier. The fields *Volt* and *Current* indicate respectively the voltage and current that the flapping DelFly model is using. The *Hz* field shows an indication of the flapping frequency. *Flapcount* is a counter that counts every flap cycle and *Throttle* gives an indication of how much throttle the user give as input. The values in the fields in the left column change with a frequency of 1860 Hz. These values are logged into a *.log* file on the computer when the program is turned off. Logging can be done continuously when *logging* is selected or it can be done for 20 seconds every 20 minutes when *log 20 sec every 20 min* is selected. This latter option is used for tests that take several hours.

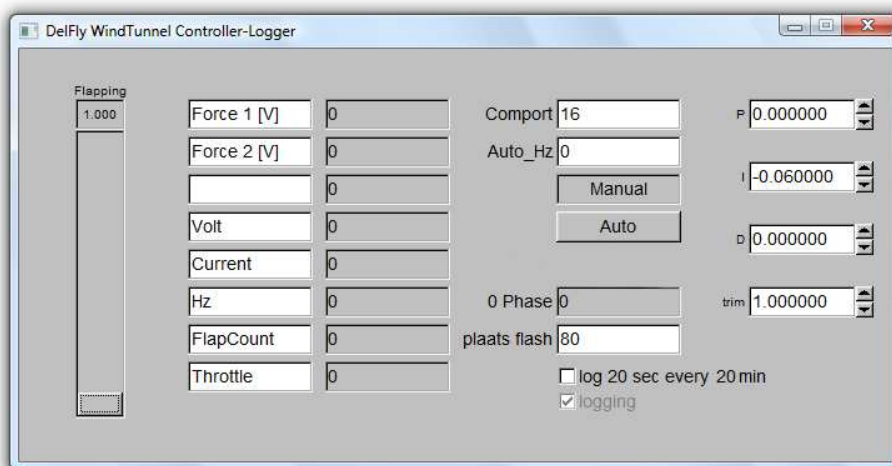


Figure 3.6: Interface of DelFly Control program.

3.2.3 Speed controller

The speed controller controls the motor and therefore the wing flapping frequency. The wing flapping frequency is measured by counting the motor pulses. Every motor revolution has three pulses. The gear ratio is 1:20, therefore DelFly flaps once every 20 revolutions of the motor. This means a total of 60 pulses per flap cycle. For the new mechanism, this gear ratio is 1:21.33, this means a total of 64 pulses per flap cycle.

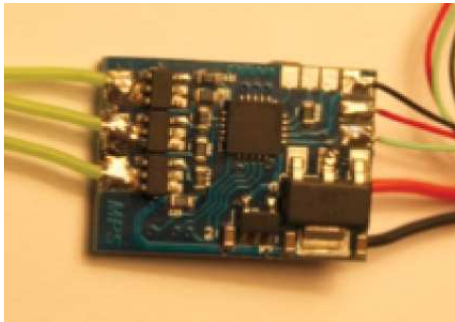


Figure 3.7: Micro Variateurs Brushless VARBL2 Speed controller (*Micro Plane Solutions* [2010]).

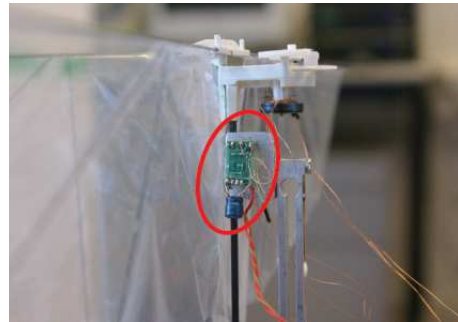


Figure 3.8: Speed controller is mounted on the DelFly model.

Note

The flapping frequency is calculated in the DelFlyControl program with the gear ratio of the DelFly model. Therefore, the *rpm*-term has to be multiplied by a factor of $\frac{64}{3}$ ($= 21.33$) (new mechanism) instead of $\frac{20}{1}$ ($= 20$) (old mechanism). This gear ratio will be further explained in section 4.2.2 of chapter 4.

3.2.4 Hall sensor

A Hall sensor (see figure 3.9) is a sensor that varies its output voltage in response to changes in the magnetic field. The type of sensor for these tests is a A3213 Micropower Ultra-Sensitive Hall-effect switch of Allegro Microsystems, Inc. The Hall sensor is placed on the gearbox of the DelFly model and a magnet is placed on the main gear. One flap cycle is equal to one revolution of that main gear. Therefore, every time the magnet travels by the Hall sensor, one flap cycle is counted. The Hall sensor sends the signal to the micro-controller board which translates the signal into a flap counter. In figure 3.10 one can see the magnet and Hall sensor mounted on the DelFly model.

Both the Hall sensor and motor pulses are used for counting the flap cycles but their information is also combined for measuring the trigger moment for the PIV equipment. The motor gives 64 pulses per revolution (the old mechanism 60 pulses per revolution). The PIV system is triggered at one of these pulses. It is important for the measurements that no time-lag will occur over different flapping cycles. If this happens, the wing will

never be at the same position when the laser is triggered. Therefore the Hall sensor is used to recalibrate the motor pulse counting for every flap cycle.



Figure 3.9: Hall sensor.

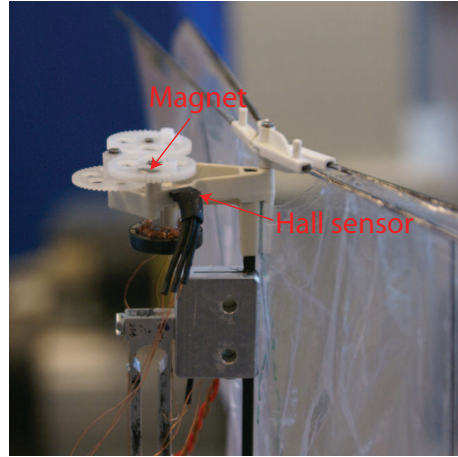


Figure 3.10: Hall sensor mounted on Delfly II model.

3.2.5 Force sensors

The lift and thrust forces which are generated due to the flapping motion of the DelFly model are measured with miniature sensors from Zemic (*Zemic* [2010]). Strain gauges are glued onto a four-bar mechanism (see figure 3.11). When a force is applied to that bar, the different strain gauges sense compression or tension in the bar, which results in respectively a decrease or increase in electrical resistance of the strain gauge. This change in resistance induces a change in voltage. Because of the small changes in voltage (millivolts), these volts are sent to an instrumentation amplifier. For this set-up, two Q70x5x9-H sensors were used. One with a capacity of 200 g for the force measurement in thrust direction and one with a capacity of 50 g for the force measurement in the direction perpendicular to the thrust direction. The 200 g capacity is necessary to measure the high vibration peaks during flapping. In the direction perpendicular to the thrust, less capacity is needed because only small forces will act in that direction during hover tests. Dimensions and more specifications of the Q70x5x9-H sensors can be found in appendix B.

3.2.6 Instrumentation amplifier

The voltages coming from the strain gauges are very small, as discussed above. Therefore the voltages of the strain gauges pass through an instrumentation amplifier. It is a PICAS amplifier from Peekel Instruments (*Peekel Instruments* [2010]). This high accuracy measurement system amplifies the measurement signal by a factor of 2096. The PICAS analog output provides the controller board with a 10 V range signal, -5 V to 5 V signal.

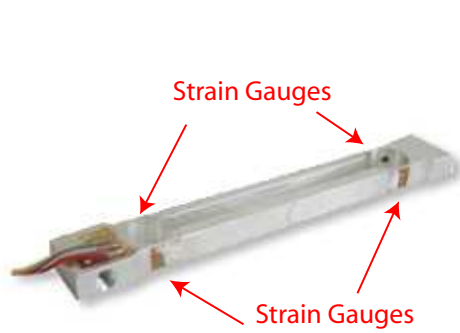


Figure 3.11: Q70x5x9-H force sensor (Zemic [2010])

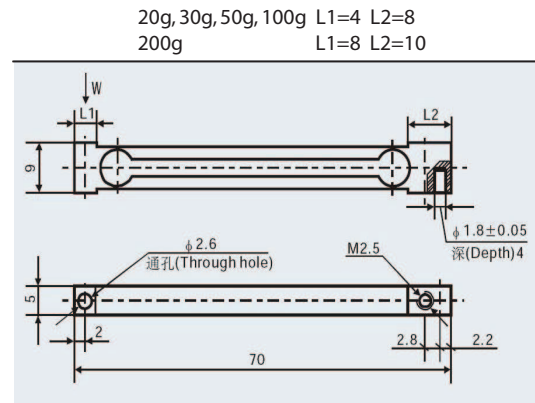


Figure 3.12: Datasheet force sensor (Zemic [2010]).



Figure 3.13: Picas amplifier.

3.2.7 Voltage, current and frequency measurement

The measurement of the current is done on the micro-controller board. The voltage is measured at the speed controller input and the frequency is calculated from the motor pulses, as explained in section 3.2.3.

3.2.8 Accuracy of the system

The bounding resolution of the system is the 10 bit resolution of the ADC in the micro-controller board. One can translate this resolution into a voltage resolution, which is equal to the measurement range, which is 10 V (-5 V to +5 V) divided by the voltage intervals, which is equal to $2^{10bit} = 1024$. This means that the voltage resolution is equal to $\frac{10}{1024} = 0.0097V$. The instrumentation amplifier is calibrated such that 1 V is equal to 20 g or 0.197 N. The resolution converted to grams or Newton is $\frac{0.0097 V \cdot 20 g}{1 V} \approx 0.2 g$ or 0.002 N. This is the resolution of one sample. The resolution of the tests will be

smaller because more samples are used for calculating the averages. Therefore, 0.002 N is a maximum.

3.3 DelFly in Forward Flight

When flying forward, the wind that travels over the wings induces a force, *Lift* or L , analogous to conventional fixed-wing aerodynamics. The vector of this lift force is positioned vertically, perpendicular to the free stream velocity, U . The *Thrust* or T , is orientated perpendicular to the plane in which the leading edges move. The angle of attack, α , is the angle between the free stream velocity and the orientation of the DelFly model.

Both sensors measure a combination of components of lift, thrust and drag:

$$force1 = L \cdot \cos(\alpha) + D \cdot \sin(\alpha) \quad (3.1)$$

$$force2 = T + L \cdot \sin(\alpha) - D \cdot \cos(\alpha) \quad (3.2)$$

Here is L the lift force, T the thrust force, D the drag force and α the angle of attack. Figure 3.14 gives a representation of the apparatus in forward flight.

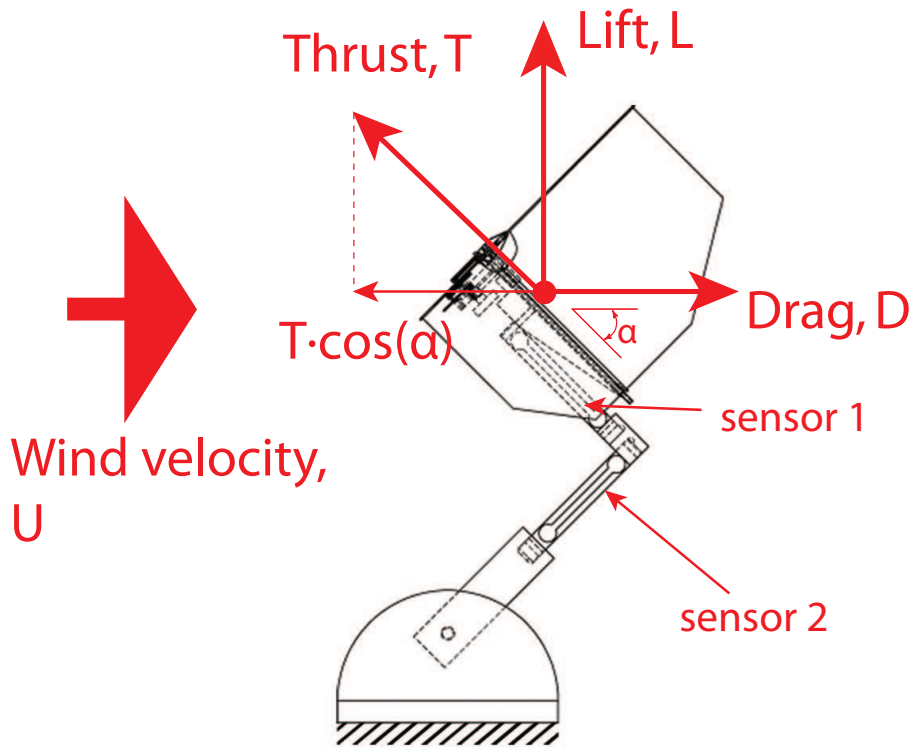


Figure 3.14: Experimental apparatus in forward flight conditions

3.4 DelFly in Hover

DelFly II is also able to stay in one place, analog to a helicopter. This condition, called "hover", is one of the advantages that DelFly II has compared to other MAV's. Hover is the most energy consuming flight mode of the whole flight envelope. This is because the thrust generated by the wings has to overcome the total weight of DelFly II. In forward flight, this is different. Less energy is needed in forward flight due to the aerodynamic advantage when flying forward (see section 3.3).

Hover can be seen as a special case of forward flight in which $\alpha=90^\circ$ and $U=0$. Although the free stream velocity is zero, the local velocity due to the downwash in order to create thrust is not equal to zero. In Figure 3.15, one can see the forces acting on the model when it is in hover position. For hover the terminology for T and L is the same. T is acting perpendicular to the plane in which the leading edges flap, which is now vertical and L is defined as the force perpendicular to the free stream velocity. During hover it is assumed that this free stream velocity is almost zero and still horizontal, therefore L is also vertical. The additional aerodynamic effect that is produced during forward flight is not applicable here.

One can expect that only the sensor that is positioned horizontally, will measure a force and that the vertical sensor will not measure any forces. In theory, this is true, but due to small mechanical vibrations, the vertical sensor will also measure small fluctuating forces.

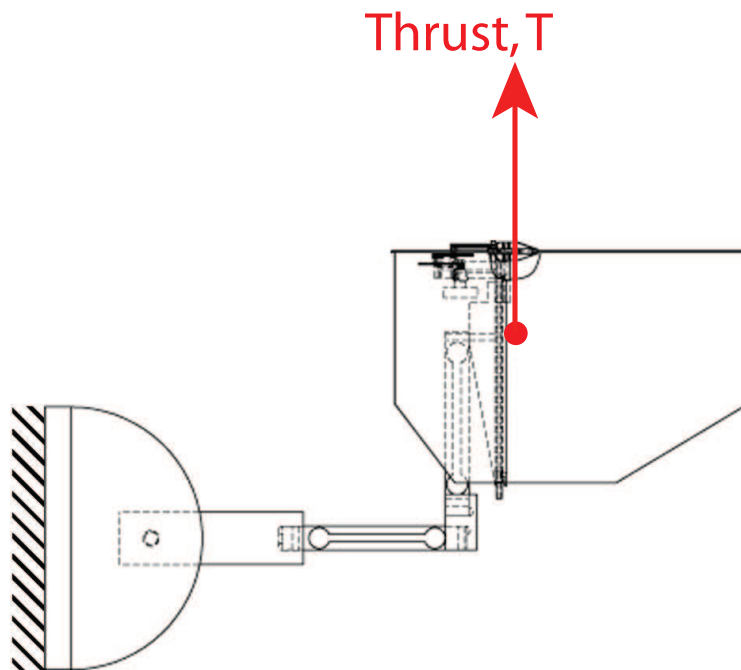


Figure 3.15: Experimental apparatus in hover conditions

New crank-shaft mechanism

The wing kinematics are strongly related to the crank-shaft mechanism that is driving the leading edges. The performance and efficiency of the crank-shaft is therefore of great importance and has a major influence on the performance of the DelFly itself. From the beginning of DelFly, a crank-shaft mechanism is used. It has always been made by hand and changed several times through the different versions of DelFly. During this thesis research a new type of crank-shaft mechanism is designed for better performance.

In section 4.1 the shortcomings of the old type of crank-shaft mechanism are discussed. Next, the different components of the new mechanism are discussed in section 4.2. After that, a weight breakdown is presented in section 4.3. Finally, a comparison between the old and new mechanism is presented in section 4.4.

4.1 Shortcomings in the old DelFly II crank-shaft mechanism

When DelFly was created in 2005, a driving mechanism was designed, based on a crank-shaft principle, see figure 2.9. This design was redesigned for the next generation, DelFly II (see figure 2.10). The DelFly II mechanism is driven by a motor which is connected through a two-stage gear set in order to have an advantageous gear ratio. Two metal crank-shafts are mounted onto the main gear on which two push rods are positioned. The push rods are connected to the hinges, which push and pull the leading edges and therefore the wings. The gearbox is a sandwich construction of a balsa core and a carbon fiber skin for lightweight and strength.

The gearbox is CNC machined, hinges are rapid prototyped and the gears are of the shelf. Nevertheless, some components such as the cranks and push rods are built by hand, therefore variation is observed between different sets of mechanisms. Consequently, one mechanism can perform better than the other, depending on the builder, wear of pushrod linkage, asymmetry due to unequal length of pushrods and not-in-line cranks.

One can understand that building this kind of mechanism by hand is an intense work and the amount of effort that is put into it, is not always proportional with the efficiency.

Another downside of this mechanism is that the forces have to be transferred across two perpendicular planes. The plane in which the gears are positioned is perpendicular to the plane in which the leading edges are moving. The push rods transfer the force from one plane to another by moving in both planes. This transfer of forces in perpendicular planes is not beneficial for the efficiency of the system.

The next section will introduce a new kind of crank-shaft mechanism in order to overcome the shortcomings that are discussed.

4.2 New crank-shaft mechanism

Figure 4.1 shows the different components of the mechanism in order to get acquainted with the terminology of the system.

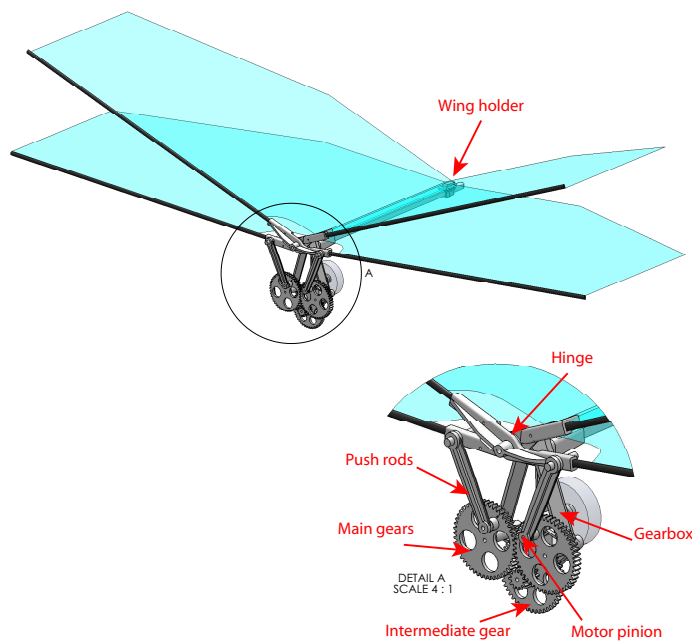


Figure 4.1: Representation of the new crank-shaft mechanism.

4.2.1 Improvements

Several aspects are improved with respect to the old mechanism:

1. The mechanism is fully symmetrical.
2. Injection molding technique is used for fabricating most of the parts. For this technique molds are constructed and then injected with a material in liquid form

which hardens when it cools down. This technique avoids imperfections in the parts. In addition, the assembly time of the crank-shaft mechanism is reduced drastically.

3. Two different hinge components are used for the old mechanism, an inner hinge and an outer hinge. The new mechanism has only one type of hinge, which is used for both wings. It is an advantage to use only one type of hinge because this reduces manufacturing costs and complexity of the system.
4. Forces are not transferred from one plane to a perpendicular plane. All forces are now in parallel planes, which is more efficient. This means more energy is left for flapping.
5. The total mass of the new system is less than the total mass of the old system. This means that less power is needed to keep the Delfly in the air so more power is left for flying and hovering. A weight breakdown can be found in section 4.3 at the end of this chapter.
6. Little or no glue has to be used. This reduces the weight as well.
7. The connection to the fuselage is integrated in the gearbox. In addition, an upside-down T-shape is connected to the gearbox, which holds the wing to the fuselage. This cancels out the carbon rod that had to be used before in order to keep the wing fixed and smooth.
8. The motorhousing is integrated in the gearbox for weight benefit.

Each of these improvements are discussed in more detail in the next sections together with a detailed description of the different components. An illustration of the new crank-shaft mechanism is given in figure 4.1.

4.2.2 Gear ratio

The gear ratio (GR) is the relation between the number of teeth of two connected gears. The gear ratio of the old mechanism is calculated as follows: The motor pinion has 12 teeth and is connected to the second gear which has 48 teeth. The gear ratio of these two gears is therefore $\frac{48}{12} = \frac{4}{1}$. The second gear has a pinion of 12 teeth that is connected to the main gear which has 60 teeth. The gear ratio of these two gears is $\frac{60}{12} = \frac{5}{1}$. These two separate gear ratios are combined into an overall gear ratio:

$$GR_{old} = \frac{48}{12} \cdot \frac{60}{12} = 20 \quad (4.1)$$

Because of different types of gear connections, size restrictions of the gears and because the size of the gears is proportional to the number of teeth, this gear ratio is slightly different for the new crank-shaft mechanism:

$$GR_{new} = \frac{48}{9} \cdot \frac{48}{12} = 21.33 \quad (4.2)$$

A gear ratio of 21.33 means that the motor pinion has to turn 21.33 revolutions in order to turn the main gear for one revolution.

More or less the same gear ratio is used for the new crank-shaft mechanism because of motor properties. The motor operates at the required voltage and power of around 18,000 rpm or 300 Hz. The required flapping frequency is around 15 Hz. Consequently the gear ratio is around $\frac{300}{15} = 20 : 1$.

Another difference between the two mechanisms, is the type of crank-shaft. The old mechanism has a double crank mounted on the main gear. The new mechanism is equipped with two counter rotating main gears. Each gear drives one push rod, see figure 2.10 and figure 2.12.

Illustrations of both gear combinations are shown in figures 4.2 and 4.3.

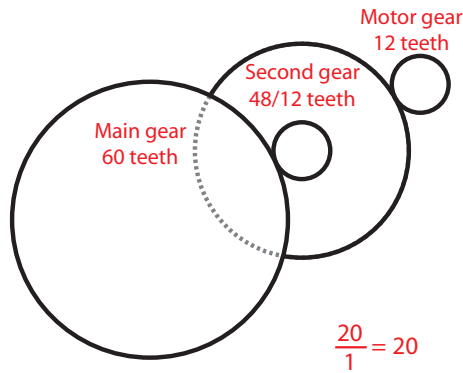


Figure 4.2: Illustration of the old gear mechanism with a gear ratio of 20.

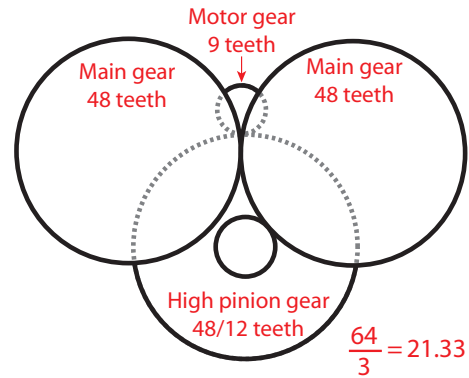


Figure 4.3: Illustration of the new gear mechanism with a gear ratio of 21.33.

4.2.3 Manufacturing of the different components

In this section the different components of the new driving mechanism are discussed in detail. The gearbox, main gears, hinge, push rods and wing holder are manufactured by PROMOLDING, a company located in The Hague and specialized in design and development of new products. 3D-CAD models are drawn and supplied to PROMOLDING. They were responsible for building the molds for the different components and the manufacturing of the different components. The intermediate gear, the motor pinion and the different steel rivets for fixing the components are obtained from DIDEL (*Didel* [2010]).

Most of the PROMOLDING parts are made of Poly Carbonate (PC), which is a strong and stiff thermoplastic. The density is between 1.20-1.24 g/cm^3 . Initially, the gears were also made out of PC but as they were a little too big. Changing the material to Polyxymethylene (POM) made it possible to keep the molds. POM has more crimp than PC but is less accurate. POM however has better wear properties than PC. The technical drawings of the different parts can be found in appendix C. The different specifications of the materials used in this section are obtained from PROMOLDING (*Promolding* [2010]).

Gearbox

The gearbox (figure 4.4) is the base of the crank-shaft mechanism. All the other components are mounted onto this single component. The gearbox is symmetrical apart of the hole where the intermediate gear fits in. The intermediate gear has to drive only one main gear and can not touch the other main gear (This can also be seen in figure 4.9 further in this chapter).

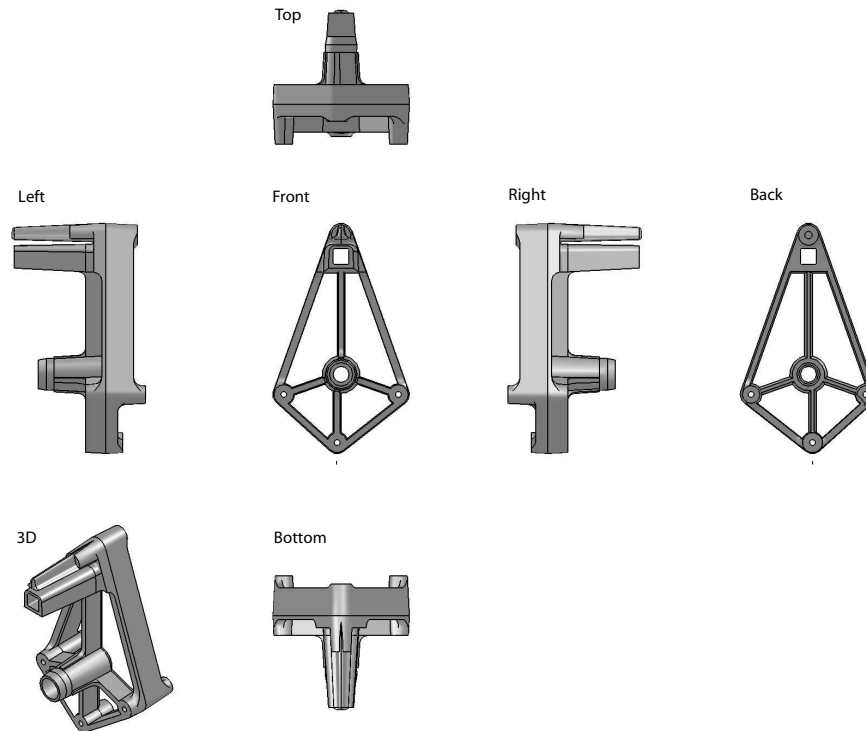


Figure 4.4: Gear box drawings. The exact dimensions can be found in appendix C.

The most important properties of this gearbox are the distances between the different holes for the rivets of the gears. The distance between two of these holes determines the distance between two gears. In order to calculate this distance, one has to know the number of teeth and the module of the gears. Equation 4.3 shows the relation between these parameters.

$$x = \frac{n1 + n2}{2} \cdot m + 0.03 \quad (4.3)$$

Here, x is the distance between the two axes of both gears in millimeter, $n1$ and $n2$ are the number of teeth of both gears. The 0.03 mm is a small extra clearance for smooth rotation (*Didel [2010]*). m is the module, which is 0.3 for all gears in this system, a unit of relative size of a gear. m is the ratio of the reference diameter, d of the gear divided by the number of teeth, n , see equation 4.4.

$$m = \frac{d}{n} \quad (4.4)$$

The distance between the motor pinion and the intermediate gear, x_1 , between the intermediate gear and the first main gear, x_2 , and between the first main gear and the second main gear, x_3 can be found in respectively equation 4.5, 4.6, 4.7.

$$x_1 = \frac{n_1 + n_2}{2} \cdot m + 0.03 = \frac{9 + 48}{2} \cdot 0.3 + 0.03 = 8.58mm \quad (4.5)$$

$$x_2 = \frac{n_1 + n_2}{2} \cdot m + 0.03 = \frac{12 + 48}{2} \cdot 0.3 + 0.03 = 9.03mm \quad (4.6)$$

$$x_3 = \frac{n_1 + n_2}{2} \cdot m + 0.03 = \frac{48 + 48}{2} \cdot 0.3 + 0.03 = 14.43mm \quad (4.7)$$

Another important feature of the gearbox is the motorhousing, which is the cylinder where the bearings of the motor axis fit into. A normal motor that is used for DelFly contains this cylinder with bearings on its own. Here, the cylinder of the motor is omitted and replaced by an integrated part in the gearbox. A cross section of this motorhousing can be found in figure 4.5 and in appendix C, figure C.2 for the exact dimensions. The two bearings fit exactly in the front and the back of the motorhousing while the stator is placed around the back of the motorhousing. Both the bearings and stator are glued with superglue. After that, the rotor can be placed inside the bearings. As one can see in figure 4.5, taper is added to the motorhousing, this is done for manufacturing reasons. The component is not able to come out of the mold if no taper is applied.

When assembling the crank-shaft mechanism, first glue the bearings in the motorhousing, followed by insertion of the stator. If this is done the other way around, the bearing does not fit nicely into the cavity and the motor axis is not straight.

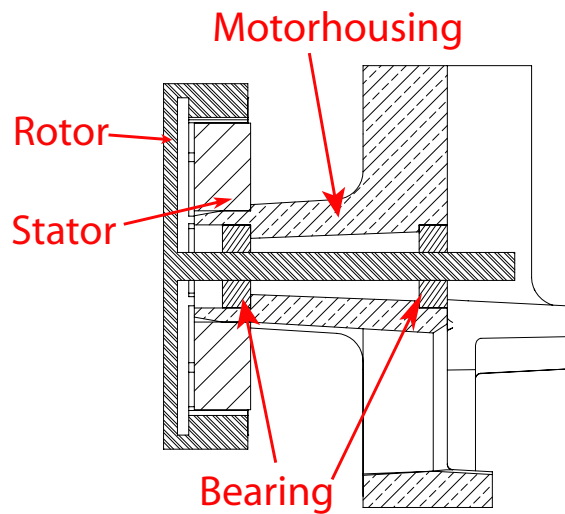


Figure 4.5: Cross section of the motorhousing together with the rotor, stator and bearings of the motor. The exact dimensions can be found in appendix C.

On top of the gearbox there are two 'pins' sticking out. A squared carbon rod can be put into the squared-shaped pin. This carbon rod functions as a fuselage. The electronics and the tail are glued onto this fuselage. The second pin in the form of an upside-down T-shaped is present for restraining the wing. This wing fits nicely between the squared-shaped pin and the T-shaped pin. If this pin was not there, no tension can be placed in the wing during flapping.

Motor pinion

The motor pinion is the gear that rotates on the axis of the rotor of the motor. It is a standard nine-teeth motor pinion, G309-097 from DIDEL (*Didel* [2010]), which is a small, module 0.3 gear with length 3.5 mm and bore diameter of 0.97 mm made out of POM.

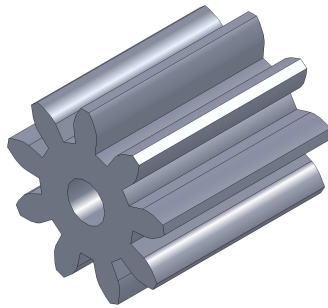


Figure 4.6: Motor pinion drawing. The exact dimensions can be found in appendix C.

Intermediate gear

The intermediate gear is the gear that is driven by the motor pinion, see figure 4.7. It is a custom made gear, designed by DIDEL that is based on the standard G348L gear (*Didel* [2010]) but the pinion is lengthened. DIDEL doubled the length of the pinion from 2.0 mm to 4.0 mm because the normal length was not high enough in order to touch the main gear in the design of the new DelFly II crank-shaft mechanism.

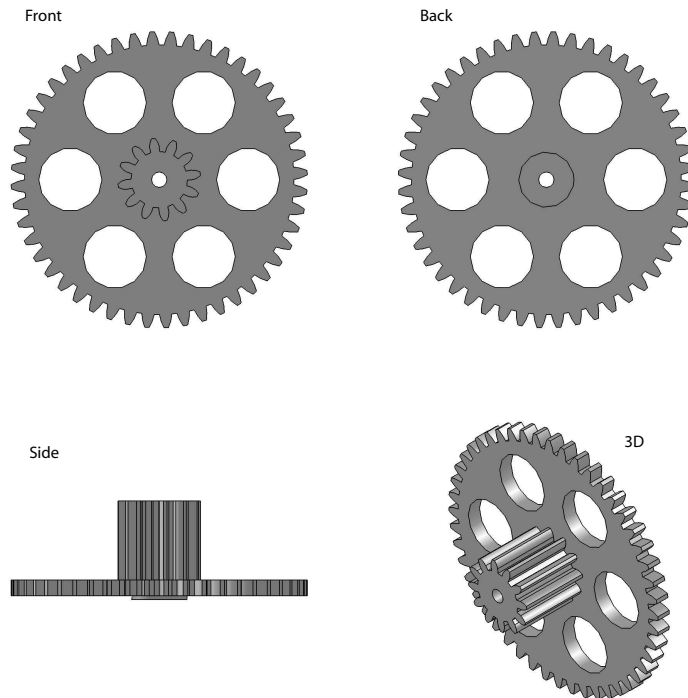


Figure 4.7: Intermediate gear drawings. The exact dimensions can be found in appendix C

Main gear

The main gear forms the crank and is responsible for pushing and pulling the push rods up and down. If the main gear turns for one revolution, one flap cycle has passed. One of the main gears also contains the magnet that triggers the Hall-sensor for counting the revolutions during testing.

The design of the main gear (figure 4.8) is, just like the intermediate gear, based on the standard G348L gear from DIDEL but manufactured by PROMOLDING. The diameter, the module and therefore also the number of teeth is the same. The pinion of the G348L gear is left away. Gears can vibrate and deform due to the high forces of pushing and pulling. This vibration can lead to slippage of the gears. To reduce the likelihood of this slippage, the thickness of the teeth is changed from 0.8 mm to 1.5 mm. The inside of the gear is not thickened to reduce weight. In order to withstand the forces some stiffeners

are applied to the back of the gear. They form a cross and extra stiffeners are placed at the hole for the push rod connection. The four holes are there for weight saving.

Both left and right main gear are the same. It is important that the main gears drive the push rods in a symmetrical way. Therefore, the hole for the push rod connection has to be exactly in line with the center and the middle of the flank of a teeth. The left and the right (which is the same as the left) main gear can be placed in such a way that the centers of both gears and the holes of the push rod connection are exactly in line two times per flap cycle. A droplet-like indicator is placed on the gear to visualize which teeth have to connect to each other, see figure 4.9.

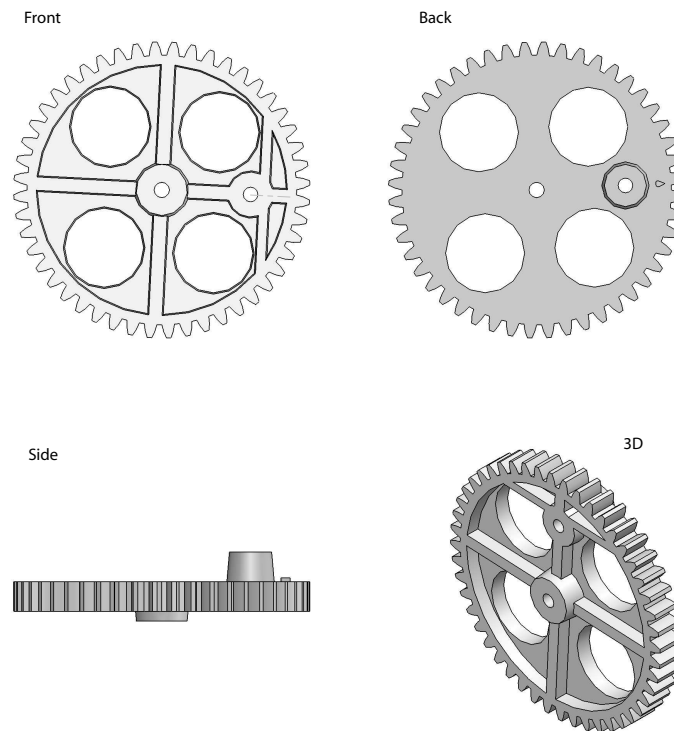


Figure 4.8: Main gear drawings. The exact dimensions can be found in appendix C.

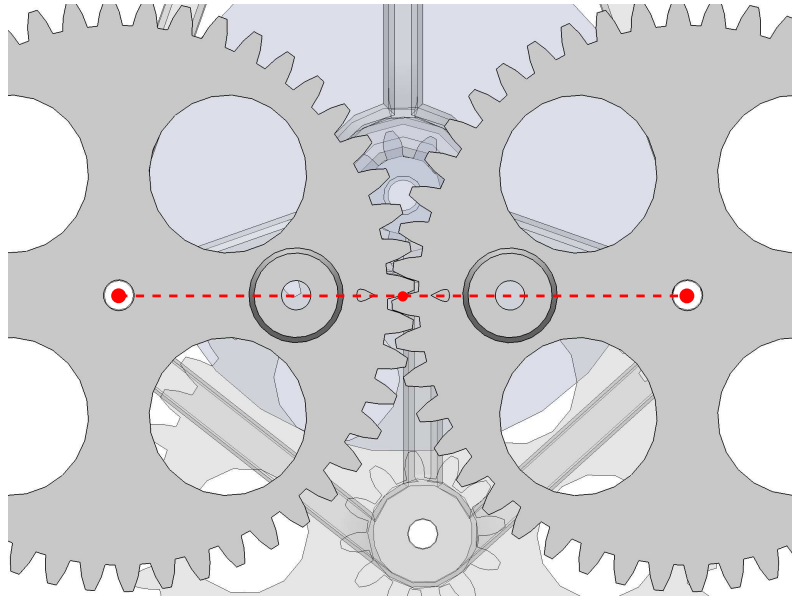


Figure 4.9: Detail of the main gear.

Push rod

The push rod, see figure 4.10, is the component that is responsible for transforming the rotation of the gears into a lateral movement of the hinges. The push rod is basically a bar that has two loose fits with both the hinge and the main gear. The cross-area of the rod is cross-shaped which gives the push rod good resistance for bending. From the middle to the small end, taper is applied for weight reduction. The length of the push rods is determined in SolidWorks such that the system is able to function. The length of the push rods has to be in such a way that when the main gear makes one complete revolution, the hinges travel one cycle from an amplitude of 0° to 44° and back to 0° . If the push rod is too short, angles close to 0° and 44° can not be reached which results in less lift generation. If the push rod is too long angles smaller than 0° and larger than 44° are be reached which will cause the system to choke. The optimal length (from axis to axis) of the push rod is 17.18 mm, see appendix C.

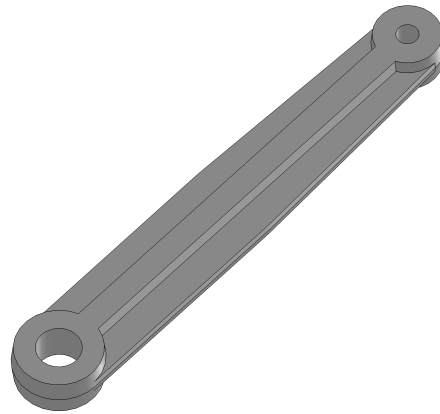


Figure 4.10: Push rod drawings. The exact dimensions can be found in appendix C.

Hinge

The hinges of the previous crank-shaft mechanism are made with a technique called Rapid Prototyping (RP). This technique is used for manufacturing components in small numbers, which is good for this project because small numbers are needed. However, the material from which the hinge is made with this process, is very sensitive to UV radiation. After a while the material starts to discolor and becomes brittle. Due to the high forces that act on the root of the leading edges and on the hinge itself, it can easily break. PC will be a better material to withstand UV light and the high forces.

The geometry of the hinge drastically changed. The two old hinges are two different hinges, an inner hinge and an outer hinge, where the outer hinge was placed around the inner, see figure 4.11. Now the two hinges are exactly the same. One hinge will fit perfectly over the other if this one is rotated for 180° , see figure 4.12.

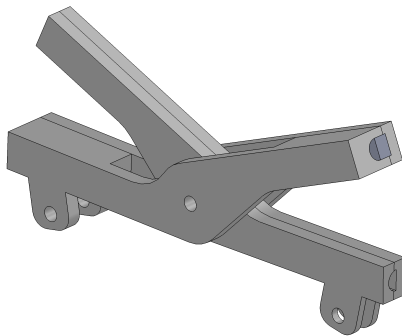


Figure 4.11: Inner and outer hinge of the old mechanism.

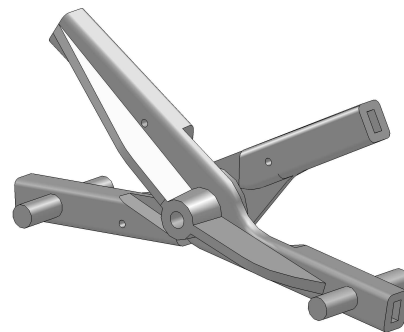


Figure 4.12: Symmetrical hinge of the new mechanism.

Figures 4.11 and 4.12 show that there are even more differences besides the symmetry of both hinges. The connection for the push rods is now on top of the hinge, this means that there is no lateral distance between the location of the leading edge in the hinge and the connection with the push rod which is a better for the energy transfer. The push rod

is kept in place by heating up the end of the small cylinder of the hinge, the PC melts a bit at the end of the cylinder and the diameter will become slightly bigger in such a way that it is impossible for the push rod to fall off. The shafts where the leading edges go into, are tapered and rectangular instead of straight and D-shaped. The reason that the shaft is rectangular is because of the symmetry. The D-shaped leading edges have to fit in both ways. The taper of the shaft is there for manufacturing reasons. In order to fabricate such a small shaft, a steel pin is inserted into the mold. If this pin is straight it is impossible for the pin to come loose. The taper prevents this. The drawback of this tapered shaft is that the leading edges have to be sanded on one side in order to fit into the shaft. The leading edge is fixed with superglue. If there is too much glue, it can escape from the small hole which is drilled in the shaft. The two ribs on both sides of the main axis of the hinge are there to make the whole component stiffer so it would not break under the high forces. They are also tapered for the same manufacturing reasons.

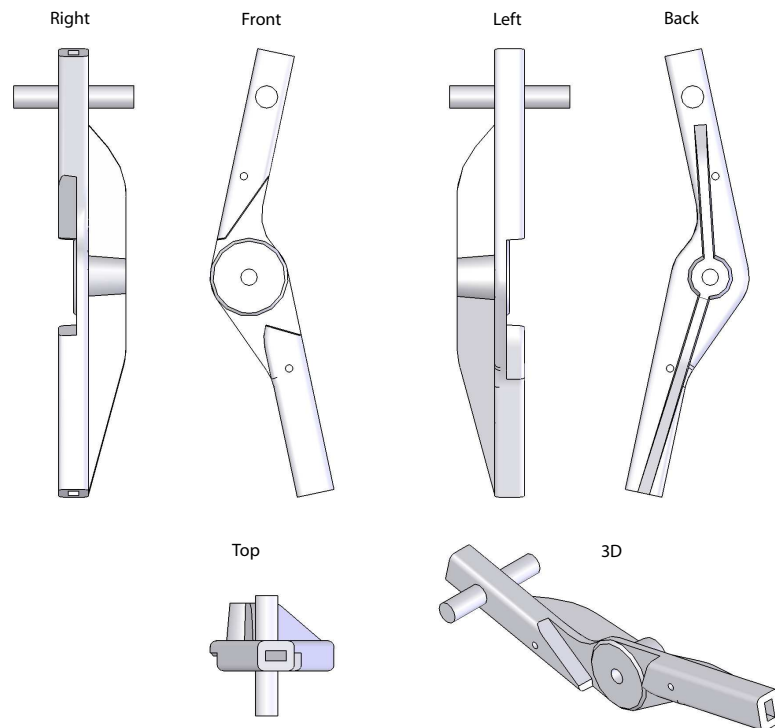


Figure 4.13: Push rod drawings. The exact dimensions can be found in appendix C.

Different rivets

The gears and push rods are kept in place with steel rivets. The rivets connect different components with push fits and loose fits. A push fit means that the two components can not move relative to each other. A loose fit means that the components can pivot, but they keep connecting while the system is working. There are three different kind of rivets.

1. The rivet that connects the hinges to the gearbox. The fit is loose at the hinges and a push fit is used at the gearbox, see figure 4.14(A).

2. The rivet that connects the gear with the high pinion to the gearbox. The fit is loose at the gear and a push fit is used at the gearbox, see figure 4.14(B).
3. The rivets that connects the main gear to the gearbox. The fit is loose at the main gears and a push fit is used at the gearbox, see figure 4.14(C).
4. The rivets that connects the push rods to the main gears. This is the same rivet as in (3). The fit is loose at the push rods and a push fit is used at the main gears, see figure 4.14(C). This rivet has to be cut to the exact length after assembly.

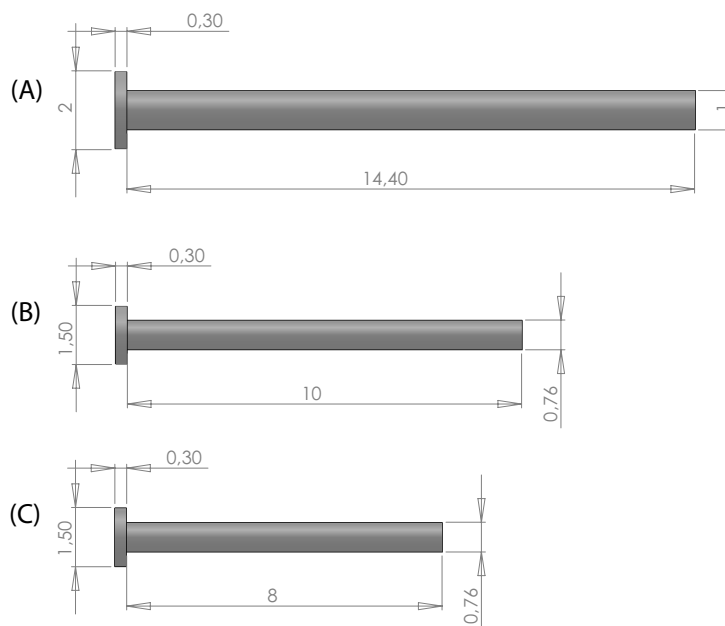


Figure 4.14: Dimensions of the steel rivets (see also appendix C).

For a push fit, the diameter of the hole has to be 0.01 mm smaller than the diameter of the rivet. For a loose fit, the diameter of the hole is 0.025 mm bigger than the diameter of the rivet. These values are according to *Didel* [2010]. For the connection between the hinge and the gearbox, the dimensions are 0.05 mm and 0.1 mm because of design restrictions. These last dimensions seem to be too large in the first prototypes. Further adjustments are necessary. Table 4.1 gives an overview of the different dimensions for a loose and push fit.

Connection	Diameter loose fit [mm]	Diameter push fit [mm]	Type of rivet
Hinge - Gearbox	1.100	0.950	(A)
Main gear - Gearbox	0.780	0.745	(C)
Intermediate gear - Gearbox	0.780	0.745	(B)
Push rod - Main gear	0.780	0.745	(C)

Table 4.1: Diameter overview for loose and push fits.

Wing holder

The wing holder, see figure 4.15, is a component that holds the middle of the trailing edge of the wings in a fixed position. This is important to keep the tension in the wing during flapping. When the old mechanism was used, the tension was kept in the foil by means of a small carbon rod that was positioned in the middle of the wing from leading edge to trailing edge. This carbon rod was fixed in place with glue. Now, the small wing holder replaces this function of the carbon rod. The wing holder is pushed over a hollow squared carbon rod (the fuselage), the hook of the wing holder hooks through a small hole in the foil at the middle of the trailing edge. Taper is applied for manufacturing reasons.

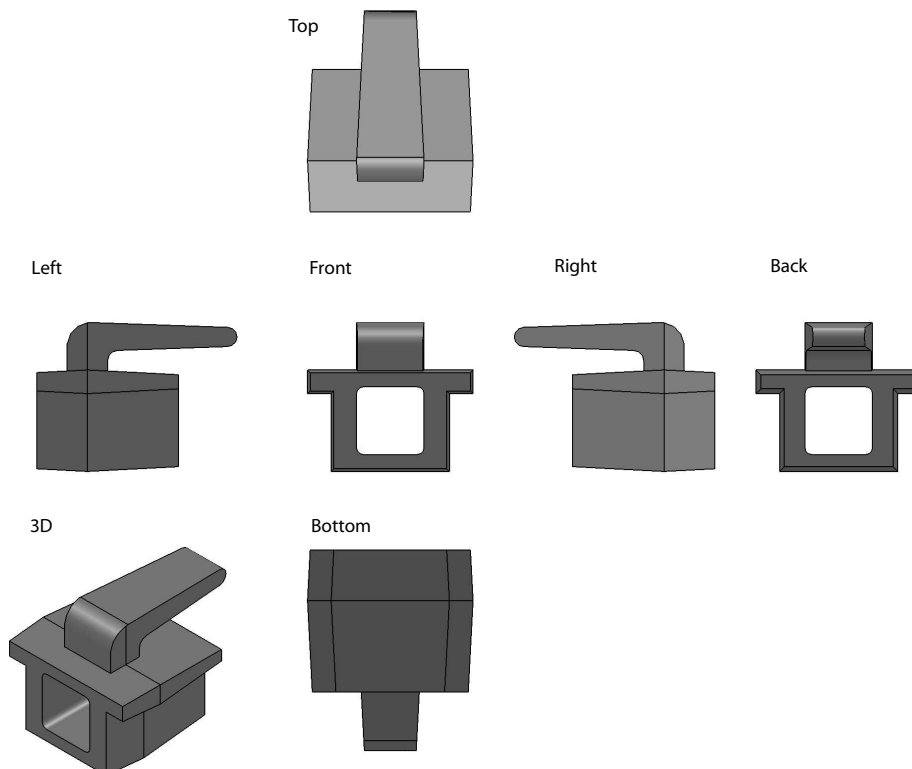


Figure 4.15: Wing holder drawings. The exact dimensions can be found in appendix C.

4.3 Weight breakdown

A final advantage of the new crank-shaft mechanism is the weight reduction with respect to the old crank-shaft mechanism. Due to the accurate manufacturing process, the use of PC and a minimum usage of glue, the new crank-shaft mechanism weights almost 2 g less than the old mechanism, which is a reduction in weight of 35%. Table 4.2 gives a comparison between the old mechanism, the prediction of the SolidWorks model with a density of 1.24 g/cm^3 for PC and the actual new mechanism. One can see that the prediction of the SolidWorks model is very accurate, up till 2%.

Component	Old mechanism model [g]	New mechanism SolidWorks model [g]	New mechanism Measured [g]
Gearbox	0.2	0.743	0.778
Hinge x2	1.1	0.436	0.444
Main gear new x2	n.a.	0.342	0.372
Main gear,second gear and motor pinion old	0.33	n.a.	n.a.
Intermediate gear	n.a.	0.160	0.164
Motor pinion	n.a.	0.022	0.022
Push rod x2	0.3	0.126	0.132
Rivet hinge	0.102	0.102	0.102
Rivet main gear new x2	n.a.	0.068	0.068
Rivet main gear with crankshaft	1.64	n.a.	n.a.
Rivet high pinion	n.a.	0.048	0.048
Rivet second gear	0.034	n.a.	n.a.
Rivet push rods	0.15	0.05	0.05
Motor:	1.63	1.362	1.362
↔ Stator	0.474	0.474	0.474
↔ Rotor	0.824	0.824	0.824
↔ Bearings x2	0.064	0.064	0.064
↔ Cylinder	0.268	n.a.	n.a.
Total	5.486	3.461	3.542

Table 4.2: Comparison of weight breakdown between old mechanism, the SolidWorks model and new mechanism.

Some notes have to be taken into account:

1. Note that the weight of the wing holder (0.05 g) is not taken into account because it is not part of the actual driving mechanism.
2. The weight of the rivets for the SolidWorks prediction is the actual weight of the rivets.
3. The weight of the motor for the SolidWorks prediction is the actual weight of the motor.

4.4 Comparison between old and new mechanism

In order to compare both mechanisms for their performance, a test is done. This test involved measuring two different wings on both mechanisms. In figure 4.16 the performance plots can be seen of these tests. The measurement points are mean values over a flapping time interval of 10 seconds. Table 4.3 shows the different cases with their mean thrust-to-power ratio. The color of the lines shows the different mechanisms. It can be seen that the difference in thrust is rather low. This will be discussed in chapter 5 when the different sets of wings are discussed. The difference between the mechanisms is found in the power. It can be seen that the old mechanism uses more power than the new mechanism. From the thrust to power plot one can see that the new mechanism performs better for both wings. When doing measurements on Wing1, the gain in thrust-to-power ratio is 21%. For Wing2 this gain is 19%. It can be stated that the gain in thrust to power performance due to the mechanism is **20%**.

Line type	Case	Mean Thrust/Power [N/W]
Dotted red line	Wing1 on old mechanism	$7.24e - 2$
Solid red line	Wing2 on old mechanism	$7.67e - 2$
Dotted green line	Wing1 on new mechanism	$8.79e - 2$
Solid green line	Wing2 on new mechanism	$9.12e - 2$

Table 4.3: Overview of different cases when comparing the old and new mechanism

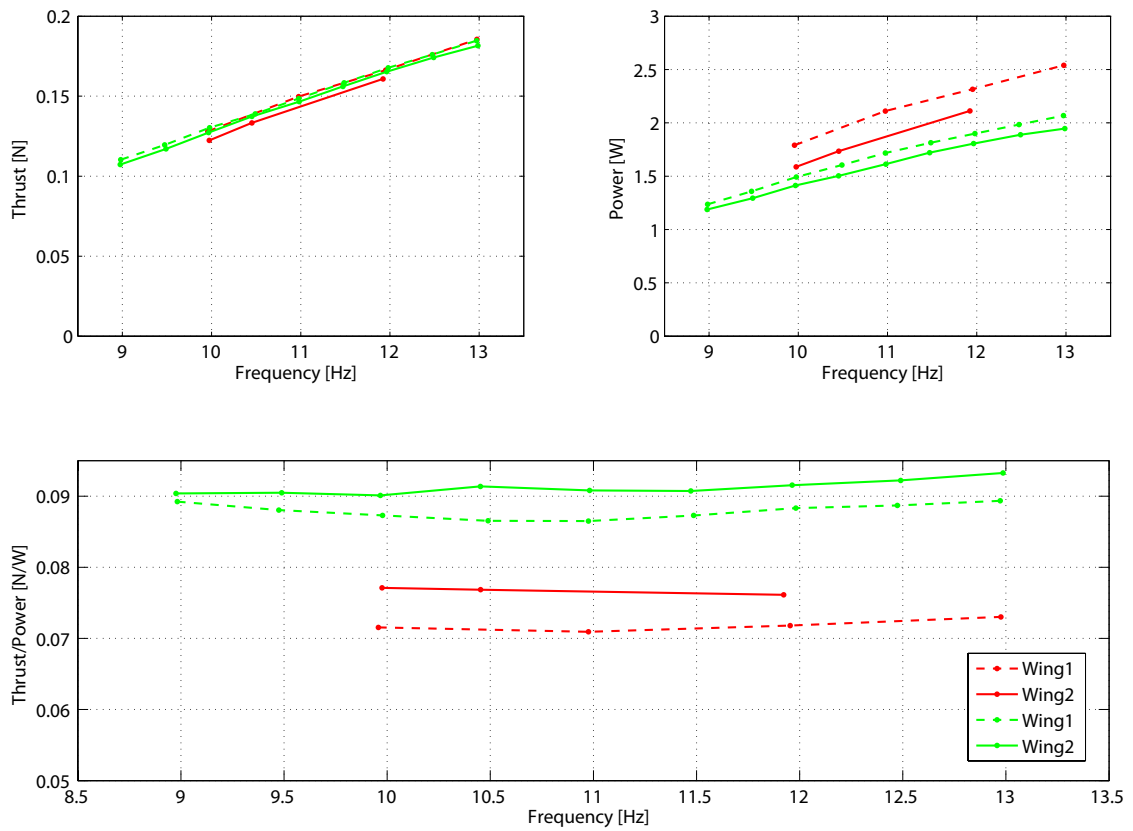


Figure 4.16: Performance plots of the comparison between old and new mechanism. The red lines represent two different wings on the old mechanism. The green line represent the same wings on the new mechanism

Results and discussion of wing study

This chapter will inform the reader about the different tests that are performed in order to obtain a better wing for DelFly II. In section 5.1, the raw data that comes out of the DelFlyControl program is analyzed. Furthermore, the way of obtaining usable data is discussed in more detail. The accuracy of the measurements is explained in this section as well. The actual steps that are taken in order to create a new and improved wing are explained by means of performance plots in section 5.2. Additional tests are performed to get a better understanding of the new wing performance in section 5.3. To conclude this chapter an overall gain in performance and the influence on the flight time is discussed in section 5.4.

5.1 Raw data processing

The raw data of one particular wing is logged in a *.log* file per measured flapping frequency. These files contain ten columns and every column contains data which is presented in table 5.1. This information, however, can not be used directly for performance measurements because of noise in the data. The actual performance plots use mean values over several flap cycles which have to be calculated from the raw data. Furthermore, due to external effects there is a standard deviation in the measurements which have to be taken into account. The next sections will explain these different issues.

5.1.1 Noise filtering

Figure 5.1 shows a plot of the raw (blue) and filtered (red) thrust data during one flap cycle when flapping at 13 Hz. The filter that is used, is a standard Matlab low pass filter with a cut-off frequency of two times the flapping frequency, 26 Hz.

This filtering is not used for the calculation of the mean values. It is only used to show an indication of the thrust generation in one flap cycle. For information about the thrust generation in one flap cycle can be found in the thesis report of Mark Groen (Groen [2010]).

Parameter	Unit
Computer time	[sec]
Force sensor 1	[V]
Force sensor 2	[V]
Force sensor 3 (not used)	[V]
Voltage	[V]
Current	[mA]
Flapping frequency	[Hz]
Throttle	[-]
Motor counter	[-]
Hall sensor counter	[-]

Table 5.1: Parameters of the *.log* file.

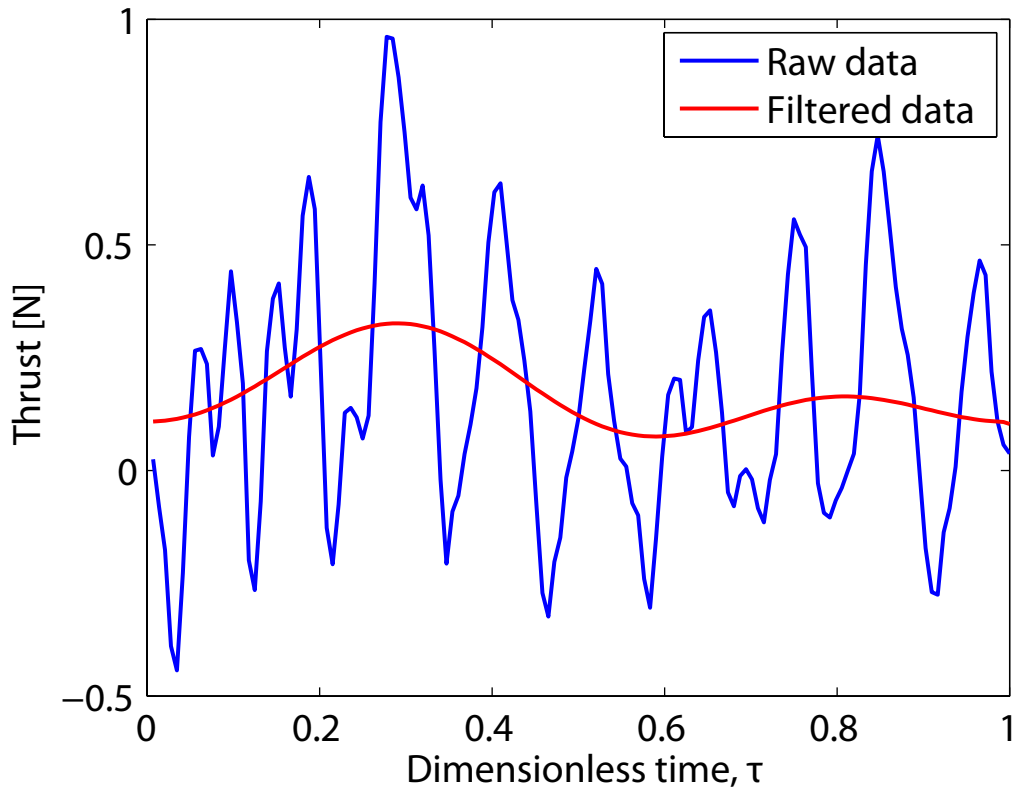


Figure 5.1: Thrust plot of both the raw (blue) and filtered (red) data of one clap cycle at 13 Hz.

5.1.2 Mean value calculation

The actual performance measurements are done with mean values of thrust, current and voltage. These main values are calculated for flapping frequencies between 10 Hz and 14 Hz over a time interval of 10 seconds. A frequency domain of 10 Hz - 14 Hz is chosen because DelFly is able to hover in this domain and it gives a nice spread to show what happens close to the hovering frequency. This hover frequency fluctuates around 12 Hz -

13 Hz depending on the weight of the DelFly and the type of wing.

In order to obtain the mean values of thrust, current and voltage, a Matlab program is written. This program makes *.dat* files per wing which contain the mean data for each measured frequency. The flow diagram of this program is presented in figure 5.2 and works as follows:

1. Enter the number of different wings that are evaluated
2. Read the first wing and enter the number of frequencies that have to be evaluated
3. Read the first frequency
4. Search file in database with corresponding wing name and frequency
5. Find maximum Hall count for throttle $\neq 0$. When the throttle is equal to zero it means that the model is not flapping. When searching the maximum Hall count for throttle is not equal to zero, the last complete flap cycle will be found.
6. Count 10 seconds from maximum Hall count. Here the time domain is captured for which the mean values are calculated. The counting is done backwards from the latest flap cycle on. This is done because the DelFly does not instantly starts to flap at the desired flapping frequency, it takes a couple of seconds. Therefore, if the measured time domain is large enough (circa 20 seconds) one can be sure that the time domain for which the mean values are calculated (10 seconds) is always at the desired flapping frequency when measuring from the latest flap cycle.
7. Mean values for thrust, current and voltage are calculated for the 10 seconds time interval. Thrust is measured in volts (strain gauges), current and voltage are respectively logged in milliamperere and volts.
8. The calculated mean values are temporarily saved in the computer memory.
9. If the loop number is smaller than the number of frequencies in step 2, step 3 will be resumed until the loop number is equal to the number of frequencies.
10. If the loop number is smaller than the number of wings in step 1, step 2 will be resumed until the loop number is equal to the number of wings.
11. All the data is saved in a *.dat* file per type of wing.

In order to obtain performance plots the thrust and power have to be calculated from the mean values. This is done as follows:

Thrust The thrust that is measured is measured in volts by the strain gauges. In order to convert this to Newtons, the measured value has to be multiplied by the calibration factor, 0.002 kg/V of the instrumentation amplifier (see chapter 3) and by 9.81 m/s^2 , see equation 5.1.

$$T = 0.002 \cdot 9.81 \cdot V_{thrust} \quad (5.1)$$

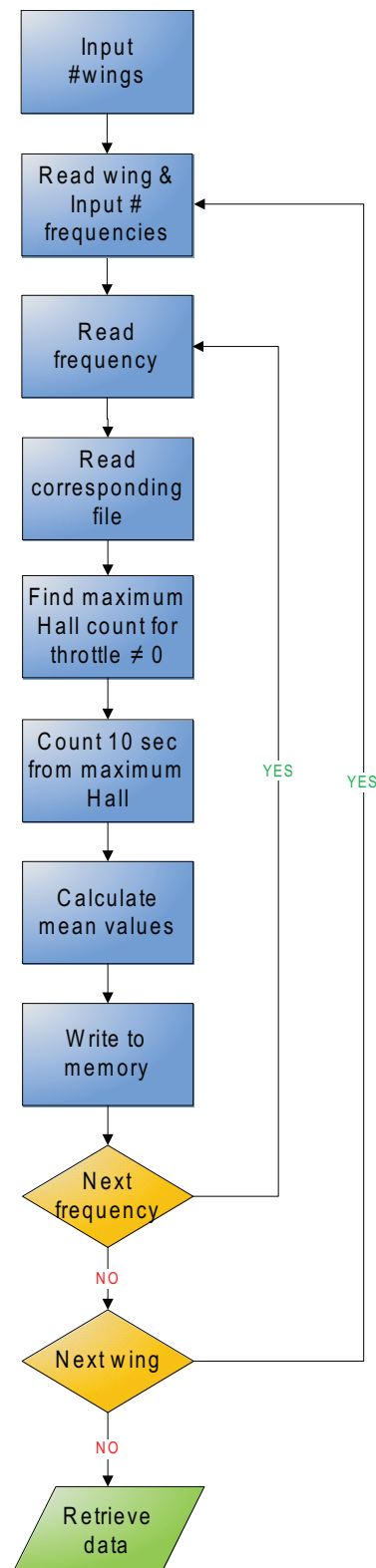


Figure 5.2: Program flow diagram.

Power The power can be obtained by applying Joule's law, see equation 5.2. In order to obtain the power in watt, Joule's law has to be divided by 1000 because the current is measured in milliampere.

$$P = \frac{I_{measured} \cdot V_{measured}}{1000} \quad (5.2)$$

Because both thrust production and power consumption are important during these tests, the driving parameter is the ratio of these two; the thrust-to-power ratio, T/P. The higher this ratio, the better the performance of the wing.

5.1.3 Accuracy of the measurements

The measurements contain small measurement errors because of different external factors. The different errors and their significance in the measurements will be explained in this section.

1. **Error due to resolution of the experimental set-up:** The resolution of the ADC of the micro-controller board results in a maximum error of **0.002 N**. This is explained in chapter 3.
2. **Error due to different air pressure:** Due to the fact that the wings are measured on different dates, there is a difference in air pressure. It is logic to assume that the thrust for flapping wings is directly proportional to the density of the air in analogy to the conventional lift formula, see equation 5.3 (J. D. Anderson [2001]).

$$T = \frac{1}{2} \rho V^2 C_T A \quad (5.3)$$

Here, T is thrust in *N*, ρ is the air density in kg/m^3 , V is the air speed in m/s , C_T is the dimensionless thrust coefficient and A is the wing area in m^2 . The density is directly proportional to the pressure, see the equation of state, equation 5.4 (J. D. Anderson [2001]).

$$p = \rho R T \quad (5.4)$$

Here, p is the air pressure in *Pa*, R is the specific gas constant. For air R is equal to 287 J/(kgK). T is the temperature in *K*.

Therefore, air pressure, p is directly proportional to the thrust generation. In order to cancel the effect of air pressure out of the measurements one can divide the thrust by the measured pressure, p and multiply it by the standard sea pressure, $p_0 = 1013.25 \text{ hPa}$ (J. D. Anderson [2001]):

$$T' = T \frac{p_0}{p} \quad (5.5)$$

Furthermore, it is assumed that the temperature stays constant in the testing room over the different days.

Figure 5.3 shows the correction of the measured data points (blue). The corrected values are presented with red dots and the green line represents a linear fit through the corrected points. The linear fit has a slope of $-8.3e-5 N/sample$. This is almost a constant line which indicates that the influence of air pressure is canceled out of the measurements. The small decay is probably due to the aging of the system. This will be discussed further in section 5.3.2 of this chapter.

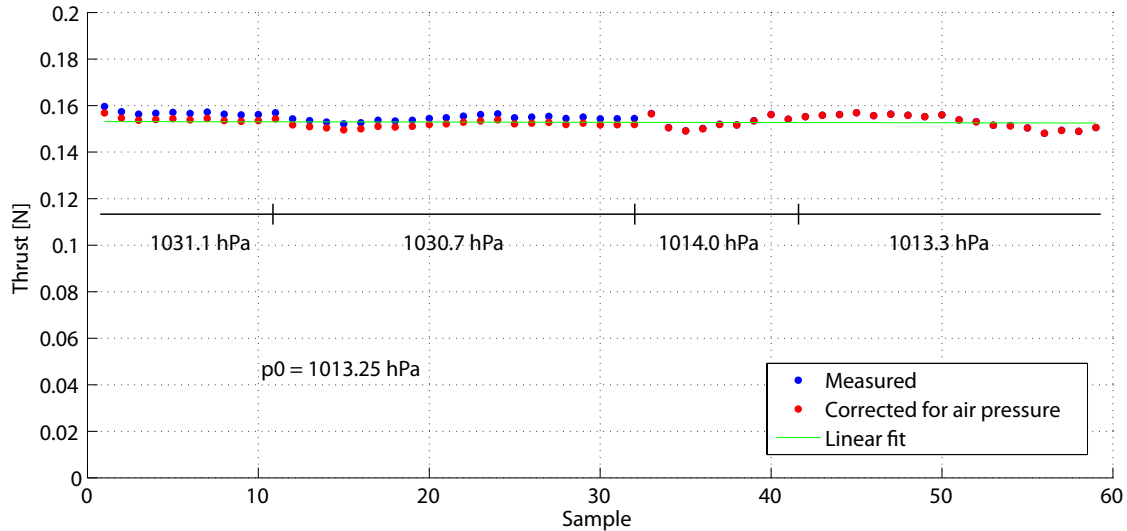


Figure 5.3: Measured thrust points (blue) are corrected for air pressure (red). The linear fit (green) through the corrected values has a slope of $-8.3e-5 N/sample$. Flapping frequency is set to 12 Hz.

It can be assumed that the power is also influenced by the air pressure. However, figure 5.4 shows that this difference can be neglected. The slope is equal to $-4.7e-5 W/sample$ and in the same order as the slope of the thrust which can be dedicated to the aging.

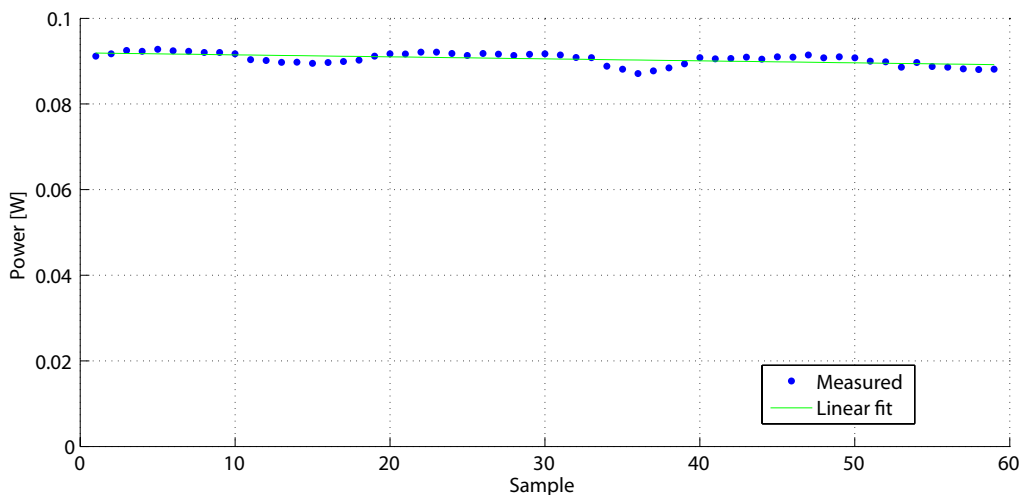


Figure 5.4: Measured power points (blue). Linear fit (green) has a slope of $-4.7e-5 W/sample$. Flapping frequency is set to 12 Hz.

3. **Assembly errors:** There are different kinds of assembly errors which can not be quantified at this point. These errors are due to:

- Different insertion of the leading edges in the hinges which leads to a different tension in the wing during flapping.
- Small manufacturing differences.
- The first measurements were done with the old mechanism. The wear of the crank-shaft and push rods of this mechanism is significant and therefore the errors are rather large (in the order of 2 grams) when the mechanism is used for several hours. In order to make it possible to neglect this measurement error, only wings will be compared that are measured in succession. Therefore, no significant wear is present between the first and last measurement.
- Decrease in performance due to aging of the wing. However, the wings are only tested for 5 minutes each. The influence of wear of the wing can be neglected as well.

As explained above, the last two assembly errors can be neglected. An estimation of the sum of the first two errors can be made by calculating the standard deviation of different measured wings of the same type where only the effect of leading edge insertion and manufacturing differences are taken into account. The standard deviation is shown in equation 5.6. This is the formula for the standard deviation of a sample of a population of measurements (Teunissen et al. [2005]). A list of the standard deviations per flapping frequency is given in table 5.2 and the different performance plots can be found in figures 5.5 - 5.7.

One can see that the standard deviations due to leading edge insertion and manufacturing error are rather small, around 1% of the nominal value.

$$\sigma = \sqrt{\frac{\sum(x - \bar{x})^2}{N - 1}} \quad (5.6)$$

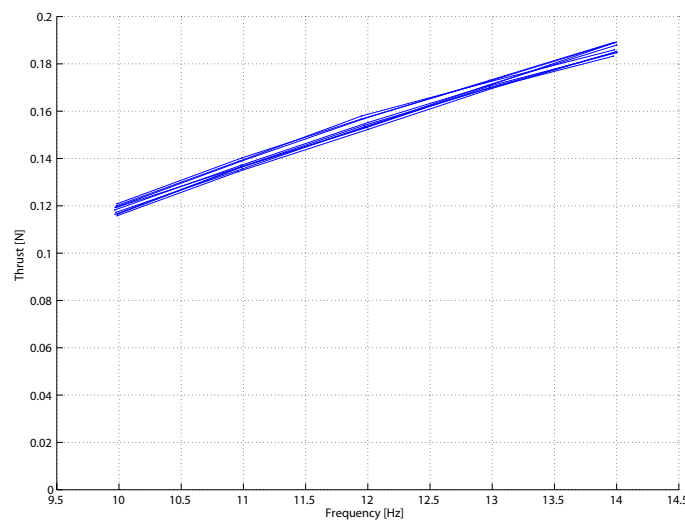


Figure 5.5: Thrust generation of 8 different wings.

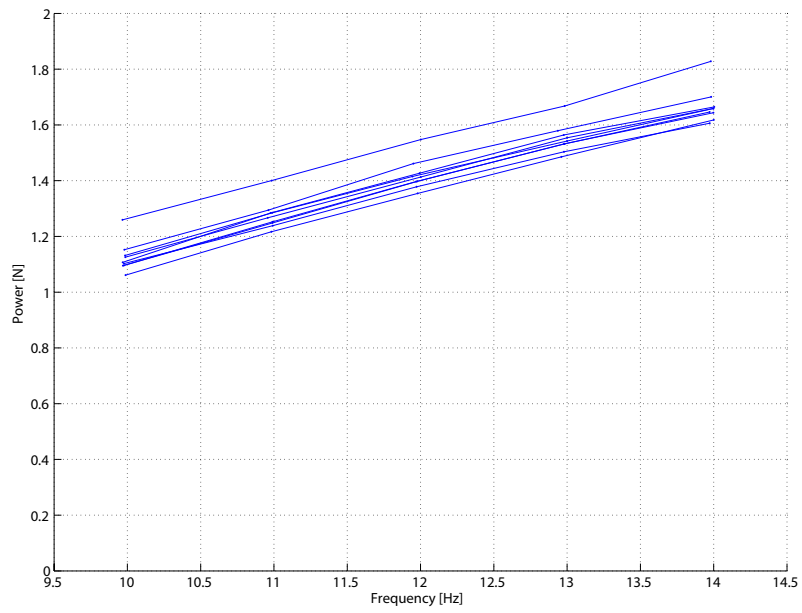


Figure 5.6: Power consumption of 8 different wings.

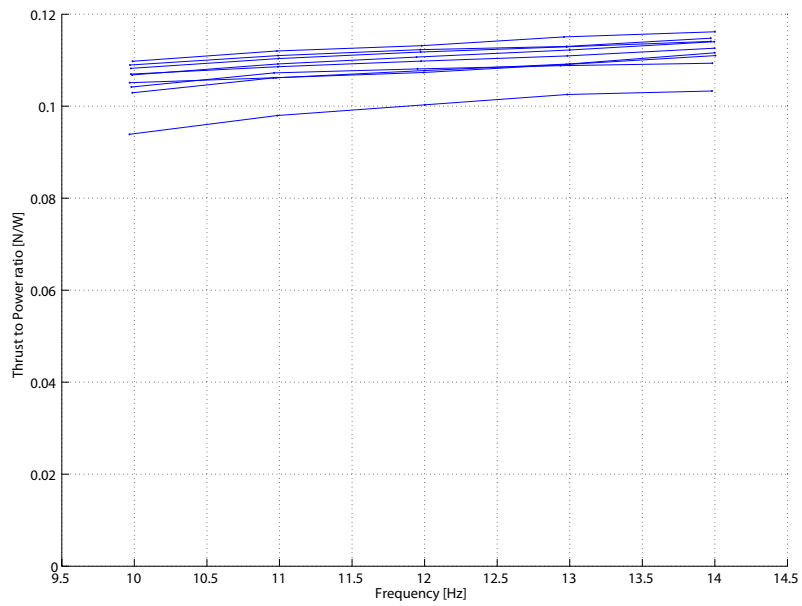


Figure 5.7: Thrust-to-power ratio of 8 different wings.

	Standard deviation of thrust [N]	Standard deviation of power [W]	Standard deviation of thrust to power [N/W]
10 Hz	0.0018	0.0565	0.0048
11 Hz	0.0018	0.0528	0.0042
12 Hz	0.0020	0.0561	0.0039
13 Hz	0.0013	0.0524	0.0036
14 Hz	0.0022	0.0654	0.0038

Table 5.2: List of standard deviations of thrust, power and thrust-to-power ratio for every measured frequency.

Now that all the errors are discussed, one can take these into account in the next sections. A standard deviation of 1% has to be taken into account in all the measurements.

5.2 Wing design

In this section, the actual wing design will be explained.

The different wing parameters are all connected to each other and therefore it is difficult to relate a certain change in performance with a certain single parameter. It can be assumed that the wing area, wing shape, stiffness of the leading edge, stiffness of the stiffeners, Reynolds number, aspect ratio, chord length and wing flapping frequency are all of great influence on the performance in terms of thrust generation and power consumption. To be able to know the influence of a certain parameter, other parameters have to stay fixed. In this research, the influence of the stiffness, orientation and therefore the location of the stiffeners is investigated, while all other parameters are kept constant. Various tests have been done with the wing shape and aspect ratio as the changing parameter. Finally the influence of the clap-and-fling on the thrust and power is investigated by looking at a single wing instead of a biplane configuration.

5.2.1 Effect of orientation and location stiffeners

The focus of this test lies on the influence of stiffener orientation and location. The orientation of the stiffeners is systematically approached, while the shape and area of the wing was not changed. This is done in different steps:

Step 1: Parallel stiffeners

First, the two stiffeners were positioned parallel to each other under five different angles with the trailing edge: 0° , 31° , 63° , 77° , 90° . The location and wing shape can be seen in figure 5.8. The results of these tests can be seen in figure 5.9. Wing31 and wing63 (respectively with the stiffeners under an angle of 31° and 63° with the trailing edge) give the best thrust-to-power ratio. The higher the thrust-to-power ratio, the more thrust generation for a lower power consumption. The wing without stiffeners (Wing Clean) has poor characteristics. For frequencies higher than 11.5 Hz, the system failed for this wing.

The same is true for wing77. The reason for failure at 11.5Hz is not yet known. The stiffeners of the standard wing are under an angle of 54° and 24° .

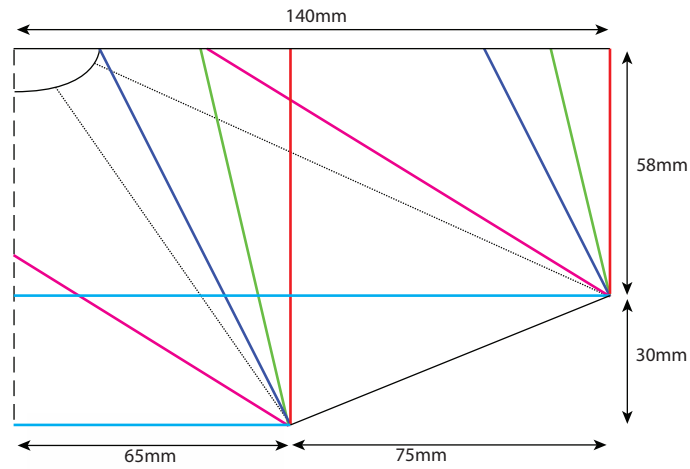


Figure 5.8: Schematic representation of half wing with stiffener location of wing0 (cyan), wing31 (magenta), wing63 (blue), wing77 (green), wing90 (red) and the standard wing (wing5424) (dotted).

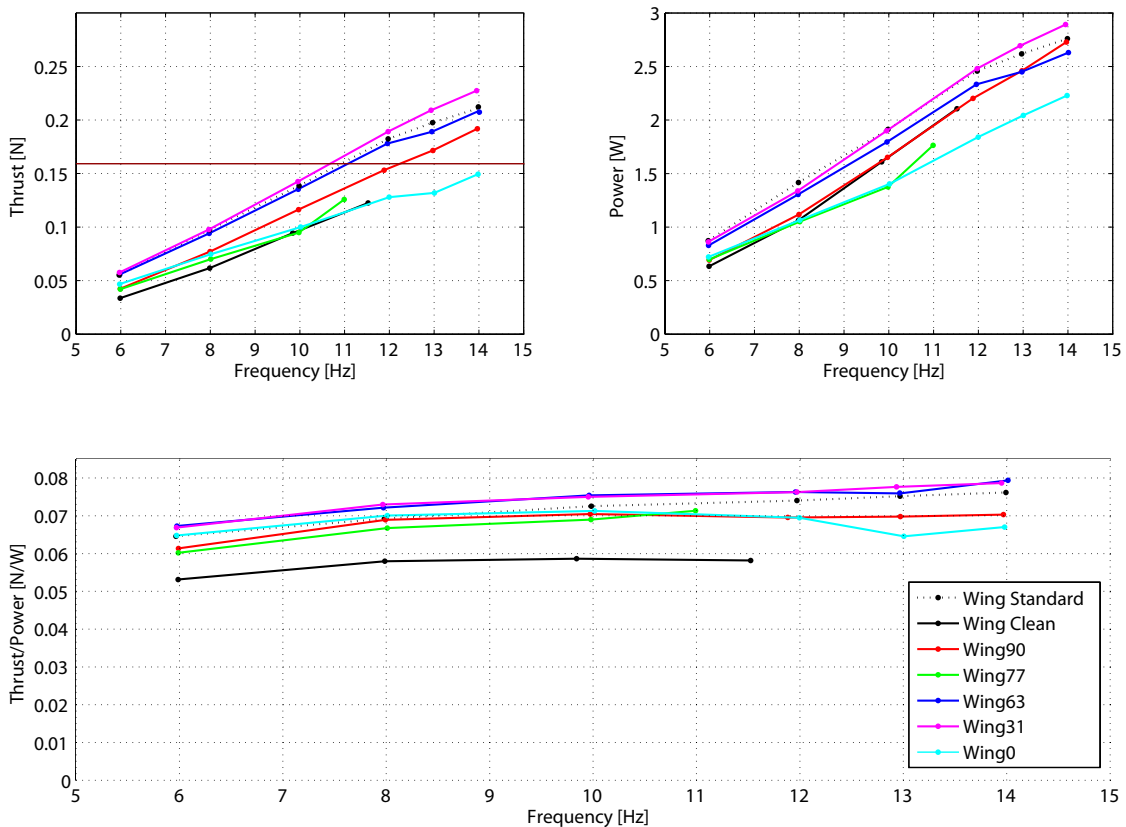


Figure 5.9: Performance plots of the parallel test series. Colors are according figure 5.8. The brown line represents a mean value of DelFly II weight at 0.16 N.

Step 2: Combine the two best wings of step 1

Wing31 and wing63 proved to be the best wings with parallel stiffeners. Now, combinations of these two wings will be made. This means that the inner stiffener of wing63 goes together with the outer stiffener of wing31, this will become wing6331 (the first two digits represent the angle of the inner stiffener and the last two digits represent the angle of the outer stiffener) and visa versa, for wing5163. Note that the angle of the inner stiffener is not 31° but 51° . This is done because the inner stiffener of wing31 penetrates through the foil at the root of the wing. This adapted wing31 is called wing5131. Therefore the stiffener is shifted to the front end of the root in order to prevent this penetration, see figure 5.10. This shift resulted in an angle of 51° . The performance plots of this combination of stiffeners can be found in figure 5.11. One can see that the absolute values of the standard wing and wing63 are not the same as in the previous plots in step 1. This is due to the wear of the mechanism. The relative relation between the different wings however is the same.

One can see from figure 5.11 that wing6331 is the best in this series. It does not produce much more thrust than the rest, but the power consumption is lower which results in the highest thrust-to-power ratio of this series of wings. Furthermore, one can see that the wings with converging stiffeners to the leading edge perform better than the wing with diverging stiffeners.

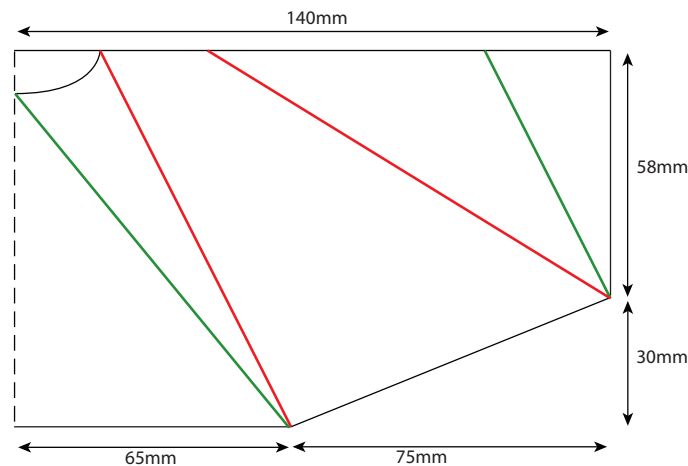


Figure 5.10: Schematic representation of half wing with stiffener location of wing6331 (red) and wing5163 (green).

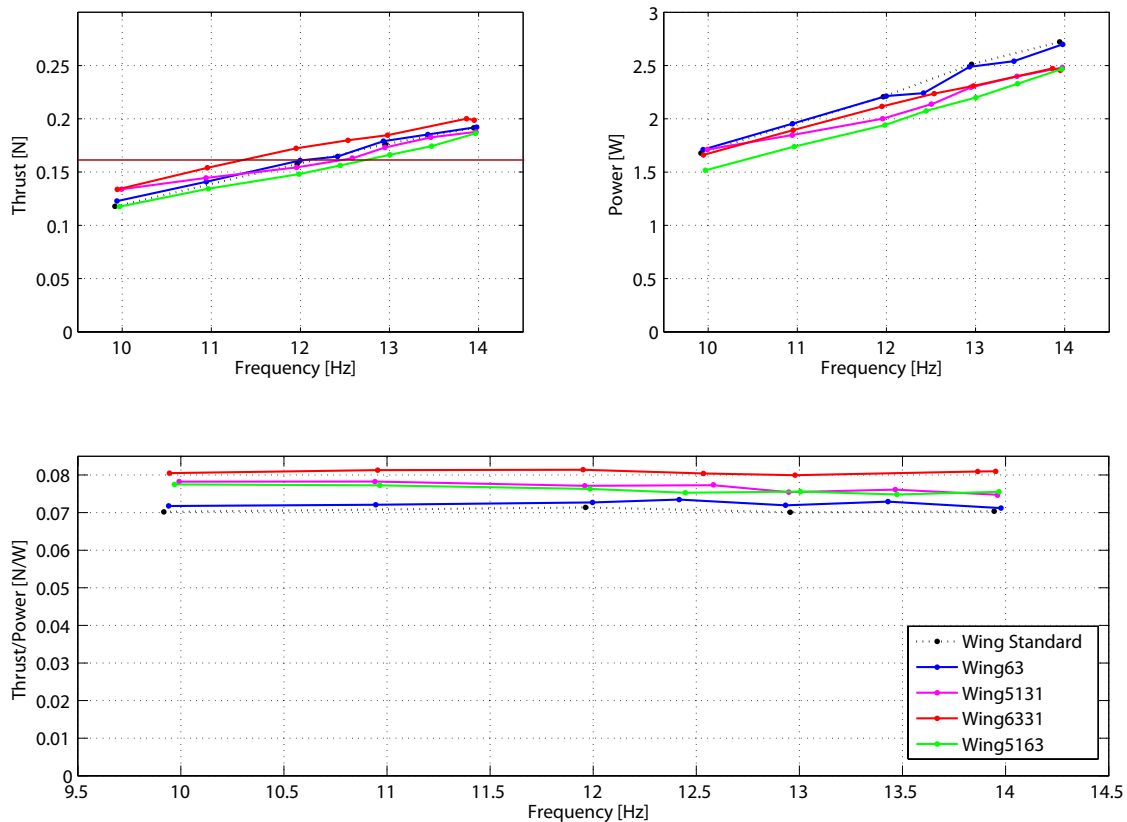


Figure 5.11: Performance plots of the parallel test series. Colors are according figures 5.8 and 5.10. The brown line represents a mean value of DelFly II weight at 0.16N.

Step 3: Combinations of converging stiffeners

Because wing6331 is the best wing in step 2, combinations of this wing are built. Converging the stiffeners towards the leading edges proved to have an impact on the performance in a positive way. Therefore, all combinations of wing6331 are converging types. Figure 5.12 shows the different types of converging wings. First wing6331 is tested again (1), after that the inner stiffener of wing6331 is kept constant (represented as a thick line in figure 5.12) and the outer stiffener is changing (2-3). The same is done for a constant outer stiffener (4-5) and a combination of two changing stiffeners (6). From the performance plots in figure 5.13 one can see that wing7731 (solid green) gives the best characteristics. The thrust is a little lower (0.006 N) than the thrust of wing6331 but the power consumption however is much lower (0.22 W) for wing7731 than for wing6331. This combination results in an increase in thrust-to-power ratio.

Wing6326, wing6931 and wing7731 converge in a way that the stiffeners almost touch each other at the leading edge. Wing7731 is the wing of which the stiffeners converge to a more outside location of the leading edge, therefore it is possible that wings with converging stiffeners to the outside of the wing perform even better. Two wings are built, (7)wing9039 (dashed blue) and (8)wing11663 (dotted blue) in order to check if this is true. These wings are also plotted in figure 5.13, the results show that wing11663 is performing

bad. Wing9039 however produces less thrust (still enough to lift a DelFly) than wing7731 but uses also less power. This results in a thrust-to-power ratio that is almost equal to the ratio of wing7731.

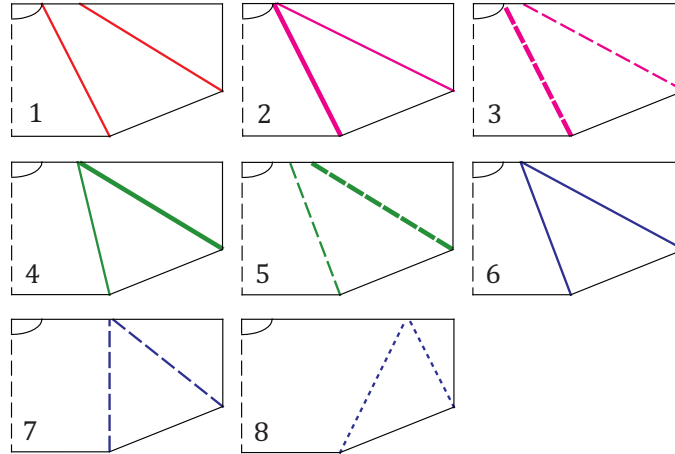


Figure 5.12: Schematic representation of half wing with stiffener location of (1)wing6331 (red), (2)wing6326 (solid magenta), (3)wing6328 (dashed magenta), (4)wing7731 (solid green), (5)wing6931 (dashed green), (6)wing6928 (solid blue), (7)wing9039 (dashed blue), (8)wing11663 (dotted blue).

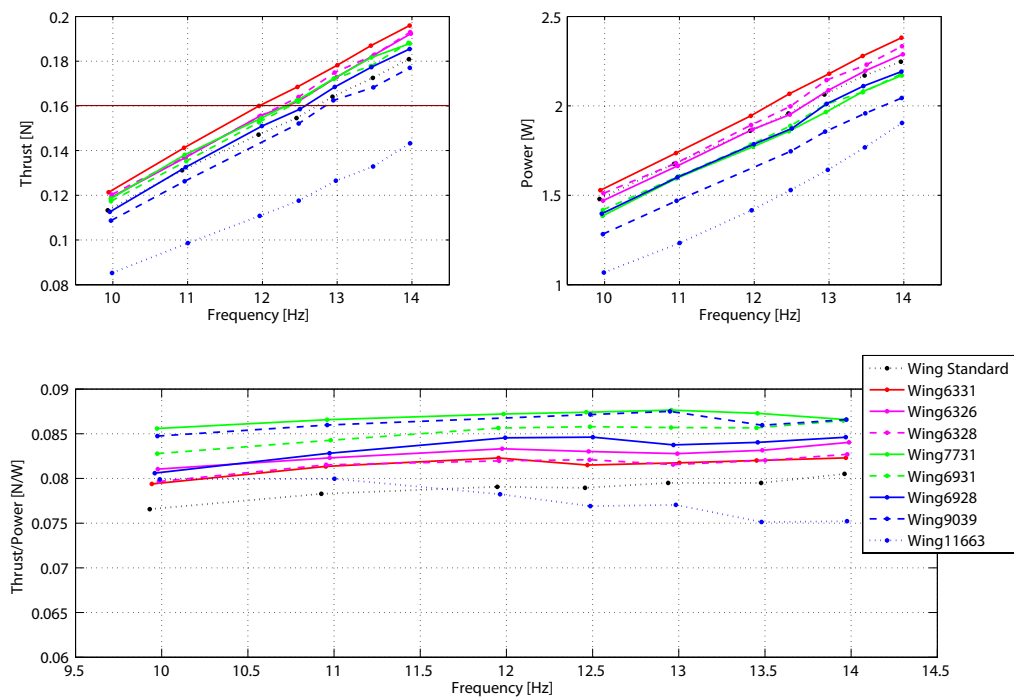


Figure 5.13: Performance plots of the converging test series. Colors are according figures 5.12. The brown line represents a mean value of DelFly II weight at 0.16N.

Step 4: Combinations of the best two converging types of step 3

The two best wings of step 3 are wing9039 and wing7731. From the previous step it appeared that moving the ends of the stiffeners at the leading edge more inwards or more outwards does not benefit the performance. Therefore a last wing is built with the ends of the stiffeners in the middle of wing9039 and wing7731. This wing is called wing8435 and can be seen in figure 5.14. In figure 5.15 the performance plots of these wings are shown. It can be seen that the performance of these wings are all close to each other. Wing8435 however gives better thrust characteristics, about 0.005 N more over the whole frequency range. This is twice as much as the standard deviation so therefore this difference is significant.

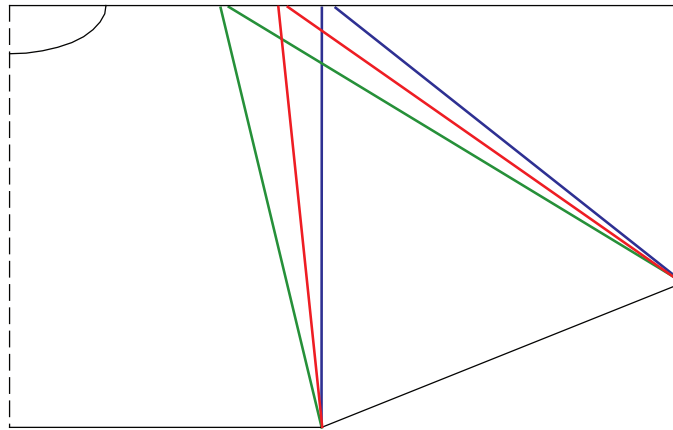


Figure 5.14: Schematic representation of half wing with stiffener location of wing7731 (green), wing9039 (blue) and wing8435 (red).

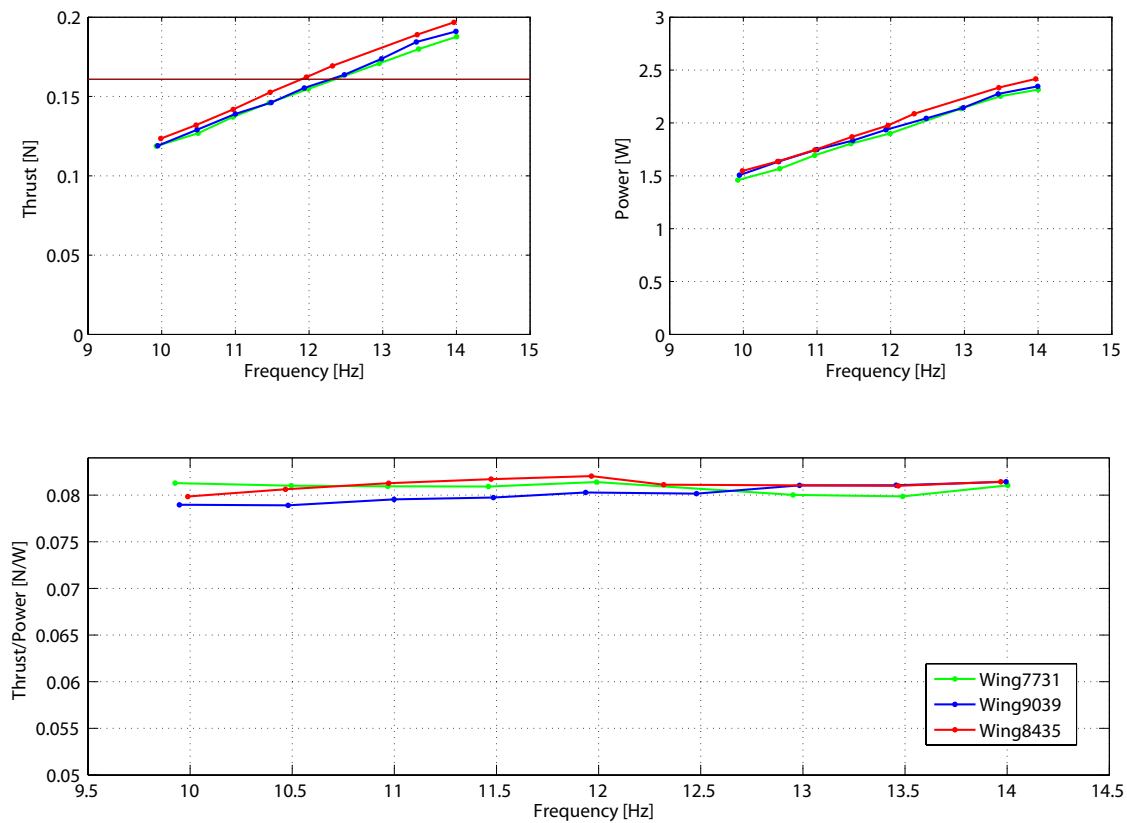


Figure 5.15: Performance plots of wing7731 (green), wing9039(blue) and wing8435 (red). The brown line represents a mean value of DelFly II weight at 0.16 N.

New versus old

Here, the new wing (wing8435) and the old wing (wing standard) are compared, see figure 5.16. The performance of these two wings is shown in figure 5.17. One can see that the thrust is more or less the same. This is probably because the main driving parameters for thrust generation such as wing area and air density (equation 5.3) are kept constant during these tests. The difference can be found in the power consumption. From the power plot a mean gain over the whole flapping frequency of $5\% \pm 1\%$ can be found. From the study of Mark Goen (Goen [2010]) it can be seen that rotational phase of the new wing occurs smoother than the rotational phase of the old wing. This can explain why there is a shift in power consumption. This gain of $5\% \pm 1\%$ is also found in the thrust-to-power ratio.

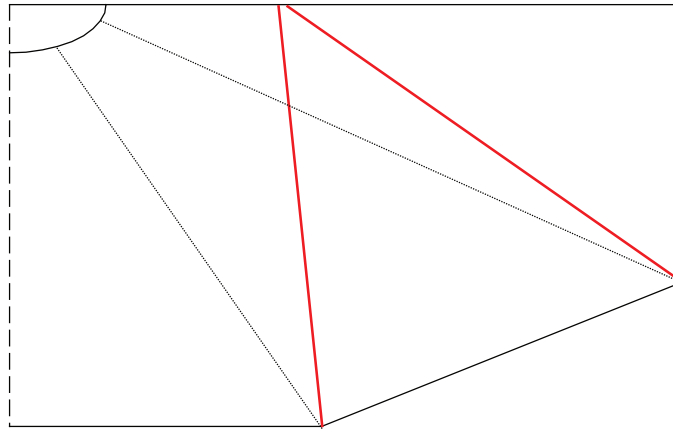


Figure 5.16: Schematic representation of half wing with stiffener location of standard wing (black) and wing8435(red).

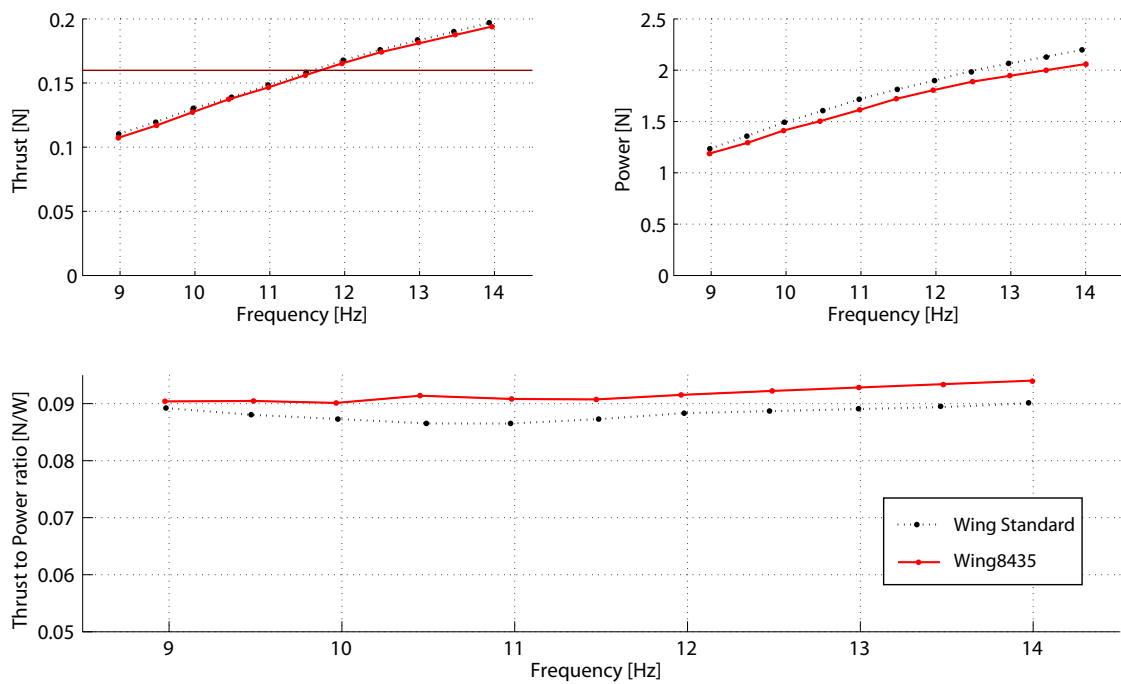


Figure 5.17: Performance plots of standard wing (black) and wing8435(red). The brown line represents a mean value of DelFly II weight at 0.16N.

5.2.2 Effect of stiffener thickness

The influence of stiffener diameter (and therefore also the influence of its stiffness) is investigated by changing the type of stiffeners from the standard 0.28 mm up to a maximum of 1.0 mm, see table 5.3. The difference in inner and outer diameter of the stiffener will result in a different deformation during flapping. This can be translated to a difference in thrust generation and power consumption. From figure 5.18 it can be observed that the thrust and power increase with the increase of cross-section area (therefore the stiffness) of the

stiffener. The thrust-to-power ratio, however, decreases with increasing cross-sectional area. A wing with 0.28 mm stiffeners has the best characteristics. The wing with 1.0 mm diameter stiffeners is not plotted in figure 5.18 because the mechanism failed at flapping frequencies of 10 Hz and higher. This wing is relatively heavy (2.2 g) in comparison to the other wings (1.1 g - 1.7 g) and therefore the motor controller is unable to control the wing flapping frequency due to the high inertial forces.

Diameter [mm]	Wing mass [g]
0.28	1.1
0.5	1.3
0.7 (outer) - 0.3 (inner)	1.4
1.0 (outer) - 0.3 (inner)	1.7
1.0	2.2

Table 5.3: Stiffener properties.

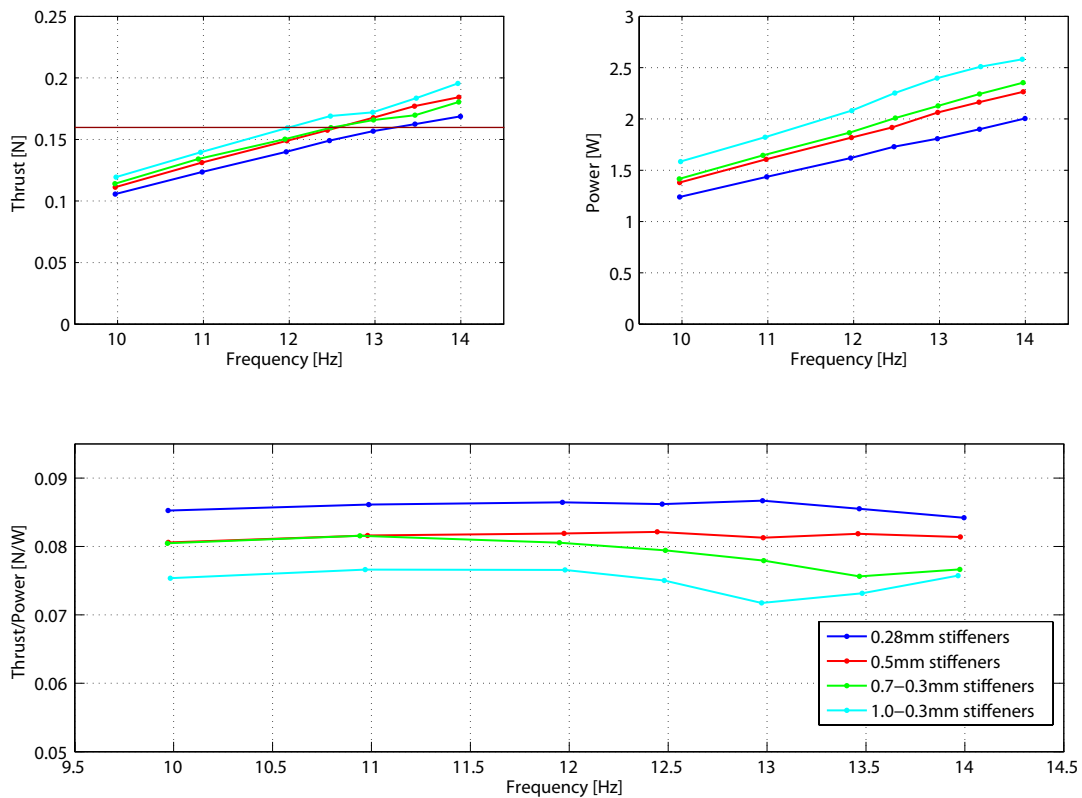


Figure 5.18: Performance plots of wings with different stiffener thickness. The brown line represents a mean value of DelFly II weight at 0.16 N.

5.2.3 Effect of different area distribution

A test is done in order to check the influence of the shape of the wing. The area of the wing is kept constant in this test, but a different area distribution is applied. Figure 5.19 shows the three different wing shapes that are measured:

1. **Normal type.** This wing is the same as wing8435 from the previous section.
2. **Bat-like type.** This wing is obtained by leaving the distances between the ends of the stiffeners at the trailing edge and the root equal to the distances of the normal type. The tip chord and root chord are equal in such a way that the area is still the same as the area of the normal type. Therefore, the root and tip chord are extended with 5 mm.
3. **Reversed type.** This wing is obtained by mirroring the normal type of wing. The tip of the normal wing is the root of the reversed wing and visa versa.

To keep the distances of both ends of the stiffeners with respect to the root equal in all three cases, the angles of the stiffeners with the trailing edge are changed. The inner and outer angle of both the bat-like wing and reversed wing are respectively 77° , 33° and 70° , 43° .

Figure 5.20 shows the performance plots of these three types of wings. One can see that the bat-like wing has the highest thrust-to-power ratio and that the thrust-to-power ratio of the reversed wing is equal to the one of the normal wing. This would imply that the bat-wing is more efficient than the normal type and that the reversed type has an equal efficiency. However, when inspecting the thrust generation, one can see that nor the bat-like wing nor the reversed wing meet the desired thrust level in order to hover (brown line), which is the weight of an actual DelFly II. Because the thrust level is so low, the power level is also lower because the system does not have to do as much effort to overcome the aerodynamic forces.

One can conclude from this test that the wing shape is of great importance for the performance when keeping the wing area constant. Further research needs to be done on this topic.

It is important to investigate the bat-like wing in forward flight conditions because of its high thrust-to-power ratio. Due to the aerodynamic advantage that a wing has in forward flight, it is possible that the desired thrust level is met in order to keep DelFly II in the air.

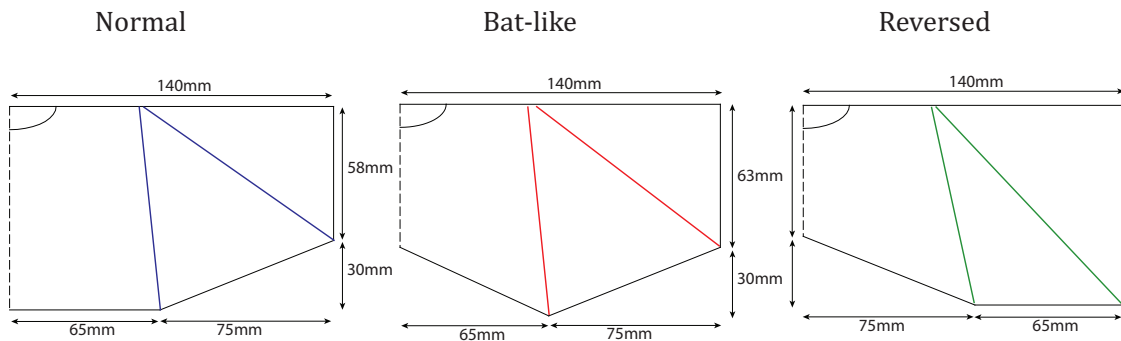


Figure 5.19: Schematic representation of wing8436 (blue), bat-like wing (red) and reversed wing (green).

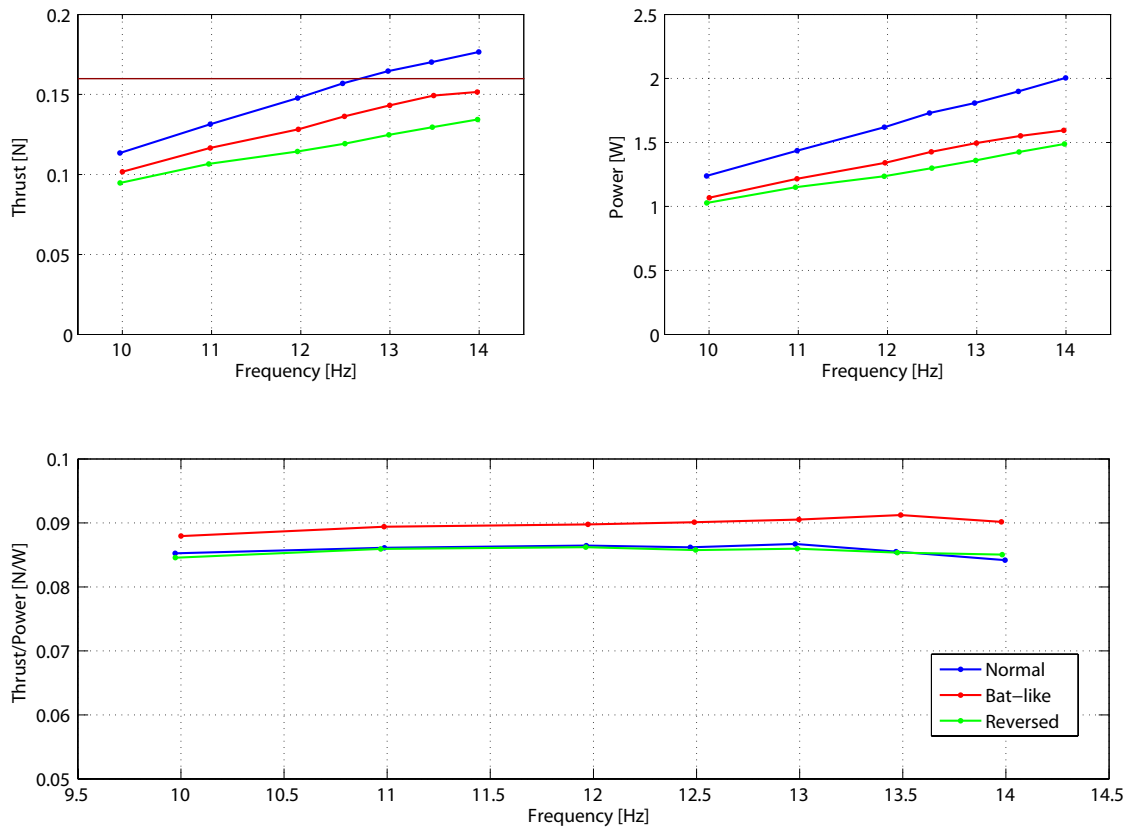


Figure 5.20: Performance plots of wing8436 (blue), bat-like wing (red) and reversed wing (green). The brown line represents a mean value of DelFly II weight at 0.16N.

5.2.4 Effect of different aspect ratio

The influence of aspect ratio (AR) on the performance is investigated by testing three different wings with three different aspect ratios, see figure 5.21. The aspect ratio is calculated with the following equation:

$$AR = \frac{R^2}{S} \quad (5.7)$$

In this equation R is the span of one wing and S is the area of one wing. In order to change the AR of a wing one can change R or S or both. In this case only S has changed because the span is one of the driving parameters of DelFly II. Therefore, the span is kept constant and the area is changed. The root and tip chords are lengthened and shortened with 20% respectively. Equations 5.8 - 5.10 show the calculation of the different AR:

$$AR_{normal} = \frac{140^2}{11195} = 1.75 \quad (5.8)$$

$$AR_{larger} = \frac{140^2}{8900} = 2.20 \quad (5.9)$$

$$AR_{smaller} = \frac{140^2}{13490} = 1.45 \quad (5.10)$$

In figure 5.22 the performance plots are shown of the three different AR wings. One can see in the thrust-to-power ratio that the normal wing gives the best performance. The wing with the higher AR however produces more thrust, especially at higher flapping frequencies. This wing has a smaller wing area, according to the equation 5.3 this wing would produce less thrust. The AR however has also influence on the Reynolds number, see equation 5.11. This Re number has influence on the flow which will result in a higher thrust generation. Further information about this flow can be found in the thesis report of Mark Groen (Groen [2010]).

$$Re = \frac{\varphi n R^2}{\nu AR} \quad (5.11)$$

Here, φ is the stroke angle, n is the flapping frequency and ν is the kinematic viscosity (C. P. Ellington [1999]). For DelFly II, $Re = 13457$ for a flapping frequency of 14 Hz.

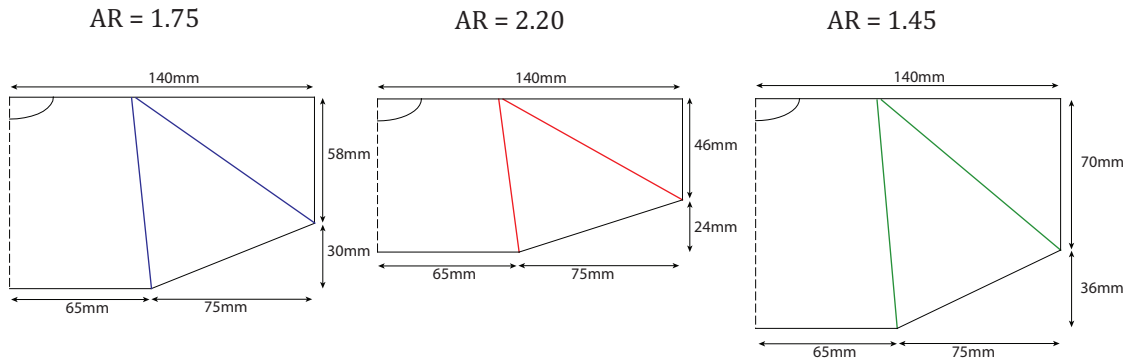


Figure 5.21: Schematic representation of wing8436 with $AR = 1.75$ (blue), wing with $AR = 2.20$ (red) and wing with $AR = 1.45$ (green).

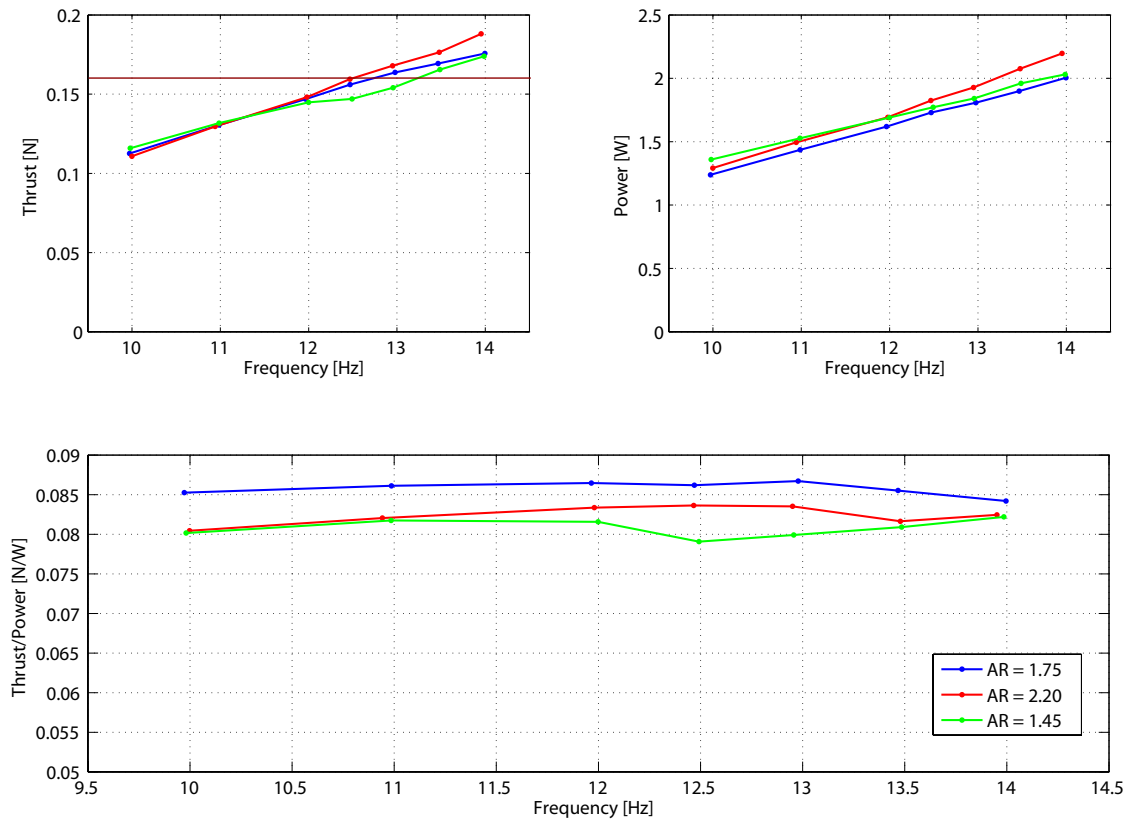


Figure 5.22: Performance plots of wing8436 with AR = 1.75 (blue), wing with AR = 2.20 (red) and wing with AR = 1.45 (green). The brown line represents a mean value of DelFly II weight at 0.16 N.

5.2.5 General remark

In all the performance plots of the previous sections one can see that the relation between frequency and thrust and between frequency and power is quasi-linear. The slopes of random measurements of thrust, power and thrust-to-power ratio are all in the same order. Table 5.4 shows the mean slopes for these three parameters. These slopes are also in the same order for the different area distributed wing. This indicates that the slope is quasi independent of area distribution and stiffener location and orientation.

An overview of the different type of wings of the wing study can be found in appendix D.

Parameter	Slope
Thrust	0.017 N/Hz or 1.7 g/Hz
Power	0.20 W/Hz
Thrust/Power	4.9e-4 N/WHz

Table 5.4: List of different slopes.

5.3 Additional measurements

As an addition to all the previous measurements for a new wing design, three other tests are performed in order to gain an even better understanding of the performance of the new model in total (new mechanism with new wing):

1. Test to investigate the effect of clap & peel on DelFly II.
2. Endurance test to see how long the new system can perform properly in order to keep the DelFly II in the air.
3. Test in vacuum and air to investigate the influence of air on the power consumption.

5.3.1 Clap & peel effect for DelFly II

One of the aerodynamic mechanisms that can be used in flapping flight is the clap & peel mechanism, as discussed earlier in chapter 2.

Clap & peel is said to gain extra thrust (lift) force. To investigate the exact gain in thrust, a single DelFly wing is tested on the model to assess the performance of one single wing. The relation between the thrust of a biplane wing configuration and the thrust of a single wing is given in equation 5.12.

$$T_{CP} = T_{biplane} - 2 \cdot T_{single} \quad (5.12)$$

The difference between the thrust generation of the biplane configuration, $T_{biplane}$ and twice the thrust generation of a single wing, T_{single} is interpreted as the "clap & peel effect", T_{CP} .

Figure 5.23 shows a plot of frequency versus thrust for a single wing (dotted blue line) and a biplane configuration (solid red line). The doubled values of the single wing are presented with a solid blue line. From this figure it can be seen that an additional 8% in thrust is gained due to the clap & peel effect. This 8% is a mean value over the whole frequency range.

This gain is lower than the gain that insects get from this aerodynamic mechanism, which is generally assessed to be around 25% on average (Marden [1987]). A study on a 20 cm MAV of 2.3 g by Kawamura (Kawamura et al. [2008]) shows an increase in thrust due to clap & peel of 40%. However, this FMAV is twice as small in spanwise direction, has a mean chord of 5 cm compared to 8 cm for DelFly II and has a stroke angle of 50° compared to 44° for DelFly II. All these differences may influence the clap & peel effect. Further investigation has to be done on this subject in order to understand the magnitude that the different features have on clap & peel.

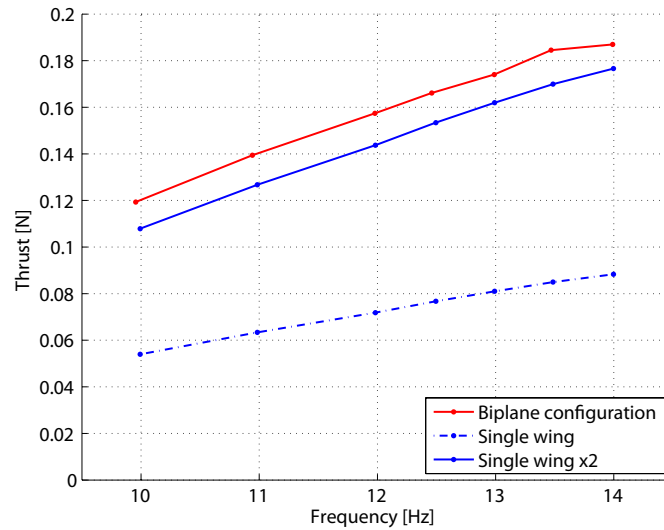


Figure 5.23: Comparison of thrust generation of a biplane DelFly II wing (red solid line) and a single DelFly II wing (dotted blue line). The doubled values of the single wing are presented by the solid blue line. The mean gain in thrust due to the clap & peel effect is 8% over the whole frequency range for DelFly II.

The power consumption is also investigated. The power consumption of a single wing (blue) is compared with a half biplane wing (green). In these two cases the motor load is the same, because the inertia of the wings is the same. The only difference is the clap & peel effect of the half biplane. As one can see in figure 5.24, the power in the two cases is almost the same. One can conclude that clap & peel has a rather small effect on the power consumption of DelFly II.

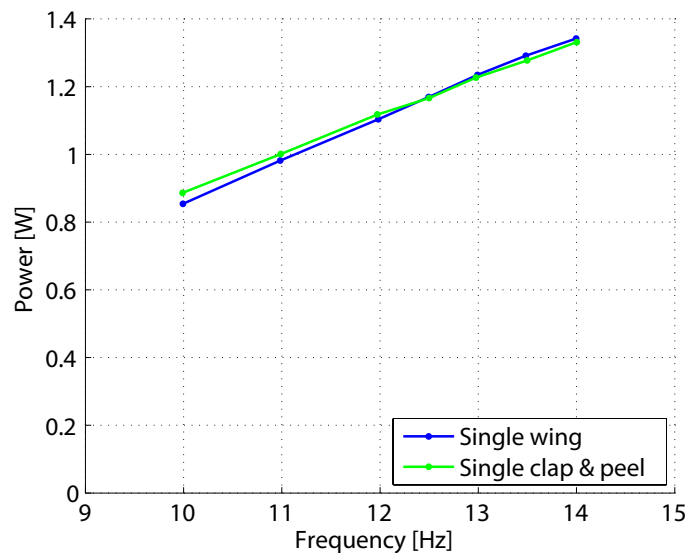


Figure 5.24: Comparison of power consumption of a single DelFly II wing (blue) and a half biplane wing (green).

5.3.2 Endurance test

An endurance test is performed as an overall test to see how long the combination of a new mechanism and a new wing would perform properly for the DelFly II to hover. During this test, the model flapped at a frequency of 12 Hz for almost 19 hours. A flapping frequency of 12 Hz was chosen because this frequency gave an initial thrust of 0.16 N or almost 16 g. The performance plots are shown in figure 5.27. The blue dots are the measuring points, the red dots are two measuring points after the wing was torn and the green line represents a linear fit through the blue dots. After almost 19 hours the thrust suddenly dropped from 0.15 N to a value of 0.10 N. This is due to the fact that one of the wings was torn at the rear of the root, see figure 5.26. Due to this rupture, the wing is not firmly attached to the fuselage anymore which causes a decrease in thrust generation of the 'limp wing'. Furthermore, the effect of clap & peel is reduced. The other wing on the other hand kept on flapping as a normal wing would do. That is the reason why the thrust is still relatively high, around 0.10 N. This is more than half of the total thrust (0.08 N) so one can assume that the 'limp wing' is still producing a small amount of thrust together with a minor clap & peel effect. There was also a small rupture in the tip of the left wing, but it is not clear from the data if this has a great influence in the performance. Pictures of the ruptured wing can be found in figures 5.25 and 5.26.

It can be seen that the linear fit is almost constant. The system degrades with a factor of 2.5×10^{-4} N/hour or 2.5 mg/hour. One can conclude from this that the system operated at a constant performance for almost 19 hours until the wing was suddenly torn. This is much better than the performance of the old system which had to be renewed after 3-6 hours because of a decrease in performance due to wear problems with gears, hinges, cranks or push rods.

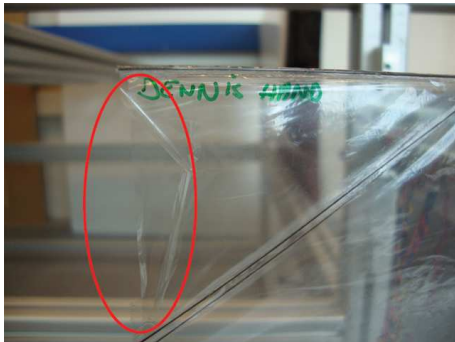


Figure 5.25: Rupture at the tip of left wing.



Figure 5.26: Rupture at the rear of the root.

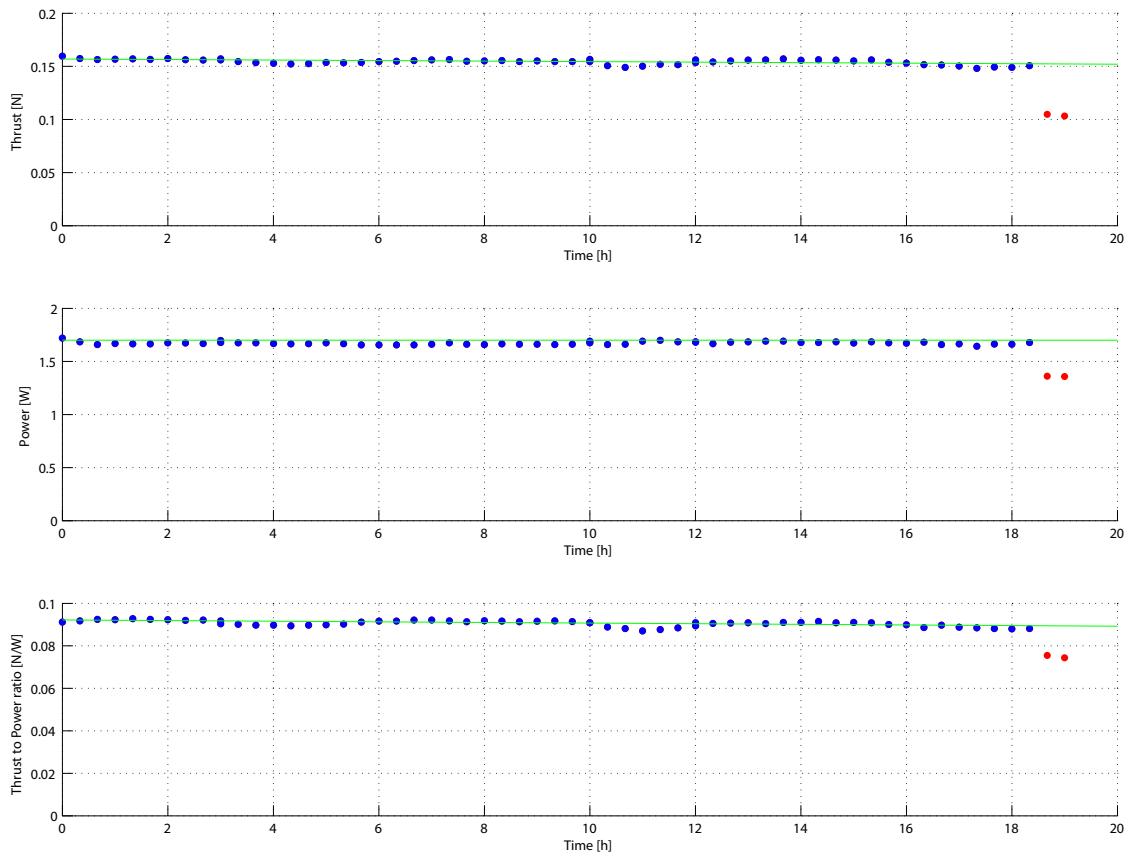


Figure 5.27: Results from the endurance test. The blue dots are the measuring points, the red dots are two measuring points after the wing was torn and the green line represents a linear fit through the blue dots.

5.3.3 Vacuum test

Vacuum tests are performed in order to measure which percentage of power and therefore of current is put into the aerodynamics and how much is put into the mechanics. Figure 5.28 shows the performance plots of eight different tests. Four different configurations are shown in this figure: old wing - old mechanism (green), old wing - new mechanism (red), new wing - old mechanism (cyan) and new wing - new mechanism (blue). All four configurations are also tested in both normal air conditions (solid line) and vacuum (dashed line). On the top left, where the thrust is plotted, one can see that in vacuum there is no thrust generation, which is logic. On the top right and the bottom, plots of power and current are shown. One can see that the power and current that is needed in vacuum is much lower than in air. This is because the system does not need to cope with the aerodynamic forces that are normally generated in air. The power and current that is needed in vacuum is necessary to overcome the inertia of the wings. In air, this is added with the power and current needed to overcome the aerodynamics. In table 5.5 the percentages of mechanical power and current are given for all four configurations. From this table one can conclude that the ratio between mechanical power and total power is around 1:4 and 1:5 depending on the configuration. This means that

75%-80% of the power is used to overcome the aerodynamics.

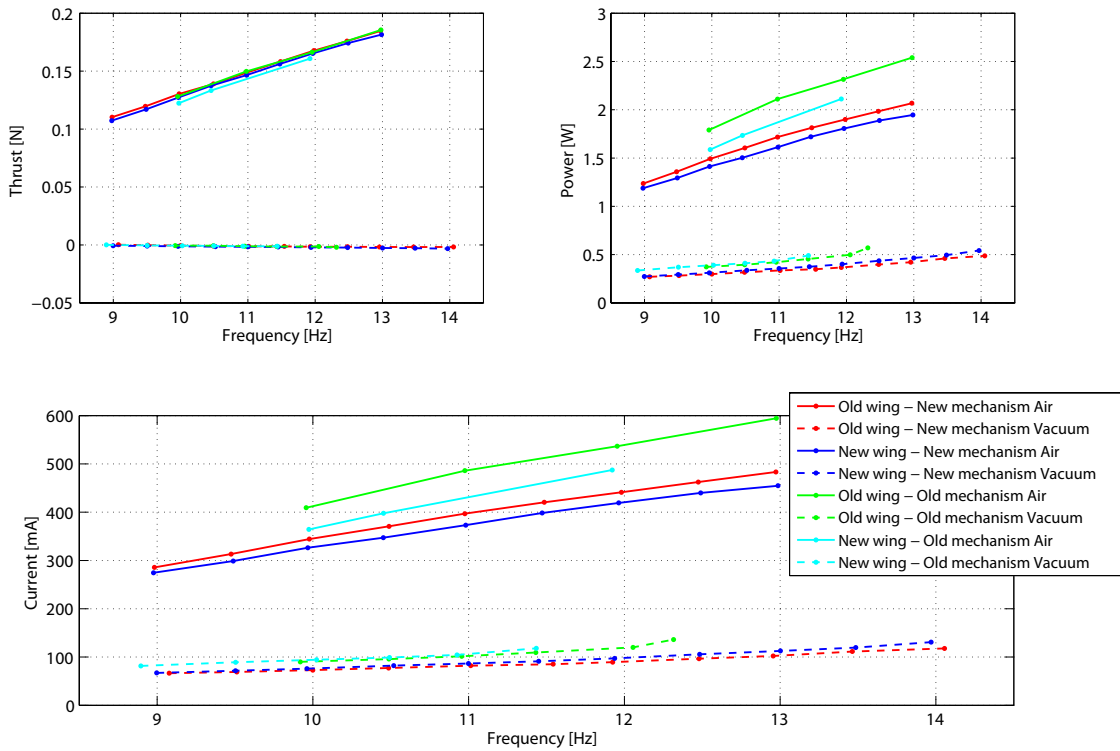


Figure 5.28: Performance plots of vacuum tests. Solid lines represent tests in normal air conditions, dotted lines are tests in vacuum.

Configuration	% of mechanical power with respect to total power
Old wing - Old mechanism	22%
Old wing - New mechanism	21%
New wing - Old mechanism	25%
New wing - New mechanism	24%

Table 5.5: List of power used for mechanics with respect to total power.

Figure 5.29 shows a plot of the current during one flap cycle both in air and in vacuum. One can see that curve of the current in air follows the curve of the thrust. The two bumps of the thrust curve are also present in the current curve. For the vacuum case however, the current stays constant during the whole flap cycle apart from a small bump, which corresponds with time when the wings are half of the out-stroke. This is also when a leading edge vortex is generated. This can be the reason of the increase in current.

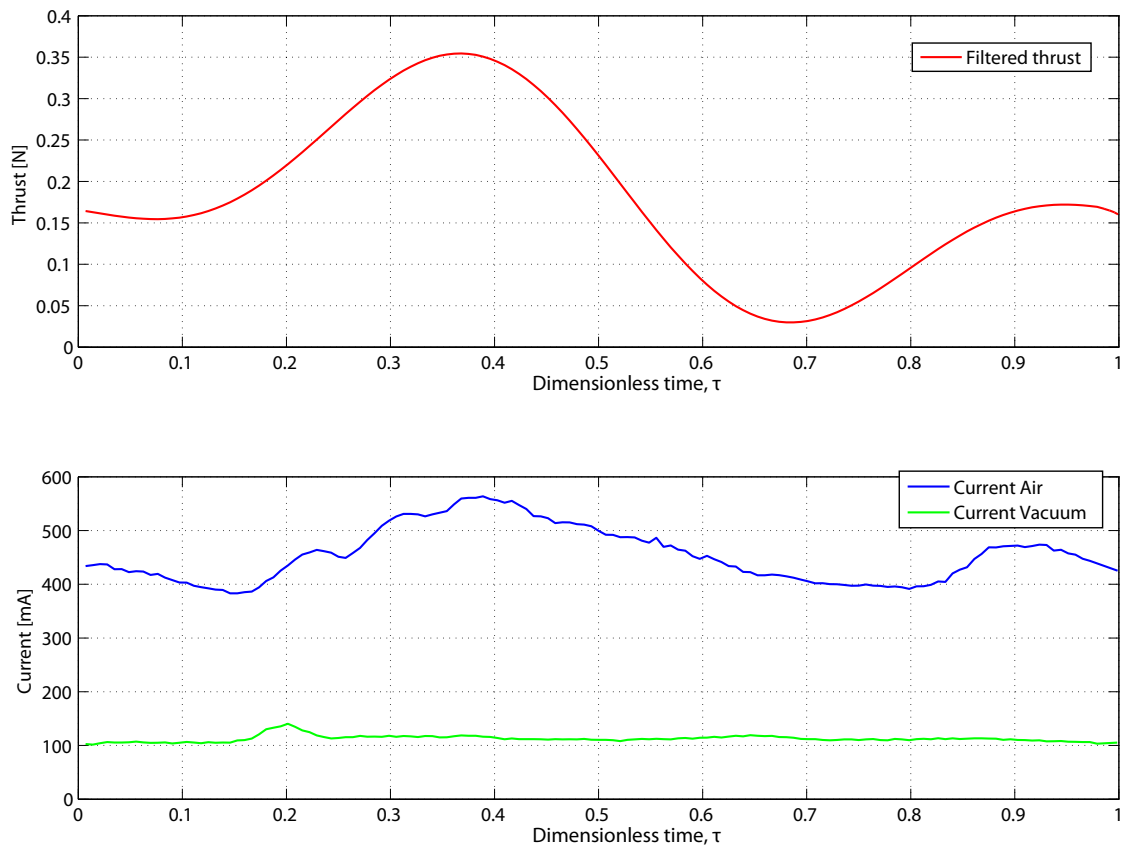


Figure 5.29: Comparison of current development at 13 Hz between a wing in air (blue) and a wing in vacuum (green) for one flap cycle. The thrust generation is shown in red.

5.4 Overall increase in performance

As explained in chapter 1 there are two ways of improving the flight performance: Improving the mechanics and improving the wing design. These two topics are covered in this report. In chapter 4 the new mechanism is discussed which is responsible for a gain in thrust-to-power ratio of approximately 20%. In this chapter the new wing design is discussed which is responsible for a gain in thrust-to-power ratio of approximately 5%. A total gain in thrust-to-power ratio of 25% is obtained during this research. The results are summarized in figure 5.30.

The gain in power is approximately 20%. An important conclusion of this improvement is that an improvement of 20% in power does not result in a gain of 20% in flight time. In figures 5.32 and 5.33 the discharge curves are shown of the 'Cyclone 130' 130mAh, 20C Lithium Polymer Cell, the battery that is used for DelFly II. From this figures one can see that when the battery is discharged at a lower current, the discharge time increases. This increase is not proportional to the decrease in discharge level. The reason for this can be explained on the hand of figure 5.31 and equation 5.13. This equation gives the formula for the motor power of a series circuit.

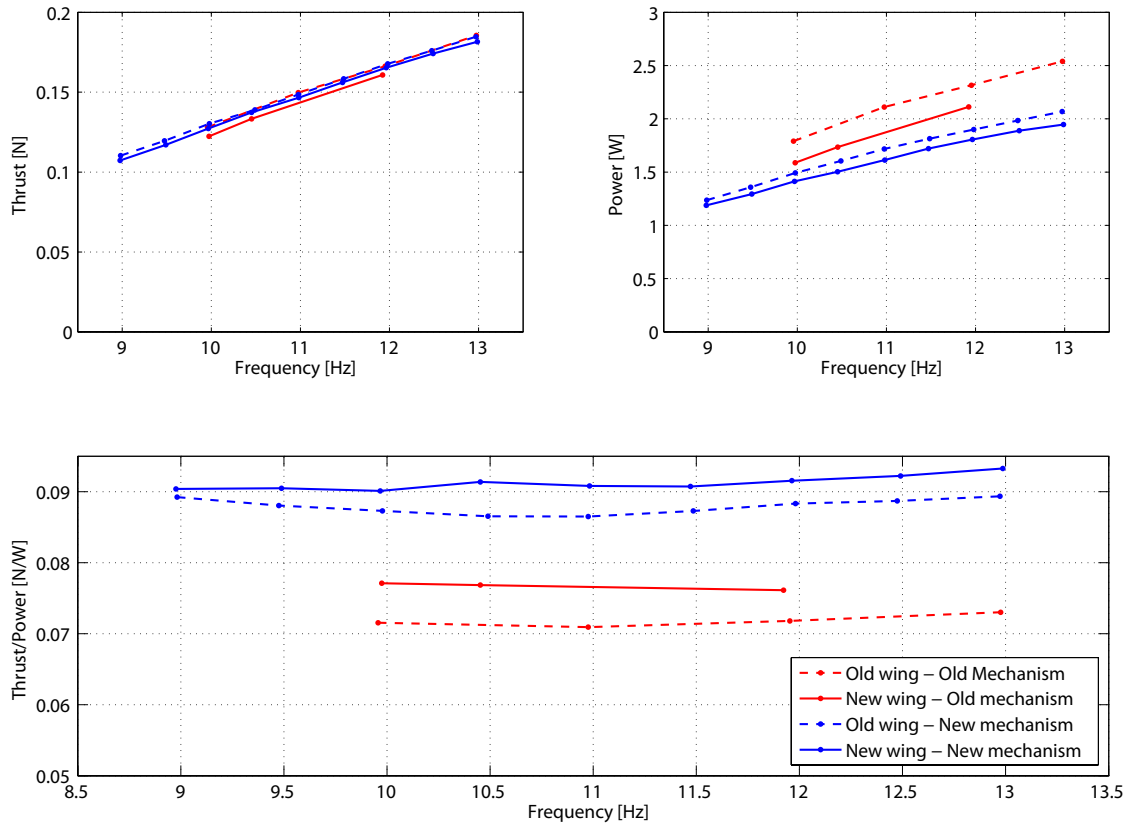


Figure 5.30: Performance plots of four cases: Old wing - Old mechanism, New wing - Old mechanism, Old wing - New mechanism and New wing - New mechanism.

$$P_{mot} = U_{mot}I_{mot} = (U_{bat} - I_{mot}R_I)I_{mot} \quad (5.13)$$

Here P_{mot} is the power that is used by the motor, U_{mot} and I_{mot} are respectively the voltage and current of the motor. U_{bat} is the voltage of the battery and R_I is the internal resistance of the battery. Reducing the power that is needed by the mechanism, P_{mot} , reduces the current that is needed, I_{mot} . This follows from the first part of the equation. Furthermore, if I_{mot} is reduced, the voltage that is lost due to the internal resistance of the battery $I_{mot}R_I$ is reduced. This means that U_{mot} has increased. Which leads to an even larger reduction of I_{mot} . This circle goes on until an equilibrium is obtained. Furthermore, with the decrease of I_{mot} , the capacity of the battery increases. Therefore, the battery can give more ampere-hour (Ah). The life time of the battery will increase as well. The effect of P_{mot} can be visualized in figures 5.32 and 5.33: decreasing the power consumption with 20% results in an increase in flight time of more than 20%. How much this increase is in practice still has to be investigated by discharging the battery at the desired current level.

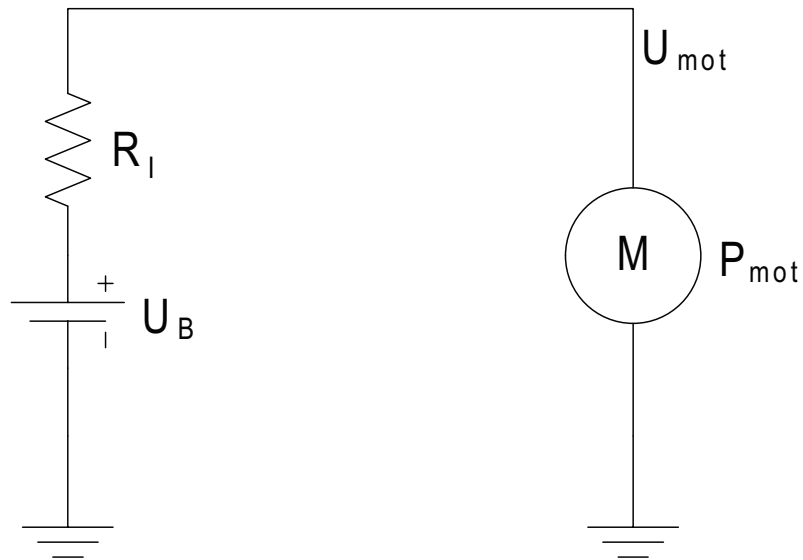


Figure 5.31: Simplified electric scheme of DelFly.

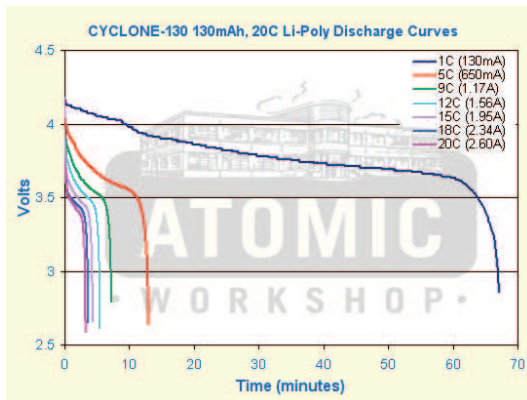


Figure 5.32: 'Cyclone 130' 130mAh, 20C Lithium Polymer Cell discharge curve (*Atomic Workshop* [2010]).

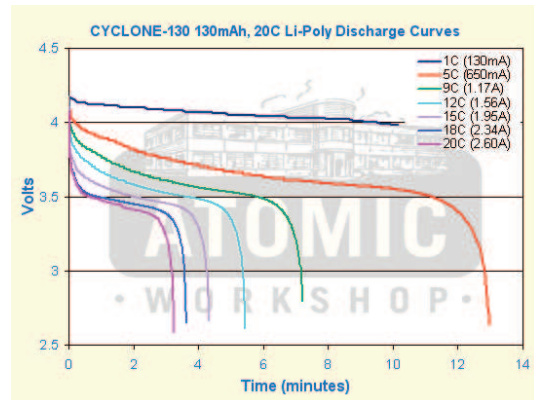


Figure 5.33: Detail of discharge curve (*Atomic Workshop* [2010]).

Wing manufacturing process

The design of a FMAV is still in its early years as described in previous chapters. The same is true for the manufacturing process of the wings. Before this project, the process of building the DelFly wings was very time consuming and the process held room for improvement in accuracy and repeatability. During a project such as this one, it is important that wings of the same type provides the same data to analyze. Furthermore, it is important to learn as much as possible in a limit amount of time, therefore the manufacturing time has to be reduced.

In addition to the project goal of this thesis, a faster manufacturing process is developed which benefits the building accuracy and decreases the Turn-Around-Time (TAT). This is the period for completing a process cycle, in this case building a DelFly wing.

This chapter clarifies the purpose of having a good and accurate manufacturing process in section 6.1 and guides the reader through the different methods that exist for building flapping wings in section 6.2. A trade-off is done between the different methods in section 6.3. A detailed description and the practical use of the best method is explained in section 6.4. Finally, a comparison is done between the current method and the new method in section 6.5.

6.1 Important building parameters

When measuring wings for a FMAV, it is important that all the wings are the same. This can only be done if the parameters which define the wing are all the same. The parameters which define a wing are listed below.

1. **Tension:** The tension in the foil has a great influence on the power consumption and the thrust generation of the wing.
2. **Wing shape:** When cutting the wing by hand, shape differences (sometimes small) will occur. This can imply a different wing area, which has a direct influence on the thrust generation.

3. **Glue:** Use of glue gives an increase in weight of the wing, which also means an increase in weight of the total FMAV. More weight means more power is needed for flying.
4. **Accuracy of the location of the stiffeners:** The location of the stiffeners has a direct influence on the stiffness of the whole wing. This wing stiffness in turn has influence on the power consumption and thrust production.

All of the points discussed above can be categorized under the term: **Human interference**. One can understand that there is much space for error and inaccuracy when the whole manufacturing process is done by hand. Therefore, the objective is to automate as much as possible in order to increase the level of accuracy and decrease the TAT.

6.2 Overview of the options

Not much possibilities are found in literature that describe methods for building flapping wings. In most studies the "Traditional cut & glue"-method is used for building wings (for example Kawamura et al. [2008], Zdunich et al. [2007] and Bolsman et al. [2009]). Another possible method makes use of Micro-Electro-Mechanical Systems technology or MEMS technology (Pornsin-Sirirak et al. [2001], Pornsin-Sirirak et al. [2000] and Yang et al. [2007]). A third method, which is not found in literature and which was developed during this research is called the "Advanced cut & glue"-method. This method is based on the traditional cut & glue method and uses a vacuum table and Computer Numerical Control-machine (CNC-machine) to increase the level of accuracy and decrease the TAT. These three methods will be enlightened in the next three sections.

6.2.1 Traditional cut & glue method

This method is the most common used method for building flapping wings. The whole process is done by hand and therefore it is not that accurate. In the next sections one can find the method description, the advantages and disadvantages of this method.

Description

First, an A4 paper with the contours of the wing (figure 6.1(1)) is placed on the table and secured with tape.

Next, a piece of Mylar is secured on top of that piece of paper with tape. This is done by taping all four corners. It is important that the builder tapes the Mylar in such a way that it is not too loose. Otherwise, the wing's membrane will be too loose which will result in a reduction of thrust generation. Furthermore, when the foil is not tight enough, wrinkles can lead to a disadvantageous flow around the wing which also results in a reduction of thrust generation during flapping. However, when the foil is too tight, there is too much tension in the wing which will result in a increase in power consumption during the flapping motion. Because there is no way of measuring the exact tension in the foil for this method, every wing will be slightly different (figure 6.1(2)).

The third step in this process is to glue the stiffeners onto the Mylar foil. These stiffeners are small carbon rods with a diameter of 0.28 mm and are cut to the appropriate length (2 x 97.0 mm and 2 x 132.5 mm) which are measured with a digital caliper. Gluing the stiffeners is done with a 0%-50% mixture of Pattex glue and Aceton. The builder has to put glue on the Mylar foil and then place the stiffener in the right place, exactly on the black line on the A4 paper beneath (figure 6.1(3)).

Next, one has to reinforce the stiffeners at the trailing edge of the wing with small pieces of tape to prevent detachment from the Mylar foil during flapping. A piece of tape in the shape of a half ellipse has to be taped on top of the Mylar where the other ends of the stiffeners come together. This is to prevent detachment and also to prevent the foil from ripping in that spot because of the high tensions during flapping (figure 6.1(4-5)).

After that, the leading edges have to be glued onto the foil. The leading edges are carbon rods with a D-shaped cross section, 0.7 mm by 1.4 mm and a length of 136.0 mm each. They are glued on the Mylar with the half circular shape bottom down, using the same 50%-50% mixture glue (figure 6.1(6)).

When all of this is done, the builder can start to cut out the contour of the wing with great care. Cutting out the ellipse shape has to be done with even more care, because tearing the foil in that particular place is easy. Parallel to the wing's leading edges extra foil has to be left on. When the wing is cut, this small piece of foil has to be glued over the flat part of the D-shaped rod. This is also done with the 50%-50% mixture (figure 6.1(6)).

The above procedure must be repeated to generate a second wing to complete the biplane wing configuration of DelFly II.

Advantages

1. The cut & glue method is a simple method.
2. It is a cheap method in terms of material and machinery costs.
3. Adaptation of the method is simple if the wing design is altered.

Disadvantages

1. Tension of the Mylar foil is different for every wing, so no comparison is possible.
2. The location of the stiffeners is never exactly the same.
3. The amount of glue that is used, differs from wing to wing, so the total weight differs also from wing to wing.
4. The accuracy and therefore also the performance of a wing depends on the person who builds it.
5. It is time-consuming and therefore expensive in man-hours.
6. It has a slow TAT.
7. The reproducibility is too low.
8. It can not be used when design variables are studied.

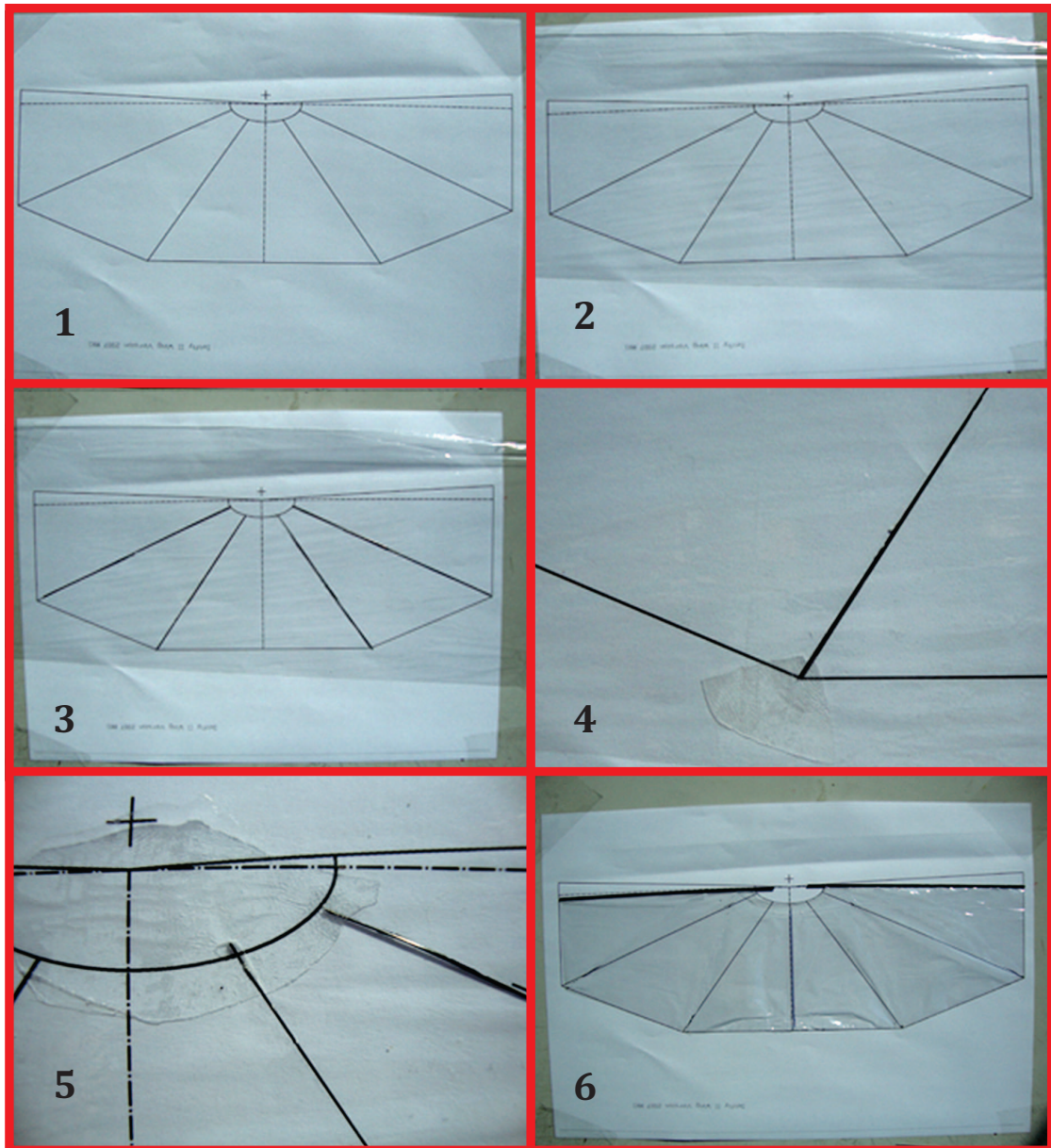


Figure 6.1: Overview of the cut & glue method. 1) A4 is taped to the table; 2) Mylar is taped over the A4 paper; 3) Stiffeners are glued to the Mylar; 4) Detail of reinforcement tape at the end of a stiffener; 5) Detail of reinforcement around the semi-ellipse; 6) Leading edges are glued to the Mylar and the wing is cut out.

6.2.2 MEMS method

Another method is a technique that uses Micro-electro-mechanical systems (MEMS) in combination with photolithography technology (Pornsin-Sirirak et al. [2000] Yang et al. [2007] Pornsin-Sirirak et al. [2001]). The wingframe is made of a titanium-alloy (Ti-alloy). Poly-monochloropara-xylylene or short parylene-C is used for the membrane of the wing. This material is selected because it can be deposited directly to the Ti-alloy at

a desired thickness. Parylene is also light and strong and can withstand high flapping frequencies without tearing (Pornsin-Sirirak et al. [2000]). In figure 6.2 the different steps are illustrated. In the next sections one can find the method description, the advantages and the disadvantages of this method.

Description

First, a Ti-alloy substrate is cleaned and dipped into a diluted Hydrofluoric (HF) solution. A dry film resist is laminated onto the substrate (figure 6.2(1)).

Then, the resist is patterned under UV-light. This makes the resist to disappear where no stiffeners are located. It is then developed into a Na_2CO_3 solution for 5 minutes (figure 6.2(2)).

When this is done, the substrate is etched in a solution of HF and HNO_3 (figure 6.2(3)).

Next, the resist is stripped of from both sides and the backside is relaminated again. This strip of resist will be used as platform for the parylene-C to deposit on. The parylene-C is vapor deposited on the top. This is a layer of $5 \mu m$ thickness (figure 6.2(4)).

Now, the resist at the backside can be stripped. This leaves behind a parylene-c membrane attached to a Ti wingframe. (figure 6.2(5)).

Finally, the backside of the frame is also deposited with the parylene-C substrate. This is for more strength. The *Ti* wingframe is now sandwiched between two layers of parylene-C (figure 6.2(6)).

Advantages

1. More wings can be manufactured simultaneously.
2. The TAT is lower than the TAT of the traditional cut & glue method.
3. It is easy to adapt the method when the wing design is changing.
4. No glue or tape is needed.
5. The level of precision is high (standard tension in the membrane, exact location of the stiffeners, CNC cut-out).

Disadvantages

1. Costs are higher than for the previous method because of the use of titanium, Parylene-C and machinery.
2. It will take a while for a person to get acquainted with this method for building wings. This is a disadvantage in the scope of the research due to the limit amount of time.
3. Higher weight of the wings due to the higher density of titanium and parylene-c with respect to carbon and Mylar.

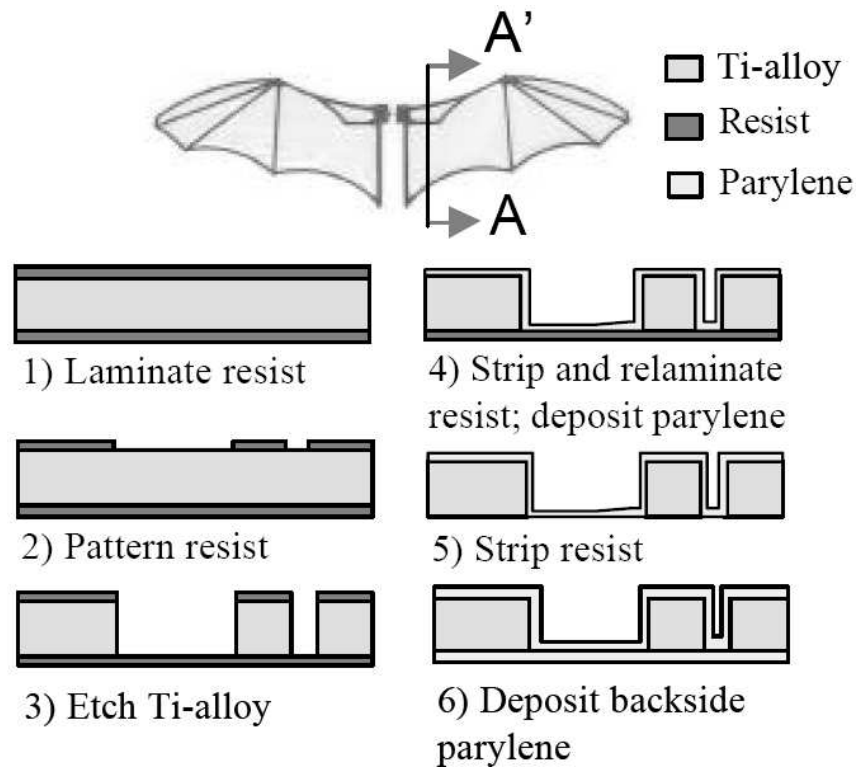


Figure 6.2: Building process of MEMS wings (Pornsir-Sirirak et al. [2000]).

6.2.3 Advanced cut & glue method

This method is developed during this research and is based on the traditional cut & glue method with the aid of a vacuum table and a CNC machine. In the next sections one can find the method description, the advantages and disadvantages of this method.

Description

The process starts with making a drawing of the wing in a CAD program. It is a simple drawing with lines for the contour, location of the stiffeners and leading edges. This drawing can be imported into a milling machine. The Computer Numerical Control-machine (CNC-machine) can now mill this drawing into a wooden plate, for example MDF. The result of this milling operation will be a wooden plate with small grooves of 0.6 mm width (depending on the tool diameter) and 0.3 mm depth which represent the contour, locations of the stiffeners and leading edges.

When the milling is finished, holes have to be drilled into the MDF plate because the MDF plate is too thick for the vacuum pump to suck the air through the plate. Without the holes, the Mylar foil would not "stick" to the plate. Both the inside and the outside of the contour has to be drilled, otherwise the side where no holes are present, will come loose when the wing is cut. In figure 6.3, a SolidWorks representation of the milled MDF plate is shown.

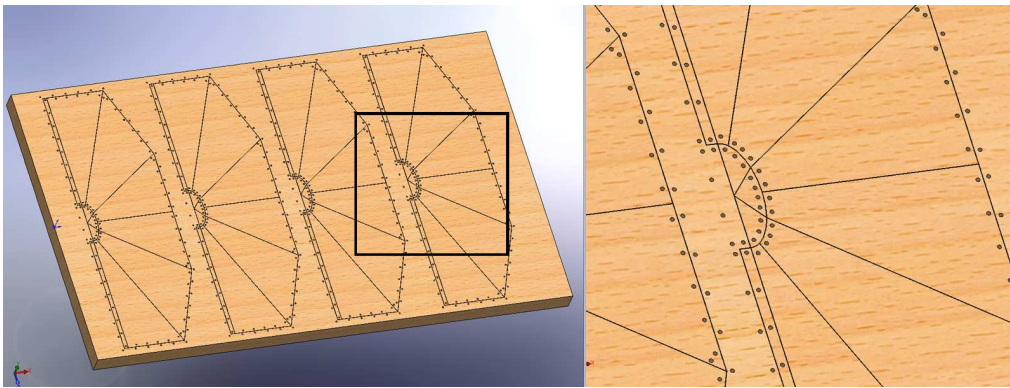


Figure 6.3: SolidWorks representation of the MDF plate after milling the wing contours and holes (left). Detail of the holes on both sides of the contour (right).

Now that the jig is finished, it can be placed on a vacuum table and the Mylar foil can be put on top of the MDF plate. The Mylar foil has a thickness of $5 \mu m$. When the whole plate is covered with the foil, the foil will be sucked onto the plate. When the foil is rolled out on the plate, wrinkles are visible in the foil. One needs to get rid of these wrinkles by stretching the foil over the plate. Stretching does not introduce tension in the foil.

This is checked with the following test: When the foil is positioned over the plate without wrinkles a line is drawn at the location of a groove. The foil is stretched elastically with the purpose to introduce tension in the foil. The line is not on top of the groove anymore. When the foil is let loose, the foil deforms again to its original state and the line is again over the groove, see figure 6.4. This means that no tension is present in the foil.

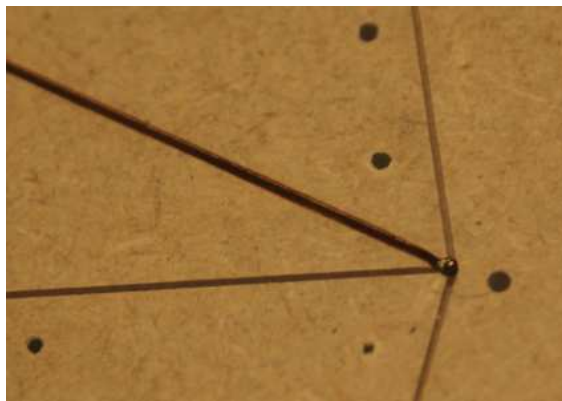


Figure 6.4: After elastically stretching the foil, the brown line is displaced again over the groove. Therefore, no tension is present in the wing.

Next, the stiffeners have to be glued onto the foil. This will be done with the same 50%-50% mixture glue as used for the traditional cut & glue method. However, the glue is now applied onto the stiffener itself instead of onto the foil. A droplet of glue is positioned on top of the stiffener while holding this vertical with tweezers. The droplet rolls down the stiffener and only little glue will stick to the stiffener, enough to secure it. The stiffeners are carbon rods with diameter 0.28 mm. After that, the stiffeners have to be secured at the ends with tape to prevent the stiffeners from delaminating. The difference with the

traditional cut & glue method is that the stiffeners are now glued with high precision because of the grooves in the jig. In figure 6.5, a representation is given of a cross section of the MDF plate at a place where a stiffener is positioned. One can see that the slot is wider than the stiffener, for clearance for the Mylar foil.

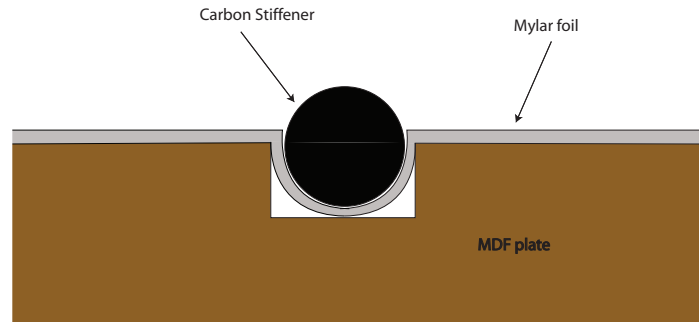


Figure 6.5: Cross-section of stiffener in jig with the Mylar.

Now the wing contour has to be cut. This is also done by making use of the same CNC-machine. The tool that is used is an engraver tool, with a very sharp head, almost like a needle (*STEP-FOUR* [2010]). The CNC-machine can follow the contour line and while the engraver is turning, it is able to cut the Mylar foil. Cutting the contour is done before gluing the leading edges onto the foil. This has a special reason. The root of the leading edges are outside the wings contour. This means that if the leading edges are glued before the contour is cut, the engraver tool has to cut through the leading edge. This is unwanted for two reasons. The first reason is that if the leading edges are cut at the contour, there is no possibility to put these leading edges into the hinges. The second reason is because it is not possible for an engraver tool to cut through a 0.4 mm thick carbon rod.

After cutting the contour, the leading edges are glued onto the Mylar, by putting 50%-50% mixture glue on the half round shape of the rod and put it in place. When this is done, simply glue the extra foil that is in front of the leading edge around it and one wing is done.

In order to have one set of wings, these steps have to be repeated for another wing. It is possible to make four wings at the same time, because four wings can fit in the MDF plate.

Advantages

1. It is easier to built a wing with this method than with the MEMS-method.
2. It is a cheap method in terms of materials. The materials used for this method are the same materials as for the traditional cut & glue method.
3. The amount of glue is kept to a minimum due to the different applying method.
4. It is easy to adapt the method when the wing design is altered.

5. The TAT of this method is much faster than for the traditional cut & glue method because wings can be built simultaneous and because of the computer tool that is involved in this method.
6. The level of precision is high (standard tension in the Mylar with the help of the vacuum table, exact location of the stiffeners, CNC cut out...).

Disadvantages

1. It is more difficult to use this method than the traditional method. Knowledge of a CNC-machine is required.
2. The precision is not of the same level as for MEMS wings because the process is not fully automated.

6.3 Trade-Off

In order to choose a suitable method for this research, a trade-off has to be done between these three methods. Trade-off criteria were chosen by looking at the advantages and disadvantages of the each method. The four most important criteria are *ease of use*, *costs*, *precision*, *turn-around time (TAT)* and *weight*. All these criteria are validated relative to each other.

The traditional cut & glue method is quite easy to start with, because no machinery is involved. It is basically, as the name of the method already tells, just glue the stiffeners onto the Mylar and cut the wing with a sharp knife. This also implies that the costs of this method are low as well. Because most of steps that are taken in this method all involve crafts, the TAT is slow, this goes at the expense of the precision. It will be difficult to validate data from wings which are made by this method.

The MEMS wings, on the other hand, are mainly made by repeatable computer controlled machines. This implies a high level of precision and a fast TAT. The process can be adapted rapidly if the design of a wing changes. It is more complicated to make a wing with this method, because one needs to get acquainted with the machines and materials. Furthermore, the use of titanium and specialized machines will increase the costs of these type of wings relative to the cut & glue wings.

The advanced cut & glue method is somewhere between the previous two methods. It is easier to use than the MEMS method and probably costs more or less the same as the traditional cut & glue method. The precision is higher than the traditional cut & glue method because of the use of a jig and vacuum pump but not that high as for the MEMS wings. Finally, the TAT is fast because multiple wings can be made simultaneous.

A trade-off diagram is illustrated in figure 6.6. The traditional cut & glue method is eliminated because of the poor level of precision and the low TAT, which are two very important parameters in this research. The MEMS method will take a lot of valuable time to get acquainted with, so that is the main reason why this method is also eliminated. The advanced cut & glue method will be used for building the wings during this research because it has overall good requirements.

	Ease Of Use	Cost	Precision	TAT	Weight
Cut-and-Glue Method	Easy	Low	Low	Low	Low
MEMS Method	Hard	Medium	High	Fast	High
Advanced Cut-and-Glue Method	Medium	Low	Medium	Fast	Low

Figure 6.6: Trade-off diagram between different methods.

6.4 Advanced cut & glue method in practice

The new method is more accurate and proves to make more consistent wings with the same properties. The process can be seen in several steps:

1. Draw the wing in a CAD program.
2. Mill the drawing into MDF plate which is positioned on a vacuum table.
3. Building the wing itself: Put foil on the MDF plate and glue stiffeners and leading edges onto the foil and cut the wing.
4. Prepare the wing to position on the DelFly.

A detailed description of the steps above is given in the next sections.

6.4.1 Draw the wing in a CAD program

The process starts with making a drawing of the wing in a CAD program. AutoCAD was used for this purpose. One can just draw the geometry of the wing including the contour, the place where the stiffeners come and the location of the leading edges. An example is given in figure 6.7. In this figure only one wing is displayed. In reality, different wings were put into one drawing because multiple wings fit onto the MDF plate.

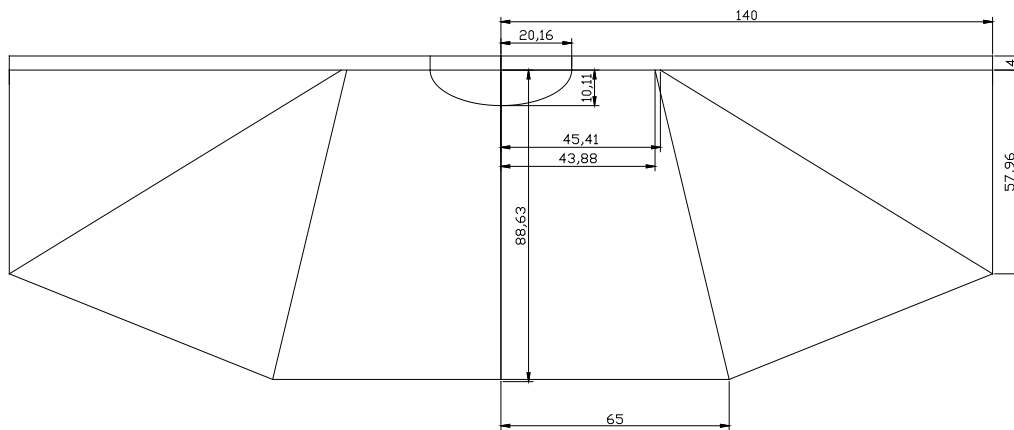


Figure 6.7: AutoCAD drawing of a wing. Dimensions are in mm.

The drawing has to be saved as a *.dxf* file. This is an extension that the milling program, *XpertMil* (see next step), can read.

6.4.2 Milling

A MDF plate is put onto a vacuum table so that the plate can not move anymore. This vacuum table is positioned on the working area of a CNC-machine. The CNC machine that is used is a *Precise 1600 Totaal Xpert* of *STEP-FOUR* (*STEP-FOUR* [2010]).

After switching on the CNC-machine, the user can set the *green* zero point, this is the point where the mill goes to when the milling is finished. The *yellow* zero point has to be set as well, this is the point where the mill starts to mill. Most common is a point on the surface of the MDF plate in one of the corners. After setting the *green* and *yellow* zero point in the *Xpert* file and aligning the points with the MDF plate, one can import the *.dxf* file with the drawing of the wing. Subsequently, mill the contour, the location of the leading edges and the location of the stiffeners with the settings given in table 6.1. The tool that is used has a 0.6 mm diameter with a flat head, see figure 6.8.

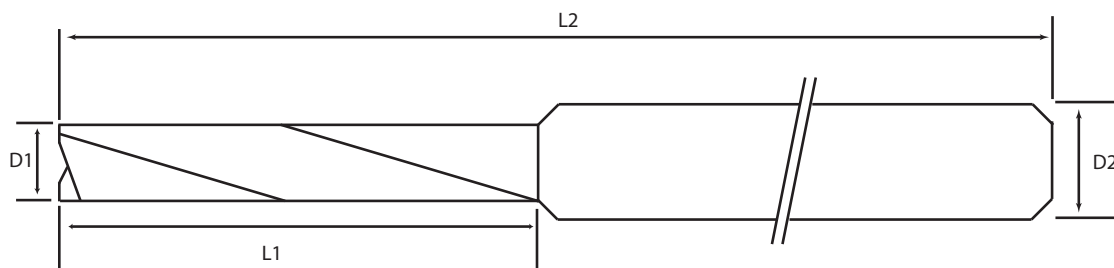


Figure 6.8: Tool for milling the contour, location of the leading edges and location of the stiffeners in the MDF plate. $D1=0.6$ mm, $L1=4$ mm, $D2=3$ mm, $L2= 38.1$ mm (*STEP-FOUR* [2010]).

When the milling of the contours, the location of the leading edges and the location of the stiffeners is done, one can drill holes both on the inner side of the contour and on the outer side of the contour. If the holes are drilled just on one side of the contour, this side

Parameter	Value	Unit
RPM	50000	[rpm]
XY feed	300	[mm/min]
Z feed	180	[mm/min]
Depth	0.3	[mm]
Steps	2	[–]
Depth per step	0.15	[mm]

Table 6.1: Milling parameters

will not stick to the plate anymore when it is cut and it will be possible for the foil to rupture. The holes have to be drilled straight through the MDF and are there for keeping the Mylar foil stick to the MDF plate. They have to be small (1 mm in diameter) because the Mylar can tear at the hole if the hole is too big because of the high suction forces of the vacuum table. The result can be seen in figure 6.9.

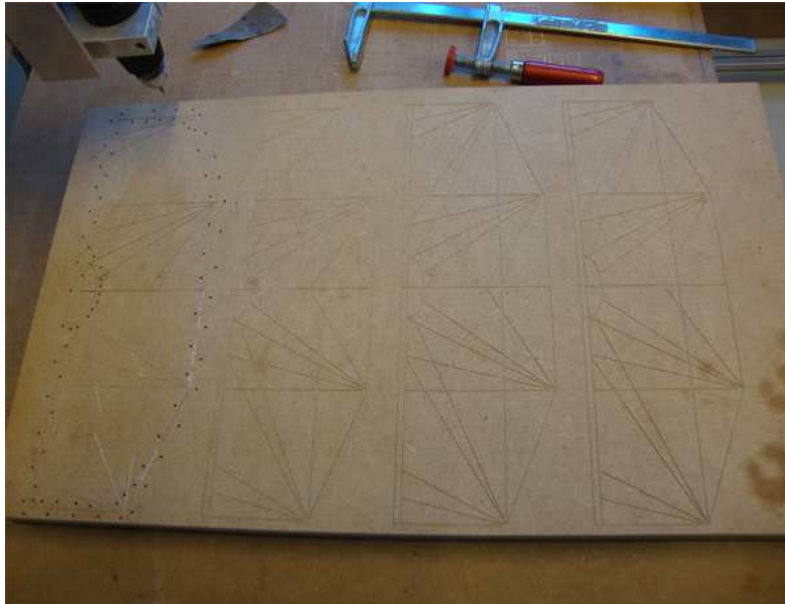


Figure 6.9: MDF plate after milling the wing contours

6.4.3 Building the wing

The actual building of the wing can be subdivided into 8 steps:

1. Placing the Mylar onto the vacuum table.
2. Glue the stiffeners.
3. Secure the stiffeners with tape.
4. Cut out the half-ellipse.

5. Glue the leading edges.
6. Cut out the contour.
7. Glue foil around the leading edges.
8. Prepare for assembly.

The steps are explained in more detail in the following sections.

Step 1: Placing Mylar onto the vacuum table.

It is very important to position the Mylar over the vacuum table in a correct way. If this is not done correctly, wrinkles can appear in the foil and therefore the tension will be different from wing to wing. The best thing to do is to slide the Mylar over the vacuum table just to avoid the wrinkles, see figure 6.11(1).

Step 2: Glue the stiffeners.

Gluing the stiffeners in the right position is easy and can be done with great accuracy thanks to the grooves that are milled into the MDF plate. The builder can put glue on the whole length of the stiffener and then position it with the help of tweezers into the correct groove on top of the Mylar. The glue that is used here is a 50% – 50% mixture of Pattex glue and Aceton, see figure 6.11(2)

Step 3: Secure the stiffeners with tape.

In order to prevent the stiffeners from delaminating, one can reinforce the endings with tape. Just like the traditional cut & glue method, small pieces of tape are positioned at the trailing edge of the wings where the carbon rods end. This is also done at the leading edge. If the stiffeners begin in the semi-ellipse near the root of the leading edge, a tape with the shape of a semi-ellipse is taped in one piece to reinforce that part of the wing, see figure 6.11(3a-3b).

Step 4: Cut out the half-ellipse.

When the stiffeners are glued and secured with tape, the semi-ellipse at the root of the leading edges is cut out with the CNC-machine for high precision with an engraver. This is a special tool with a thin cutting edge as can be seen in figure 6.10. The semi-ellipse has to be cut before the leading edges are glued because the roots of these leading edges are outside the contour of the wing. This means that when the leading edges are glued before the cutting of the semi-ellipse, the engraver has to mill through the leading edges and that is not possible, see figure 6.11(4).

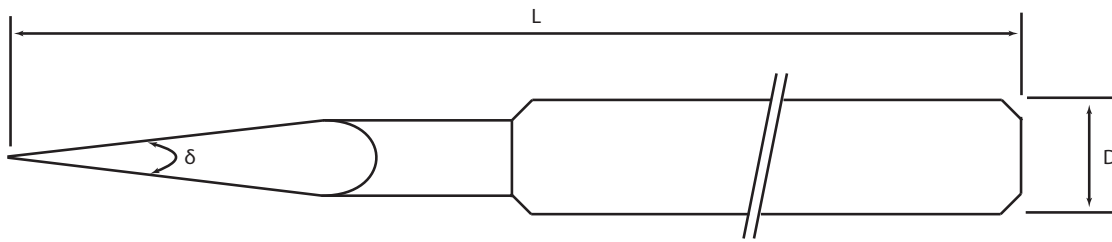


Figure 6.10: Tool for cutting the contour of the Mylar foil. $D=3\text{mm}$, $L=40\text{mm}$ and $\delta = 15^\circ$
(STEP-FOUR [2010])

Step 5: Glue the leading edges.

After cutting out the semi-ellipse, the leading edges can be glued. The leading edges are D-shaped carbon rods with a cross-section of 1.4 mm by 0.7 mm and with length 136.0 mm. They have to be glued with the curved side down in the groove, see figure 6.11(5).

Step 6: Cut out the contour

Now that both stiffeners and leading edges are glued to the Mylar, it is time to cut out the contour. This is done with the same engraver as for the semi-ellipse. The engraver cuts out the whole contour except the semi-ellipse to prevent collapsing with the leading edges, see figure 6.11(6).

Step 7: Glue foil around the leading edges.

The extra strip of foil that is in front of the leading edge is glued. This strip is there to be wrapped around the leading edge such that this can not disconnect from the foil during flapping, see figure 6.11(7). When the builder starts to glue the strip to the leading edge, he will notice that the foil is not sucked into the vacuum table anymore, this is because more and more sucking holes are not covered with the foil anymore because of the cutting. One should be careful not to tear the foil in a certain place.

Step 8: Prepare for assembly.

If all the previous steps are done, one DelFly wing is finished. Simultaneously, one can built three other wings. The builder can built two sets of DelFly wings at once. When two wings are built, they can be prepared to put on a DelFly. This means that in the middle of the trailing edge, a small hole has to be punched into the foil after that area is reinforced with tape. This is the location where the wing holder secures the wing to the fuselage, see chapter 4 and also see figure 6.11(8)

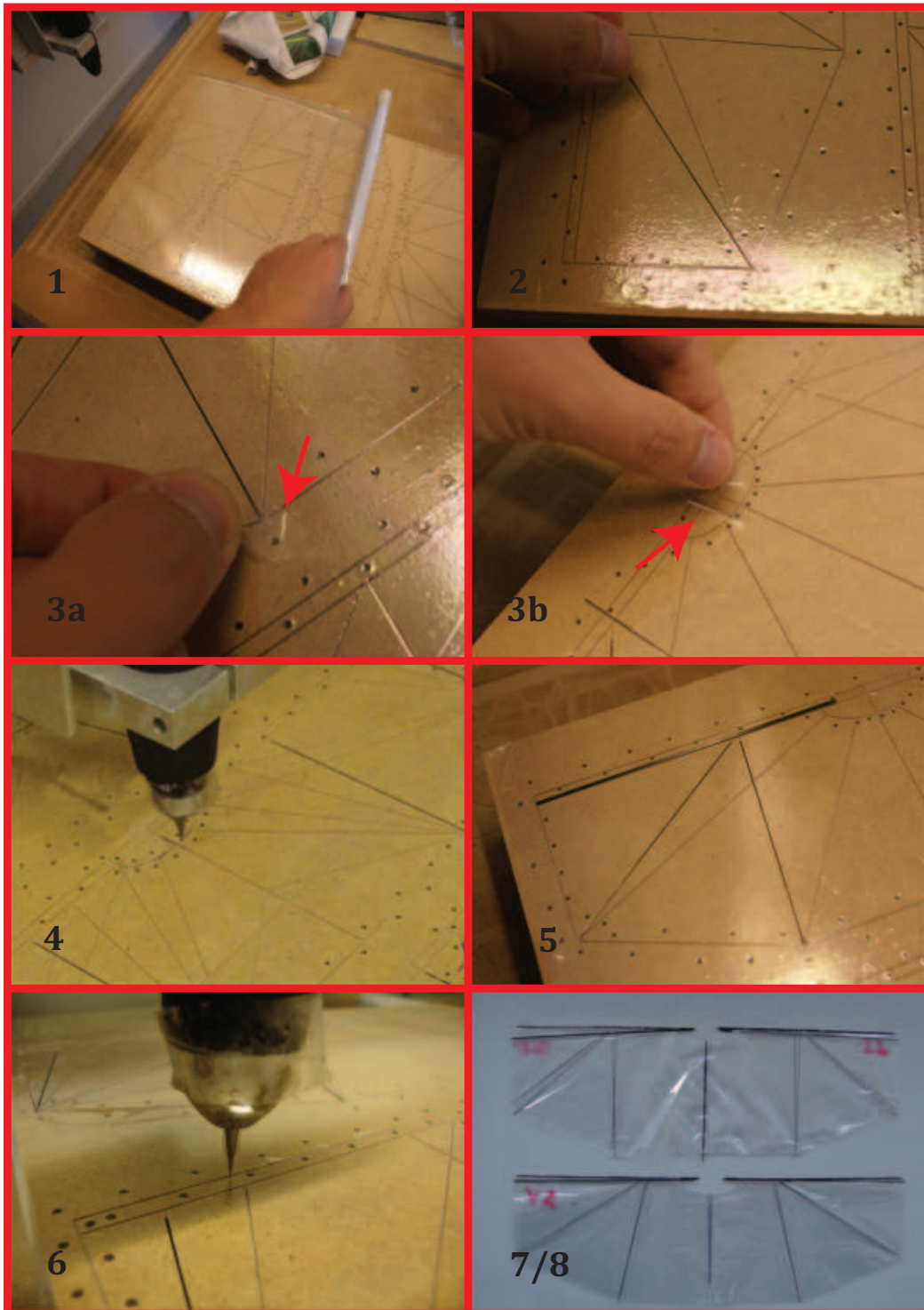


Figure 6.11: Overview of the advanced cut & glue method. 1) Placing the Mylar onto the vacuum table; 2) Glue the stiffeners; 3) Secure stiffeners with tape; 4) Cut out the half-ellipse; 5) Glue leading edges; 6) Cut out the contour; 7) Glue foil around leading edges; 8) Finished.

6.4.4 Some remarks

1. During the whole process it is important not to move the vacuum table because the reference point of the CNC-machine has to stay fixed to cut the contour in the exact position with the engraver.
2. The depth of the engraver cut is set to 0.15 mm below the surface of the MDF plate. This is just deep enough to cut the foil over the whole contour because there is a small difference in surface height because of small imperfections of the plate. If the cut is too deep, the Mylar foil will start to tear, especially when it cuts the areas where the tape is located. Cutting specifications are given in table 6.2

Parameter	Value	Unit
<i>RPM</i>	50000	[rpm]
<i>XY feed</i>	100	[mm/min]
<i>Z feed</i>	50	[mm/min]
<i>Depth</i>	0.15	[mm]
<i>Steps</i>	1	[–]

Table 6.2: Engraver cutting specifications

3. The speed with which the engraver cuts the foil has a great influence on the roughness of the cutting edge as can be seen in figures 6.12 to 6.14. Three different speeds are tested in order to have an idea of the roughness: 12 mm/min, 100 mm/min and 500 mm/min. From the figures one can conclude that a speed of 100 mm/min results in the smoothest edge. The smoothness of the edge is important to counteract the tearing of the foil during flapping. A comparison is also done with a cut from a razor blade, see figure 6.15. One can see that this cut is even smoother than the one with an engraver with speed 100 mm/min. The cut is done by hand, but with the aid of the grooves in the jig. Therefore, it is possible to make a precise cut along the edges of the wing. Furthermore, the cutting with the razor blade is done faster than the CNC-machine. The result of this study is that CNC-cutting is possible, but the actual cutting will be done with a razor blade.



Figure 6.12: Microscopic view of an engraver cut with speed 12 mm/min.

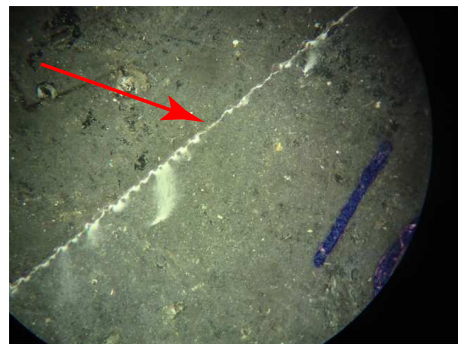


Figure 6.13: Microscopic view of an engraver cut with speed 100 mm/min.

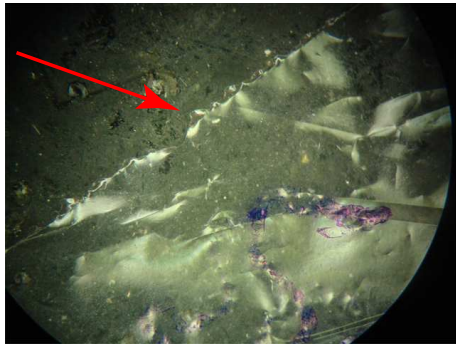


Figure 6.14: Microscopic view of an engraver cut with speed 500 mm/min.



Figure 6.15: Microscopic view of a razor blade cut.

- The significant differences between the Traditional method and the Advanced method are summarized in table 6.3.

	Traditional Method	Advanced Method
Placing and preparing the Mylar	Fix Mylar with tape. This introduces tension in the foil.	Fix the Mylar on a vacuum table. This introduces no tension in the foil.
Gluing the stiffeners	Glue them onto the Mylar with the CAD drawing as a guideline. Gluing will not be exact.	Glue them onto the Mylar in the grooves for the exact positioning.
Cutting out the contour	By hand. Lot of margin for error.	With the aid of the jig and razor blade. Cut is precise.

Table 6.3: Differences between the Traditional and Advanced method

6.5 Comparison of advanced cut & glue method with traditional cut & glue method

In order to verify the findings in of the previous sections, a comparison of both the traditional cut & glue method and advanced cut & glue method are done. Two aspects are examined: The manufacturing time and the difference in quality of the wings.

6.5.1 Manufacturing time comparison

The manufacturing time is an important parameter in this thesis. Because of the great amount of wings that have to be manufactured and tested, lots of time can be saved by reducing this manufacturing time per wing.

Four different persons were asked to built wings. They did this by using the traditional cut & glue method and the advanced cut & glue method. Some persons are familiar with

building DelFly wings, other are totally not familiar with the subject. Table 6.4 shows the time that different test persons need to built one set of DelFly wings. Note that the building time of person 1 is neglected in the calculating of the mean value because no building time for the advanced method was known.

	Traditional method	Advanced method	Gain in %
Person 1	82 min	/	/
Person 2	55 min	25 min	54%
Person 3	45 min	20 min	56%
Person 4	54 min	23 min	54%
Mean time	51min	23min	55%

Table 6.4: Overview of building time of one set of DelFly wings (two wings) for both traditional method and advanced method

One can see that the building time is reduced with **23 minutes** on average, this is equal to a gain of **55%** on average.

6.5.2 Quality comparison

In order to compare the wings that are built with the advanced method and the wings that are built with the traditional method, one needs to investigate the performance plots. These plots can be found in figure 6.16. Both thrust, power and the ratio of the two are evaluated against the flapping frequency. The blue lines indicate wings that are built with the traditional method. The red lines indicate wings that are built with the advanced method. One can see that the differences in thrust are relatively low. This is because all wings are of the same type (shape and stiffener location are the same) and therefore have the same aerodynamic properties. This results in a thrust generation that is more or less equal.

When looking at the power consumption, larger differences are present between the different wings. Both blue and red lines are scattered. There is no clear relation between the wings built with the traditional method. The performance of the wings built with the advanced method however are concentrated per two wings. Advanced 1 and Advanced 2 have nearly the same thrust-to-power ratio. This is also true for the wings Advanced 3 and Advanced 4. The reason for this is due to the fact that Advanced 1 and Advanced 2 are built at once as well as Advanced3 and Advanced4. One can built four wings at once on one MDF plate. The tension in the foil when building the wings is therefore exactly the same when building the wings on one MDF plate and therefore the performance is also the same.

The blue lines are scattered more in the power and thrust to power plot. The standard deviation for the blue lines is 0.0091 N/W. For the red lines this standard deviation is in the order of 3e-4N/W for Advanced 1/2 and for Advanced 3/4.

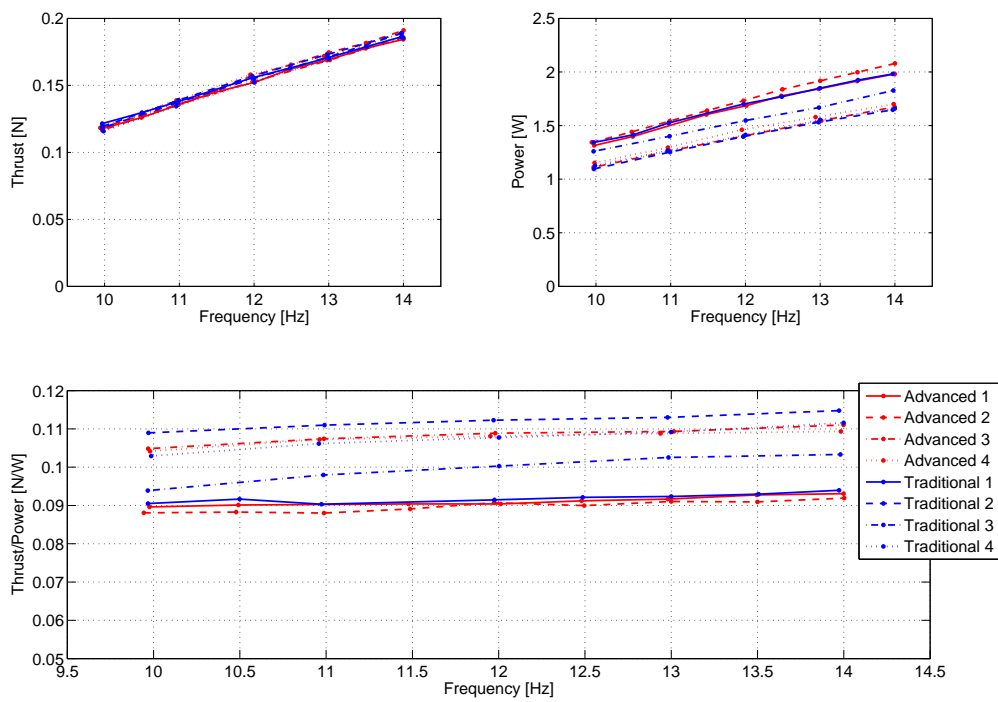


Figure 6.16: Performance plots of wings made with the advanced method (red) and wings made with the traditional method

Conclusions & Recommendations

7.1 Conclusions

As a final chapter of this thesis research, conclusions are drawn and recommendations for future research on this topic are suggested.

At the beginning of this report the following project goal is stated:

Project Goal

”Improve the flight performance of DelFly II in hover by improving wing design and driving mechanism”

This goal consists of two parts: Improving the wing design and improving the driving mechanism.

A systematic approach of altering the wing design has improved the thrust-to-power ratio of the new wing with approximately **5%**. Furthermore, using a crank-shaft mechanism that is manufactured with an injection moulding technique and that has a different set of gear connections for different energy transfer, has proven to give an increase in thrust-to-power ratio of approximately **20%** with respect to the old crank-shaft mechanism. A total gain in thrust-to-power ratio of approximately **25%** is obtained during this research. Therefore, it can be stated that the project goal is achieved.

Further conclusions are given in the next sections, they can be subdivided into four groups: Experimental set-up, new crank-shaft mechanism, results of wing study and manufacturing method.

7.1.1 Experimental set-up

A new experimental set-up has to be built because the old set-up was not stiff enough to counteract the vibrations that occur due to the flapping of the wings. In order to

counteract these vibrations, the set-up is made stiffer and heavier. However, even with the current stiffness, not all vibrations have disappeared. High frequency mechanical vibrations are still present. Furthermore, the new set-up has to be able to do measurements in both hover and forward flight conditions. Therefore, two force sensors are used instead of one force sensor. These sensors are placed in a L-shaped form so that when the model is under an angle of attack both sensors measure components of thrust and lift force. During this study only measurements in hover condition are performed.

Although the mechanism is made stiffer, one can still observe the presence of noise in the data. This noise can be filtered out of the data by means of a standard low-pass filter when analyzing the data in one flap cycle. This filtering method shows the desired pattern of thrust generation during one flap cycle, which indicates that the data can be trusted. For the performance measurements, this filtering is not necessary because mean values are used over a time period of 10 seconds.

7.1.2 New crank-shaft mechanism

During this research a new driving mechanism is designed in order to improve the performance of the system. This mechanism is designed in SolidWorks and manufactured by Promolding, a company that is specialized in designing and developing new products. The new mechanism is different from the old mechanism in two main aspects. First, this new mechanism is made with a technique called injection molding. The materials that are used for are PC and POM for the gears. Using this technique increases the reproducibility of the DelFly system. The old mechanism is assembled by hand and most components were also built by hand which has a negative effect on the reproducibility and efficiency. Second, another way of transferring the energy of the motor into mechanical energy in order to move the leading edges is applied. The motor, gears, push rods and leading edges all move in parallel planes. When using the old mechanism, the energy has to be transferred to perpendicular planes which is less energy efficient.

These two main features make the new driving mechanism more efficient, more durable and more robust than the old mechanism. An increase of thrust-to-power ratio of 20% is measured with respect to the old mechanism. Endurance tests showed that the new mechanism can perform at the same level for a minimum of 19 hours, after that the foil in the wing teared and therefore the performance dropped. Wear properties of this new mechanism are far better than those of the old mechanism.

Furthermore, the weight of the driving mechanism is reduced with 35% with respect to the old driving mechanism.

7.1.3 Results of wing study

More than 100 different wings are measured during this research in order to investigate the influence of different parameters which define wing performance. The main focus in this research lies on the effect of the following parameters: Location and orientation of the stiffeners, thickness of the stiffeners, area distribution and aspect ratio.

A systematic study is performed to investigate the influence of stiffener location and orientation. This study resulted in a increase in thrust-to-power ratio of approximately

5% leaving parameters such as wing area, wing shape, aspect ratio untouched. The stiffeners of the old wing are under an angle of 54° and 24° with the trailing edge for respectively the inner and outer stiffeners. For the new improved wing, wing8435, these angles are 84° and 35° . Performance plots also show that the increase in thrust is almost zero, but the difference lies in the power consumption. The power consumption of the new wing is significantly lower than the power consumption of the old wing. The stiffeners of the new wing are shifted more to the tip of the wing, therefore the stiffness distribution of the whole wing is shifted more outwards. Furthermore, PIV measurements of Mark Groen (Groen [2010]) show that the foil of the new wing is much smoother during the rotational phase of the flap cycle than for the old wing. These two effects have their influence on the power consumption and need to be investigated in more detail.

The influence of thickness (and therefore the stiffness) of the stiffeners is investigated while leaving all other parameters unchanged. Tests show that the thrust generation increases with the increase of thickness. The actual reason for this is yet unknown. Further research has to be done on the aerodynamics and flow visualization.

Tests on different area distribution show that this also has an effect on the performance while leaving the actual wing area untouched. A bat-like wing has a significant higher thrust-to-power ratio than the standard wing shape. The thrust production of the bat-like wing however is much lower, the wing does not reach the thrust level for hover flight. This can indicate that a bat-like wing is better in forward flight because of the gain in thrust due to forward flight aerodynamics and the higher thrust-to-power ratio.

The effect of aspect ratio is also investigated. Tests show that the wing with a higher aspect ratio generates more thrust at higher frequencies although this wing has a smaller wing area.

Finally, additional tests are performed in order to gain a better understanding of the performance of the new model in total (new mechanism with new wing). First, the effect of clap & peel for DelFly II is investigated. The performance of a biplane wing configuration is compared with the performance of a single wing. If the thrust of a single wing is doubled, it is 8% lower than for the biplane configuration. This difference is due to clap & peel. For smaller MAV this gain can be up to 40%. The influence of clap & peel in the power consumption is practically zero. An endurance test is performed on the new model. A new wing flapped for 19 hours with the new driving mechanism and shows a decrease in thrust of around 2.5×10^{-4} N/hour or 2.5 mg/hour. This is far better than for the old mechanism. Experience with this old mechanism proves that. Tests in vacuum are performed in order to investigate the part of power and current consumption that goes to the mechanics and the part that goes to the aerodynamics. The tests show that 20 - 25% of the total power consumption goes to the mechanics and the rest is needed for the aerodynamics.

An overall gain of 20% is obtained for the power consumption due to improving the wing design and driving mechanism. This results in a gain in flight time that is larger than 20% because of the way the battery is discharged.

7.1.4 Manufacturing method

A new manufacturing method for producing DelFly wings is created during this research. The method is called "Advanced cut & glue method". It is a method based on the traditional cut & glue method with the aid of a CNC-machine and a vacuum table. The intention is to reduce the building time of DelFly wings and to create more consistent wings in terms of performance. Using this advanced method, the production time is reduced with 55%. The level of consistency improved as well but there are still small differences in performance of the wings.

7.2 Recommendations

In order to structure the recommendations, the same subdivision as for the conclusions is used. These recommendations can help further researchers in their work.

7.2.1 Experimental set-up

- The set-up is ready to use in the wind tunnel in order to do forward flight measurements, because of the positioning of the two force sensors and the hinging point. However it is wise to add the possibility of being able to set and measure the angle of attack as accurate as possible. Furthermore, when changing the angle of attack with this test set-up, the height of the DelFly model changes respectively to the nozzle of the wind tunnel. This can be non-profitable for the measurements.
- One can make the construction even more stiffer, in such way that the mechanical vibrations are outside the regime of the measurements.
- It is also important to obtain a high mechanical resonance frequency. This also ensures that the noise domain is outside the measured domain which makes filtering easier.
- Another way to obtain clean data is by filtering the raw data. For this research a standard low-pass filter is used which gave good results. Further research in advanced filtering can be done.
- Improve the accuracy with which the wings are fixed onto the DelFly model.

7.2.2 New crank-shaft mechanism

- Extra improvements can be done on the new mechanism in order to make it even more robust and resistant to vibrations and deformations.
- Dimensions of the connection between the rivet of the hinge and the hole in the gearbox need to be adjusted a little bit for a perfect push fit.
- The hole that has to be made at the back of root of the wing for placing the wing holder is cut with a razor. For the future it is better to punch a perfect hole in the wing in order to reduce the risk of tearing.

- All the electronics, mechanical components and fuselage should be protected in a light-weight foam shell such that they are all secured from the surroundings. This shell can also prevent damage due to crashes. DelFly is a fragile piece of technology and deserves some safety measures.

7.2.3 Experiments

- Keep a good logbook during the testing phase of the project with detailed information about air pressure, temperature and state of the system because all these factors have their influence (small or large) on the measurements.
- More research has to be done on the shape of the wing and influence of Re number and/or AR, possibly by using a rigid wing.
- Further investigation needs to be done on bat-like wings in forward flight
- Implement the data in an aerodynamic tool in order to do preliminary simulations on DelFly.
- Further research can be done on the effect of span, chord, AR and Re number for clap & peel.

7.2.4 Wing manufacturing process

- A detailed study of the MEMS method has to be done to validate the possibility of building DelFly wings with this method and to see if different wings are more consistent in terms of performance.
- Improve the advanced cut & glue method by implementing the ability to measure the tension in the wing foil when manufacturing the wing.

References

- Ansari, S. A., Knowles, K., & Zbikowski, R. (2008). Insectlike Flapping Wings in the Hover Part 1: Effect of Wing Kinematics. *Journal of Aircraft*, Vol.45 (6), pp. 1945 – 1954.
- Atomic workshop*. (2010, October 01). [http://http://www.atomicworkshop.co.uk](http://www.atomicworkshop.co.uk).
- Bolsman, C., Goosen, J., & Keulen, F. van. (2009). Compliant Structure Design for Reproducing Insect Wing Kinematics in MAV'S. *Proceedings of IFASD conference, Seattle, Washington, Vol.1*, pp.21-25.
- Croon, G., Clercq, K. D., Ruijsink, R., Remes, B., & Wagter, C. D. (2009). Design, Aerodynamics and Vision-Based Control of the Delfly. *International Journal of MAV, Vol.1(2)*, pp. 71–97.
- De Clercq, K. M. E. (2009). *Flow visualization and force measurements on a hovering flapping-wing mav 'DelFly II'*. M.Sc. Thesis, Delft University of Technology, Delft, The Netherlands.
- Delfly*. (2010, July 14). <http://www.delfly.nl>.
- Didel*. (2010, July 14). <http://www.didel.com>.
- DSE. (2005). *Design of a Flapping Wing Vision-Based Micro-UAV*. Design Synthesis Exercise, Delft University of Technology, Delft, The Netherlands.
- Ellington, C., Berg, C. V. den, Willmott, A., & Thomas, A. (1996). Leading-Edge Vortices in Insect Flight. *Nature*, Vol.384, pp. 626–630.
- Ellington, C. P. (1995). Unsteady Aerodynamics of Insect Flight. *Symposia of the Society for Experimental Biology*, Vol.49, pp. 109 – 129.
- Ellington, C. P. (1999). The Novel Aerodynamics of Insect Flight: Applications to Micro-Air Vehicles. *Journal of Experimental Biology*, Vol.202, pp. 3439 – 3448.

- Groen, M. (2010). *PIV Measurements on the Flapping Wing MAV DelFly II: An Aerodynamic and Aeroelastic Investigation into Vortex Development*. Master Thesis, Delft University Of Technology, Delft, The Netherlands.
- J. D. Anderson, J. (2001). *Fundamentals of Aerodynamics*. USA: McGraw-Hill.
- Kawamura, Y., Souda, S., Nishimoto, S., & Ellington, C. P. (2008). Clapping-wing Micro Air Vehicle of Insect Size. *Bio-mechanisms of Swimming and Flying, Vol. Chapter 26*, pp. 319 – 330.
- Lehmann, F. O. (2004). The Mechanisms of Lift Enhancement in Insect Flight. *Naturwissenschaften, Vol.91 (3)*, pp. 101 – 122.
- Lehmann, F. O., & Pick, S. (2007). The aerodynamic Benefit of WingWing Interaction depends on Stroke Trajectory in Flapping Insect Wings. *Journal of Experimental Biology, Vol.210*, pp. 1362 – 1377.
- Marden, J. (1987). Maximum Lift Production During Takeoff in Flying Animal. *Journal of Experimental Biology, Vol.130*, pp. 235–258.
- Micro plane solutions*. (2010, September 13). <http://www.microplanesolution.com>.
- Peekel instruments*. (2010, July 15). <http://www.peekel.nl>.
- Pornsirakul, T. N., Tai, Y. C., Nassef, H., & Ho, C. M. (2000). Unsteady-state Aerodynamic Performance of MEMS Wings. *International Symposium on Smart Structures and Micro Systems 2000, Vol.1*, pp. G1 – 2.
- Pornsirakul, T. N., Tai, Y. C., Nassef, H., & Ho, C. M. (2001). Titanium-alloy MEMS Wing Technology for A Micro Aerial Vehicle Application. *Sensors and Actuators, A: Physical, Vol.89 (1-2)*, pp. 95 – 103.
- Promolding*. (2010, July 14). <http://www.promolding.nl>.
- Sane, S. P. (2003). The Aerodynamics of Insect Flight. *Journal of Experimental Biology, Vol.206 (23)*, pp. 4191 – 4208.
- Step-four*. (2010, August 25). <http://www.step-four.at>.
- Teunissen, P. J. G., Simons, D. G., & Tiberius, C. C. J. M. (2005). *Probability and Observation Theory*. Delft: Faculty of Aerospace Engineering.
- Weis-Fogh, T. (1972). Quick Estimates of Flight Fitness in Hovering Animals, Including Novel Mechanisms for Lift Production. *Journal of Experimental Biology, Vol.59*, pp. 169–230.
- Yang, L. J., Feng, C. K., Hsu, C. K., Ho, J. Y., Feng, G. H., Shih, H. M., et al. (2007). Flapping MAV (Micro Aerial Vehicle) with PVDF-Parylene Composite Skin. *Hangkong Taikong ji Minhang Xuekan/Journal of Aeronautics, Astronautics and Aviation, Vol.39A (3)*, pp. 195 – 202.

Zdunich, P., Bilyk, D., MacMaster, M., Loewen, D., DeLaurier, J., Kornbluh, R., et al. (2007). Development and Testing of the Mentor Flapping-Wing Micro Air Vehicle. *Journal of Aircraft*, Vol.44 (5), pp. 1701 – 1711.

Zemic. (2010, July 15). <http://www.zemic.nl>.

Appendix A

DelFly II parameters

Parameters	Unit	Formula	Value
Mass	[g]	m	17
Flapping frequency	[Hz]	n	13 – 15
Amplitude	[°]	ϕ	44
Wing semi-span(one wing)	[mm]	R	140
Wing span	[mm]	b	280
Wing area	[mm ²]	S	11195
Aspect ratio	[-]	$AR = \frac{R^2}{S}$	1.75
Mean wing chord	[mm]	$\bar{c} = \frac{S}{R}$	80.0
Wing loading	[N/m ²]	$\frac{W}{S} = \frac{mg}{4S}$	3.72
Mean wingtip velocity	[m/s]	$\bar{U}_t = 2\phi n R$	3.01
Reynolds number (C. P. Ellington [1999])	[-]	$Re = \frac{\bar{c} \bar{U}_t}{\nu}$	13457

Table A.1: Design parameters of DelFly.

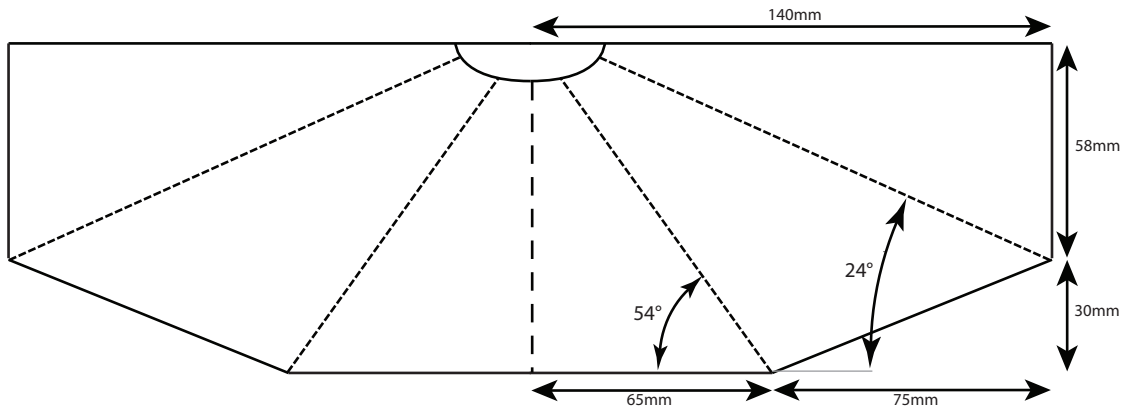


Figure A.1: Geometry of the old DelFly II wing.

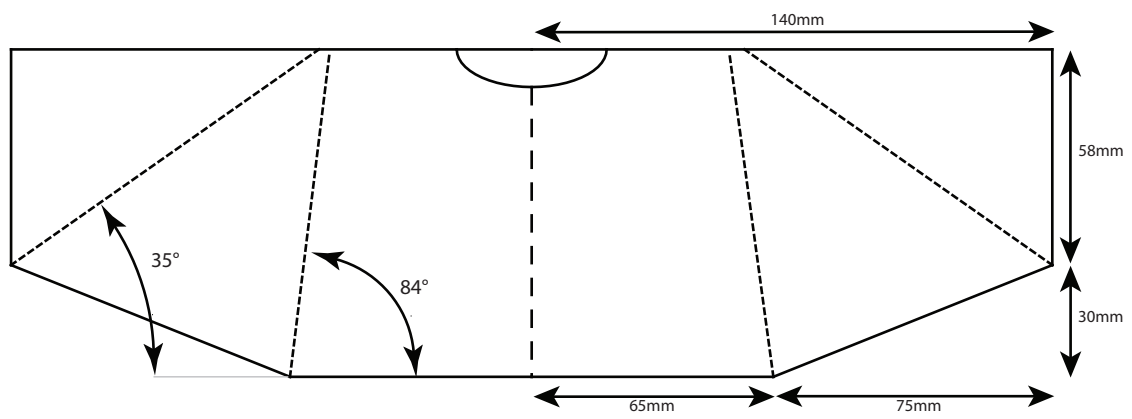


Figure A.2: Geometry of the new DeIFly II wing.

Appendix B

Specifications of Q70x5x9-H sensors

Specifications	
Capacity [g]	20, 30, 50, 100, 200
Output Sensitivity [mV/V]	0.5 ± 0.15
Combined Error [%FS]	± 0.05
Non-linearity [%FS]	± 0.05
Non-repeatability [%FS]	± 0.05
Hysteresis [%FS]	± 0.05
Creep [%FS/30min]	± 0.05
Zero Balance [mV/V]	± 0.5
Temp. effect on zero [%FS/10°C]	± 2.0
Temp. effect on span [%FS/10°C]	± 0.05
Input Resistance [Ω]	1055 ± 10
Output Resistance [Ω]	1055 ± 10
Insulation Resistance [$M\Omega$]	$\geq 2000(50VDC)$
Excitation, Voltage [V]	≤ 6
Temperature, Operating [°C]	$-10 \sim +40$

Table B.1: Specifications of Q70x5x9-H sensors (Zemic [2010]).

20g, 30g, 50g, 100g L1=4 L2=8
 200g L1=8 L2=10

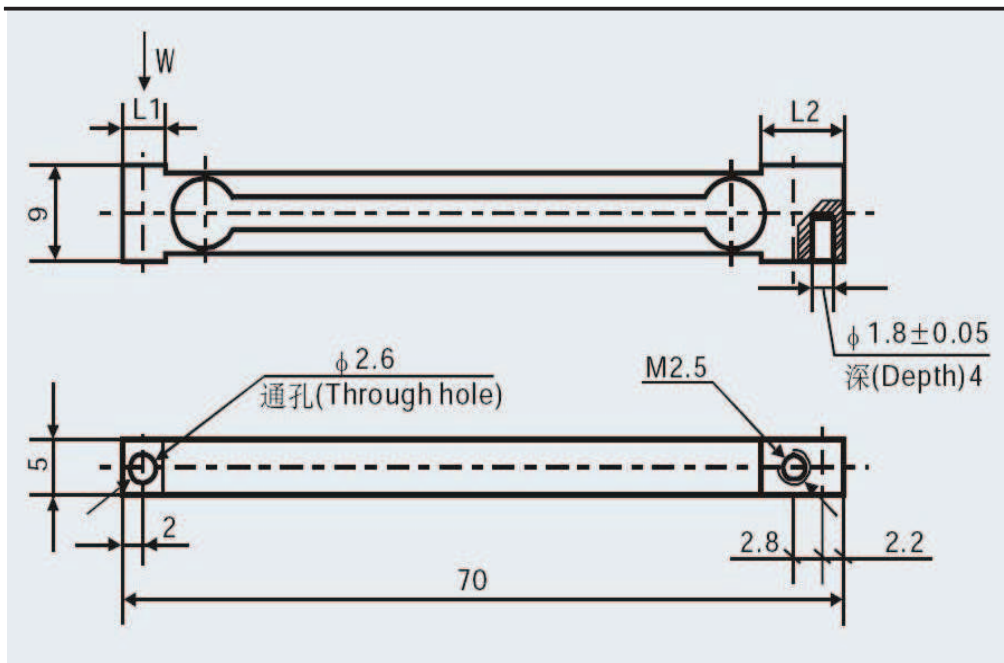


Figure B.1: Dimensions of the force sensor (Zemic [2010]).

Technical drawings of the new crank-shaft mechanism

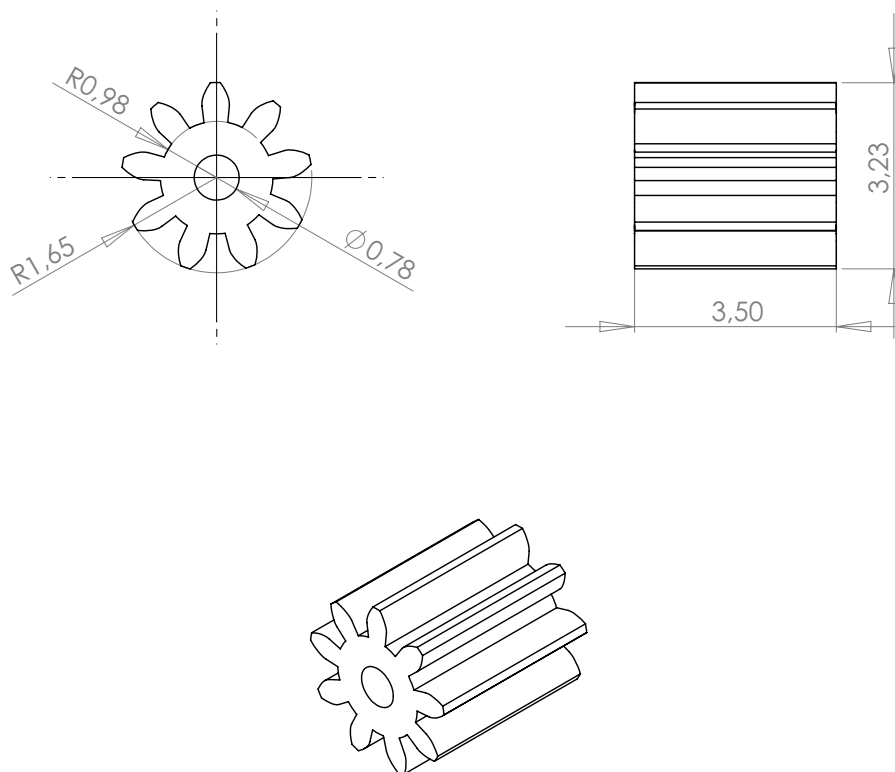


Figure C.1: Dimensions (in mm) of the motor pinion.

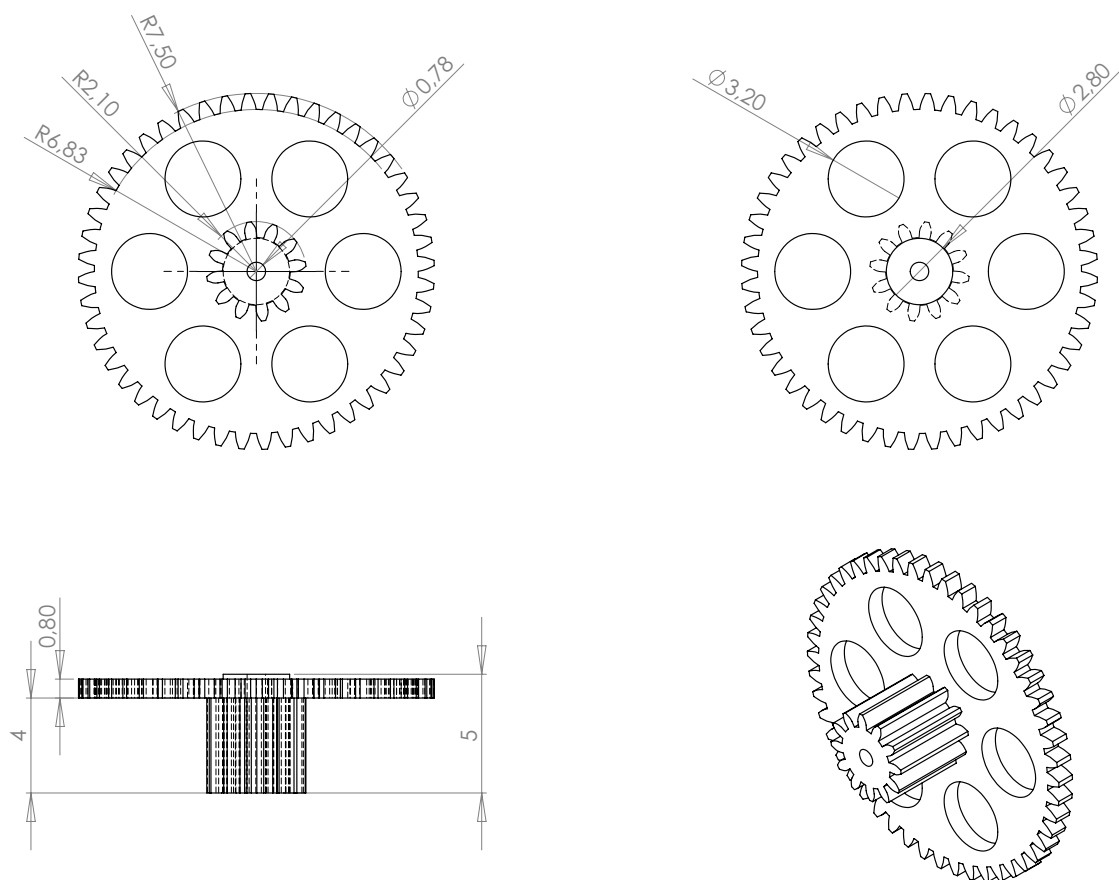


Figure C.3: Dimensions (in mm) of the intermediate gear.

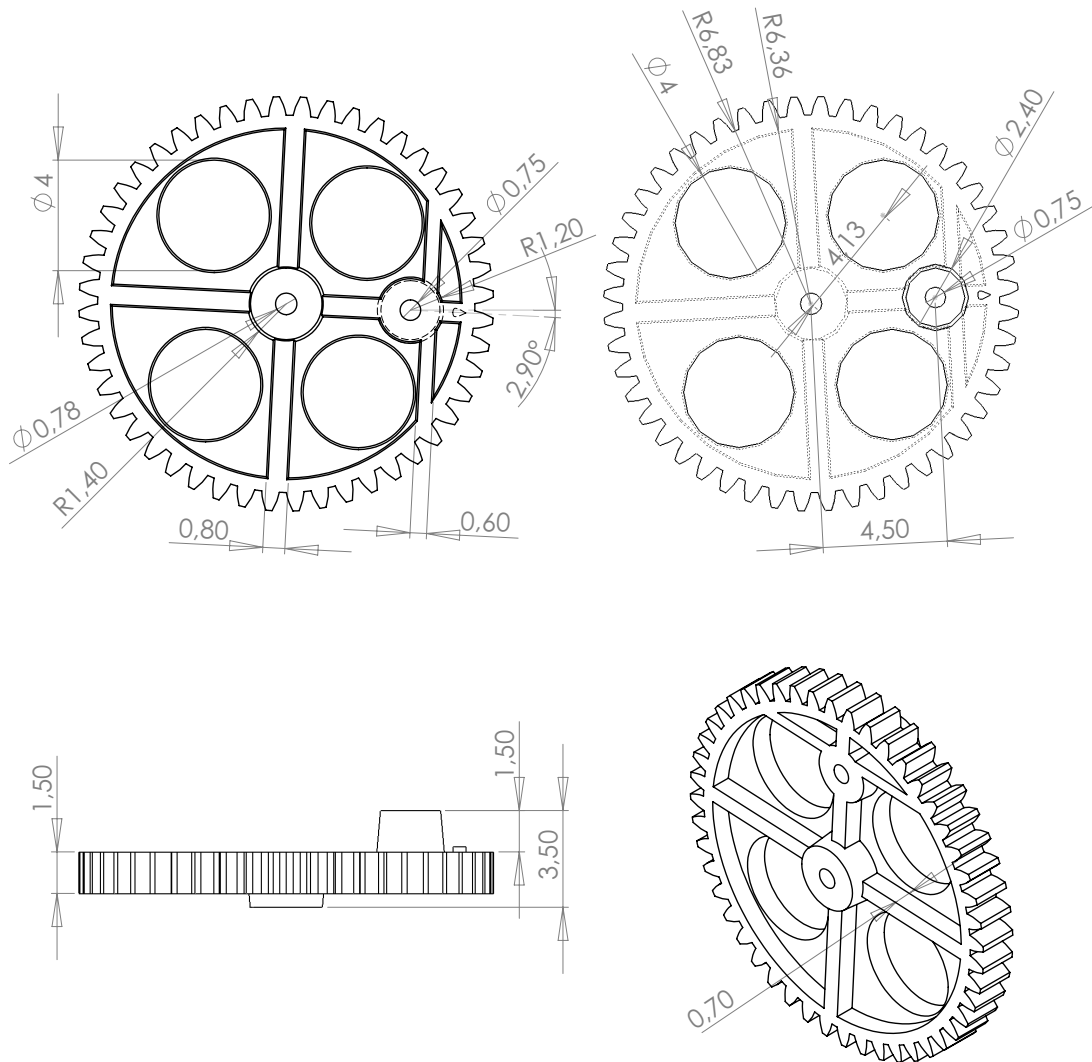


Figure C.4: Dimensions (in mm) of main gear.

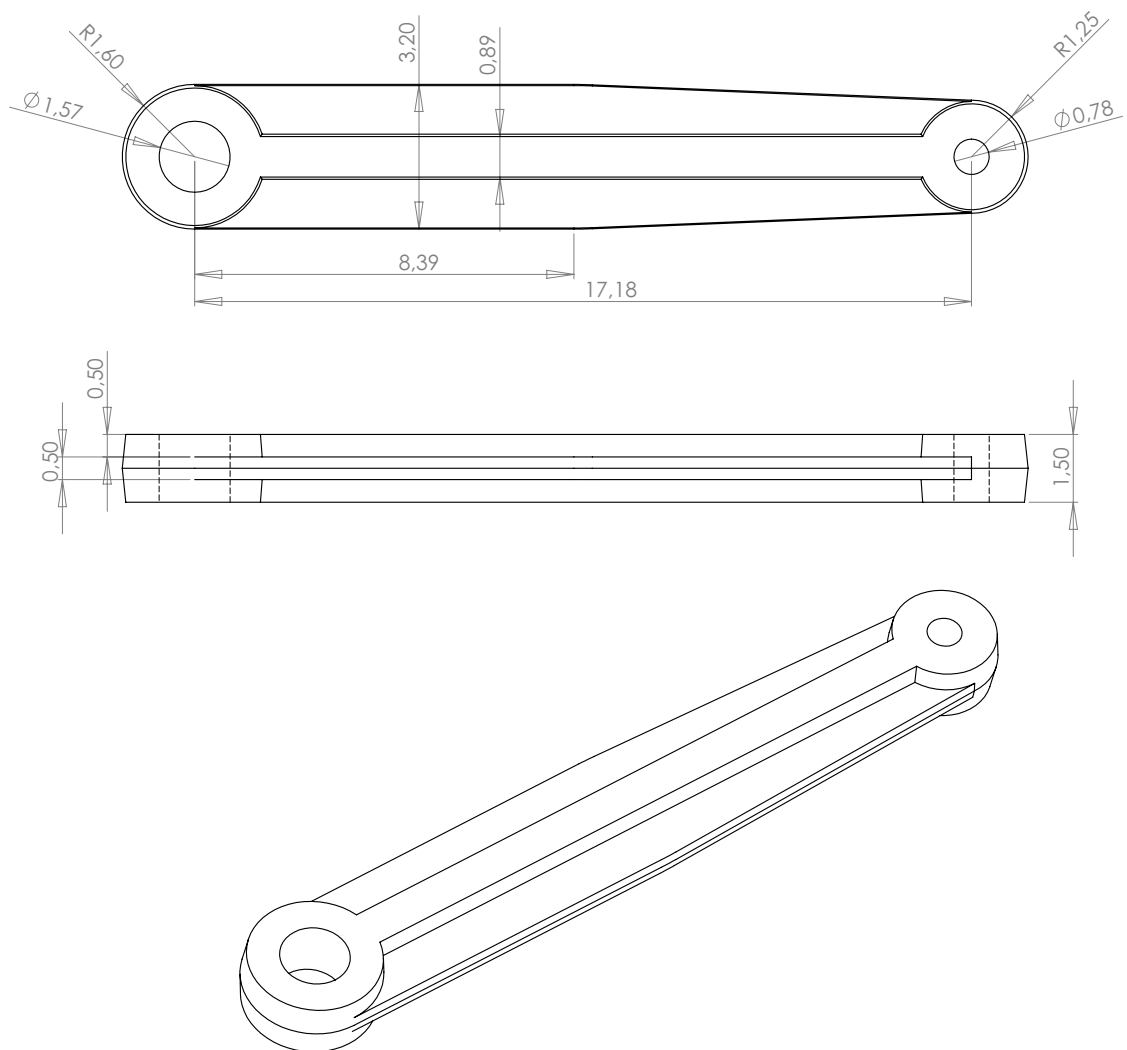


Figure C.5: Dimensions (in mm) of the pushrod.

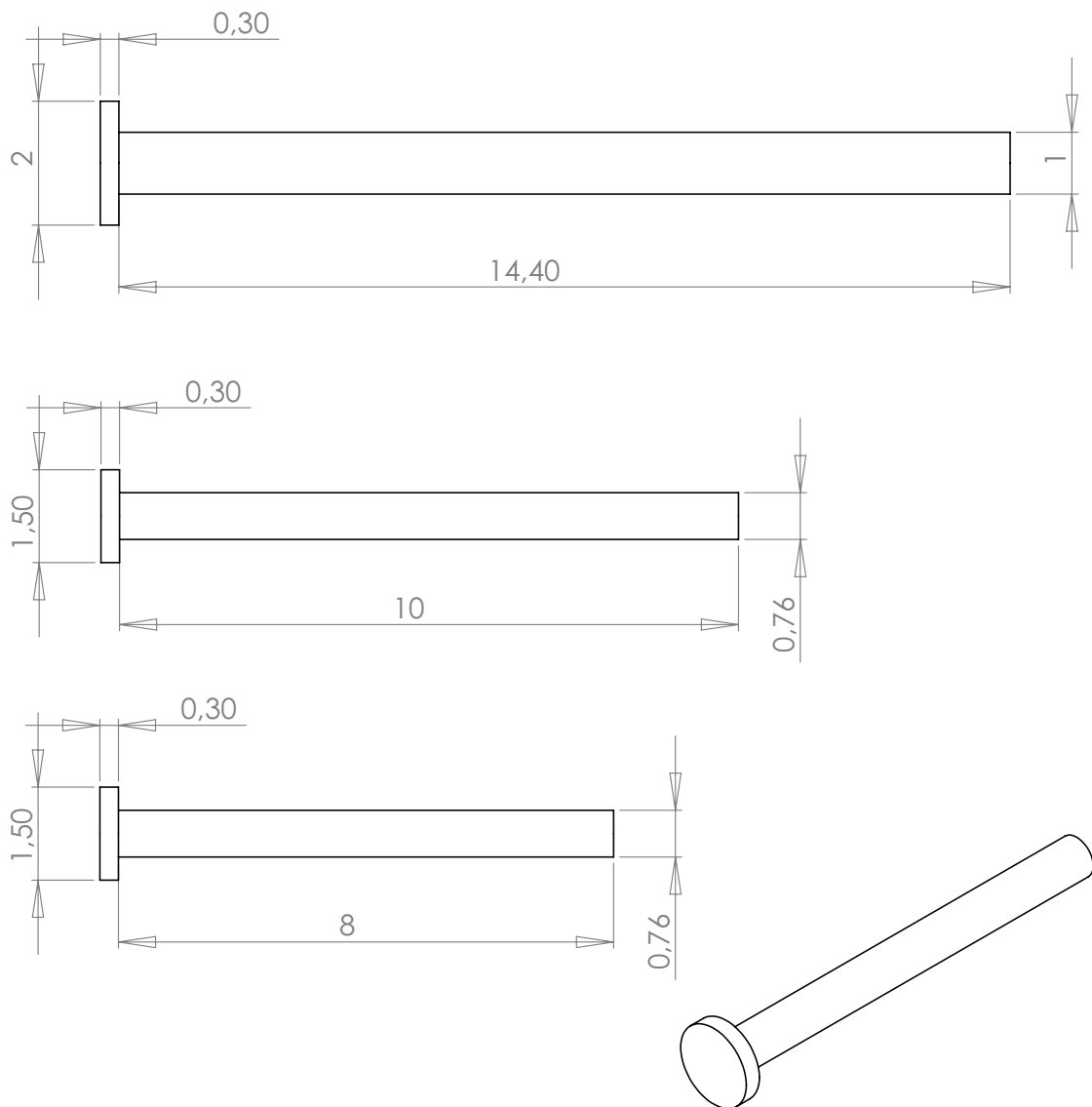


Figure C.7: Dimensions (in mm) of the steel rivets.

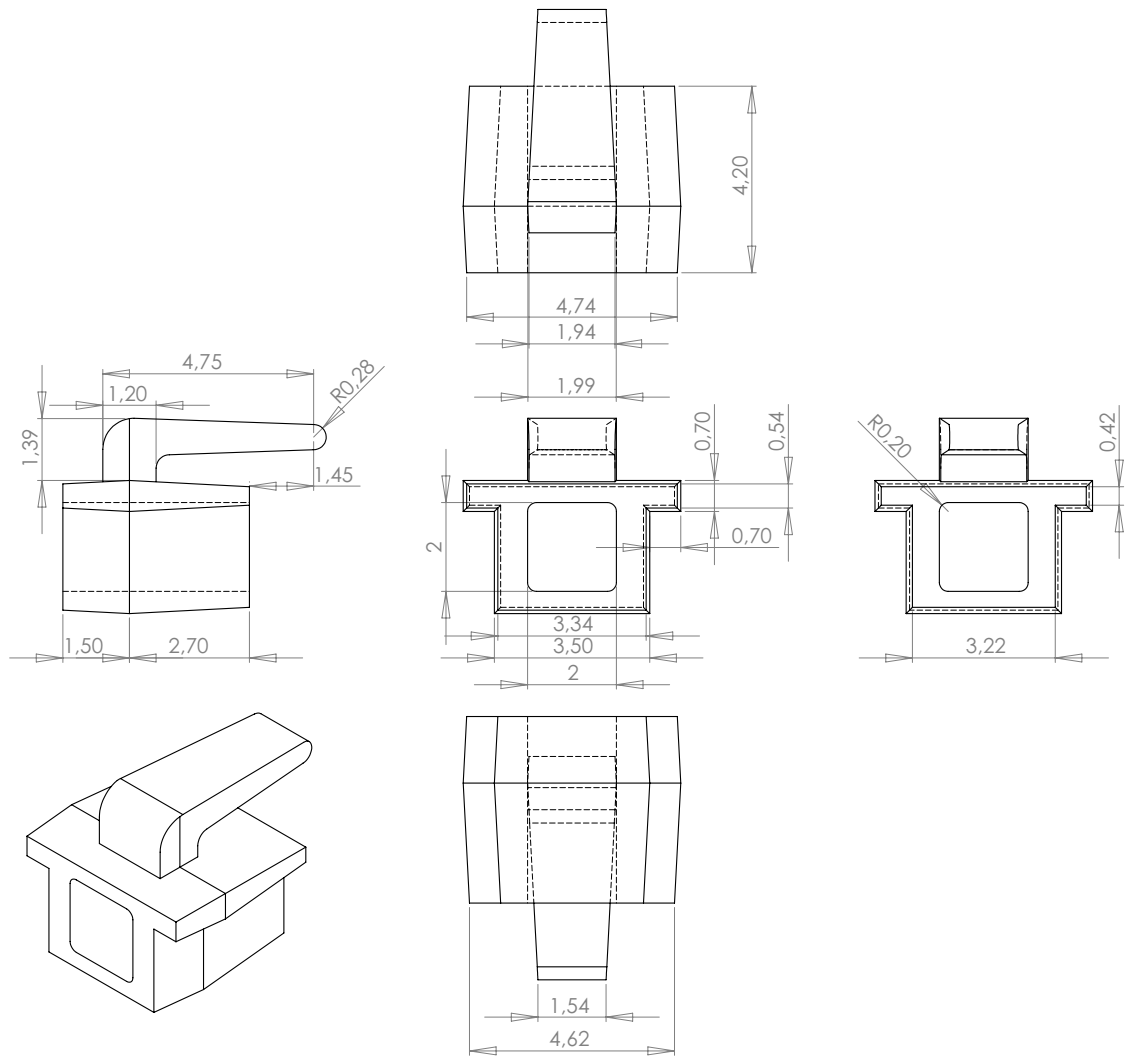


Figure C.8: Dimensions (in mm) of the wing holder.

DeFly II wing design

D.1 Influence of stiffener location

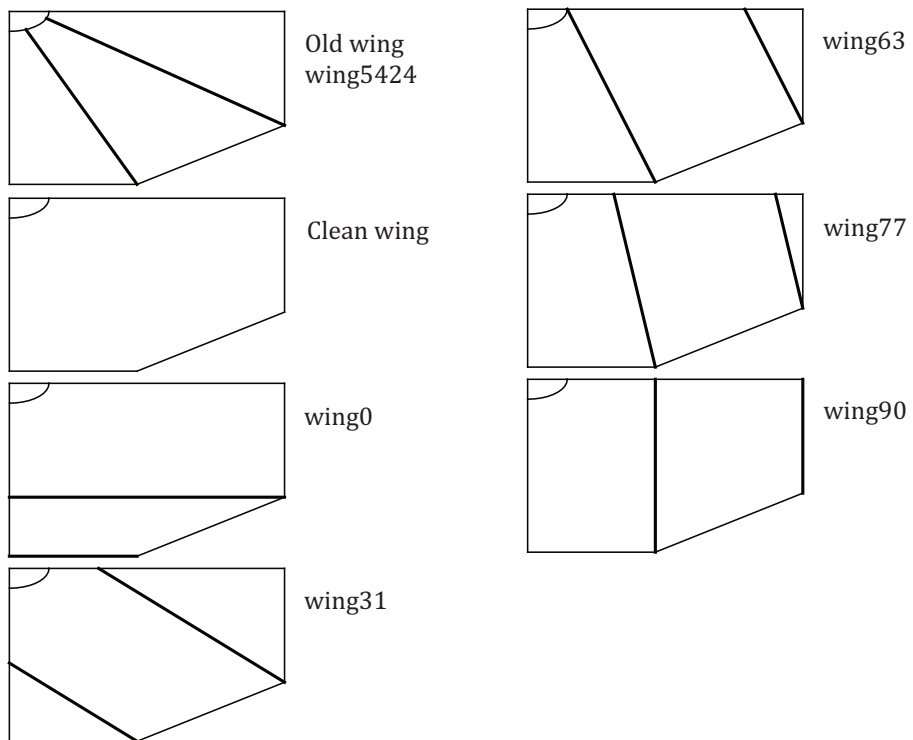


Figure D.1: Step 1.

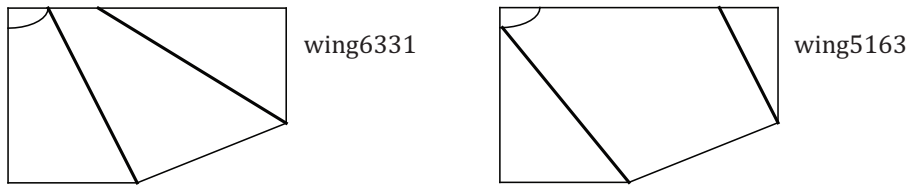


Figure D.2: Step 2.

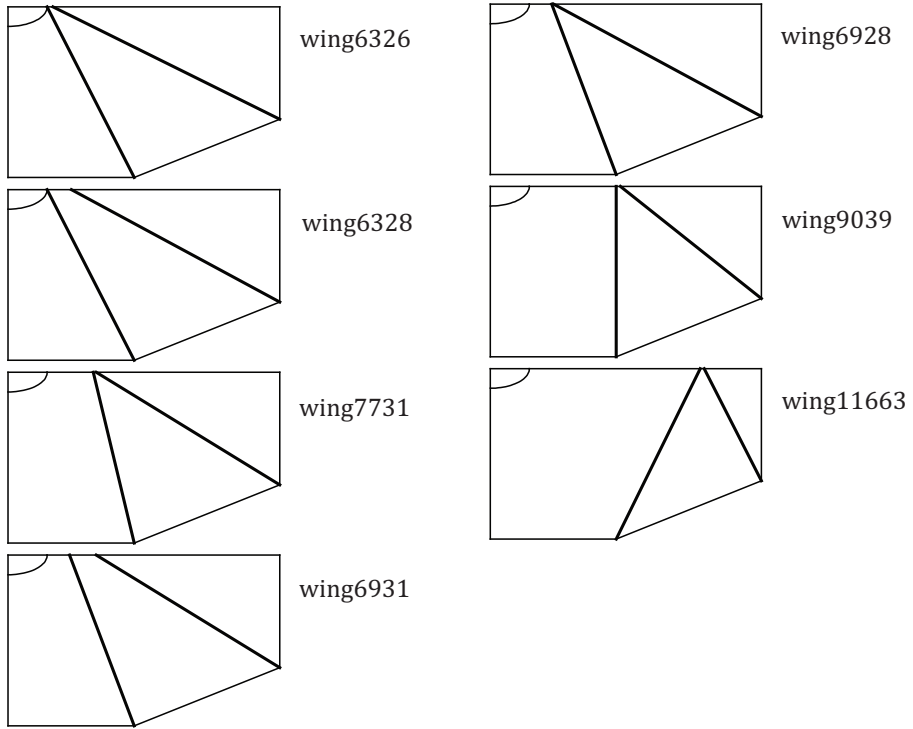


Figure D.3: Step 3.

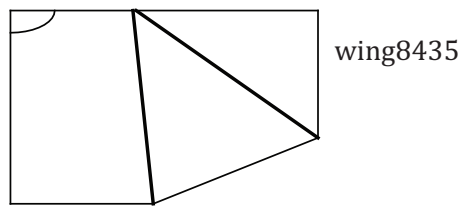


Figure D.4: Step 4.

D.2 Influence of area distribution

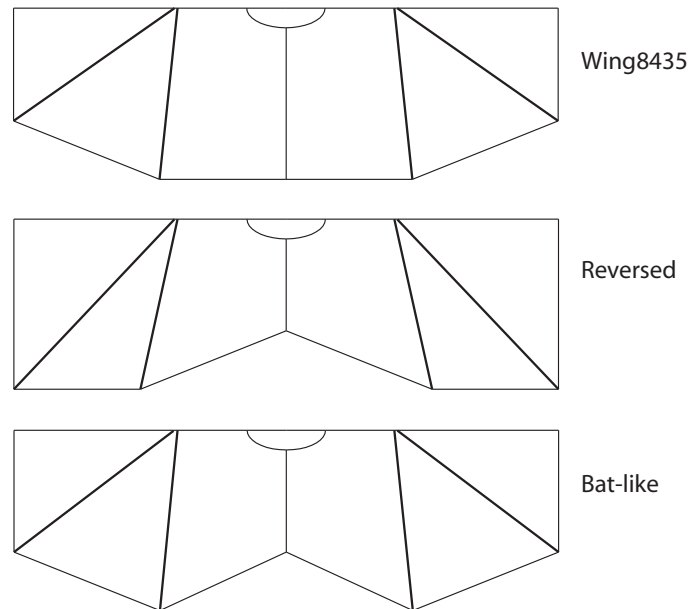


Figure D.5: Area distribution.

D.3 Influence of aspect ratio

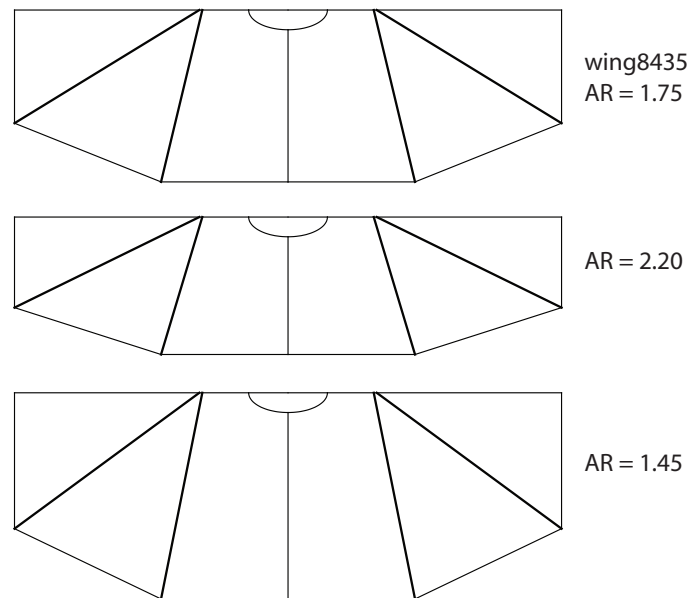


Figure D.6: Aspect ratio.